

# **Piezoelectric and dielectric properties of polymer-ceramic composites for sensors**

PROEFSCHRIFT

Ter verkrijging van de graad van doctor  
aan de Technische Universiteit Delft,  
Op gezag van de Rector Magnificus Prof. Ir. K.C.A.M. Luyben,  
Voorzitter van het College voor Promoties,  
In het openbaar te verdedigen op 17 Juni 2015 om 12:30u

Door

***Nijesh K James***

Master of Science in Physics

St. Berchman's College, Kerala, India,

Geboren te, Kozhikode, Kerala, India

Dit proefschrift is goedgekeurd door de promotor:

Prof. dr. ir. S. van der Zwaag

Prof. dr. W. A. Groen

Samenstelling promotiecommissie:

Rector Magnificus                      voorzitter

Prof. dr. ir. S. van der Zwaag      Technische Universiteit Delft – promotor

Prof. dr. W. A. Groen                      Technische Universiteit Delft – promotor

Prof. Andrew Bell                      Universiteit Leeds, UK

Prof. dr. S. J. Picken                      Technische Universiteit Delft

Prof. dr. ing. A. J. H. M. Rijnders      Universiteit Twente

Prof. dr. E. H. Brück                      Technische Universiteit Delft

Copyright © 2015 by Nijesh K James

All rights reserved. No part of the material protected by this copyright notice may be reproduced or utilized in any form or by any means, electronic or mechanical, including photocopying, recording or by any information storage and retrieval system, without prior permission of the author.

Printed in The Netherlands by Ipskamp Drukkers B.V., Enschede

ISBN: 978-94-6259-697-9

Author email: [nijeshkjames@gmail.com](mailto:nijeshkjames@gmail.com)

*To my family*

---

*To my family*

---

**Table of contents**

<b>1</b>	<b>Introduction .....</b>	<b>1</b>
1.1	Introduction to piezoelectricity and piezoelectric materials.....	3
1.2	Piezoelectric aocomposites.....	6
1.3	Scope and outline of the thesis .....	10
	References.....	13
<b>2</b>	<b>Piezoelectric and mechanical properties of structured PZT- epoxy composites .....</b>	<b>17</b>
2.1	Introduction .....	19
2.2	Theory.....	20
2.3	Experimental .....	22
2.4	Results and discussion .....	26
2.5	Conclusions.....	35
	References.....	35
<b>3</b>	<b>Piezoelectric and mechanical properties of fatigue resistant, self-healing PZT-ionomer composites .....</b>	<b>39</b>
3.1	Introduction .....	41
3.2	Theory.....	42
3.3	Experimental .....	44
3.4	Results and discussion .....	47
3.4.1	Microstructure .....	47
3.4.2	Poling behaviour .....	49
3.4.3	Piezoelectric and dielectric properties .....	53
3.4.4	Mechanical properties .....	54
3.4.5	Self-healing properties .....	58
3.5	Conclusions.....	60
	References.....	60

<b>4</b>	<b>Analysis of the state of poling in granular PZT-polymer composites by High Energy Synchrotron X-ray diffraction.</b>	<b>65</b>
4.1	Introduction .....	67
4.2	Experimental procedure.....	68
4.3	Results and discussion .....	71
4.4	Conclusions.....	82
	References.....	83
<b>5</b>	<b>Exploring the Lead Zirconium Titanate (PZT) phase diagram for high sensorial properties in piezoelectric ceramic polymer composites .....</b>	<b>85</b>
5.1	Introduction .....	87
5.2	Theory.....	88
5.3	Experimental .....	90
5.4	Results and discussion .....	92
5.4.1	Crystallographic phase analysis and microstructure characterization ...	92
5.4.2	Dielectric and piezoelectric properties.....	97
5.5	Conclusions.....	109
	References.....	109
<b>6</b>	<b>Structured and unstructured Lead-free (K, Na)<sub>x</sub>Li<sub>1-x</sub>NbO<sub>3</sub> (KNN) piezoelectric ceramic - epoxy composites with a high piezoelectric voltage coefficient .....</b>	<b>113</b>
6.1	Introduction .....	115
6.2	Theory.....	117
6.3	Experimental .....	119
6.4	Results and discussion .....	120
6.4.1	Optimization of calcination process .....	120
6.4.2	Microstructure .....	125
6.4.3	Dielectric and piezoelectric properties.....	128
6.5	Conclusions.....	133
	References.....	133

TABLE OF CONTENTS

---

<b>Summary .....</b>	<b>137</b>
<b>Samenvatting .....</b>	<b>143</b>
<b>Acknowledgements .....</b>	<b>149</b>
<b>Curriculum vitae.....</b>	<b>155</b>
<b>List of publications .....</b>	<b>157</b>

TABLE OF CONTENTS

---

CHAPTER **1**

**Introduction**

---



## 1.1 Introduction to piezoelectricity and piezoelectric materials

Piezoelectricity was discovered by Jacques Curie and Pierre Curie as early as in 1880. Analogous to temperature change induced charges in pyroelectric crystals, they observed electrification under mechanical pressure of certain crystals, including tourmaline, quartz, topaz, cane sugar and Rochelle salt. This effect was distinguished from similar phenomena such as “contact electricity” (friction-generated static charge) [1]. In the direct piezoelectric effect, when these material are subjected to mechanical stress, this generates electric charge proportional to the applied stress. In contrast, piezoelectric materials can generate a mechanical strain when an electric field is applied to them. This is known as the inverse or converse piezoelectric effect. The phenomenon of piezoelectricity can be considered as a reversible process in which there exists a linear electromechanical coupling relation between the strain and electrical field. The phenomenon occurs in non-centro symmetric crystalline class of material [1, 2]. Piezoelectric materials form the backbone of several components utilized in communication systems, defence, industrial automation, medical diagnostics, and energy harvesting applications.

The equations of state relating the elastic and electric variables due to piezoelectric phenomenon can be represented by a pair of linear constitutive equations as follows [3]:

$$D = dT + \varepsilon^T E \quad \rightarrow \text{Direct Piezoelectric Effect} \quad (1.1)$$

$$S = s^E T + dE \quad \rightarrow \text{Inverse Piezoelectric Effect} \quad (1.2)$$

Where,

D is the dielectric displacement and S is the mechanical strain,  $s^E$  is the compliance for constant electric field E,  $\varepsilon^T$  is the permittivity under constant stress T. The superscripts T in  $\varepsilon^T$  and E in  $S^E$  denote the electrical and mechanical boundary conditions.

The important parameters for a piezoelectric material are [2]: the *Piezoelectric Charge Constant* ( $d$ ), the *Piezoelectric Voltage Constant* ( $g$ ) and the *Dielectric Constant* ( $\epsilon$ ).

The piezoelectric charge constant reflects the polarization generated per unit mechanical stress applied to a piezoelectric material (or) the mechanical strain experienced by a piezoelectric material per unit of electric field applied [4]. For zero mechanical stress ( $T=0$ , unloaded condition) it relates to the magnitude of induced strain  $S$  due to an electric field as shown in Eq. 1.3 [2] and can be expressed using two units – ( $C/N$ ) in case of direct effect and ( $m/V$ ) in case of inverse effect.

$$S = dE \quad (1.3)$$

The piezoelectric voltage constant is the electric field generated per unit applied stress by a piezoelectric material (or) the mechanical strain experienced by a piezoelectric material per unit electric displacement applied [3]. The values of  $g$  are expressed either in terms of  $V.m/N$  or  $m^2/N$ . At open circuit condition,  $\mathbf{D}=0$  the piezoelectric voltage coefficient relates the induced electric field  $E$  to an external stress  $T$  as well as piezoelectric charge coefficient to dielectric constant of the material as follows:

$$E = gT \quad (1.4)$$

$$g = \frac{d}{\epsilon_0 \epsilon_r} \quad (1.5)$$

The relative dielectric constant,  $\epsilon_r$ , commonly called the dielectric constant, is the ratio between the charge stored between a pair of electrode plates separated by a medium and the charge that can be stored under the same conditions by the same electrodes when separated by vacuum [5].

$$\epsilon_r = \frac{\epsilon}{\epsilon_0} \quad (1.6)$$

---

## 1.1 Introduction to piezoelectricity and piezoelectric materials

---

In polycrystalline ferroelectric ceramics the piezoelectric effects of individual domains will cancel each other out and thus the sintered piezoceramics do not possess any net piezoelectric property. Fortunately, these randomly oriented domains in piezoceramics can be aligned by the application of a strong electric field at elevated temperature, known as the poling process, by which a majority of the randomly oriented domains gets (more or less permanently) aligned in the direction of the applied field, resulting in a material having net polarisation [6, 7]. Piezoceramics have a high stability and high electromechanical coupling, can be machined into shape and are suitable for mass production [8]. The main types of commercial piezoceramics are based on barium titanate, lead zirconium titanate (PZT), lithium niobate and lithium tantalate [2]. PZT based ceramics are the most widely used materials and serve as the reference material in this field. In addition, a lot of research is devoted to the development of lead-free piezoceramics (apart from  $\text{LiNbO}_3$  and  $\text{LiTaO}_3$ ) to overcome the health and environmental hazards as a result of lead content in PZT based piezoceramics. However, there is no equivalent substitute for PZT; therefore, its use is still continued. This may be a temporary respite, but the legislation certainly impressed the researchers to develop alternative lead-free piezoelectric materials in order to replace lead-based materials.

The main drawback of PZT ceramic is their brittleness, which makes it difficult to process and shape into required forms. The maximum operating temperature of piezoelectric materials is dependent on their Curie temperature. As a rule of thumb the maximum operating temperature should not be higher than half of the Curie temperature [9]. In addition, the variation of the piezoelectric properties with temperature, pressure and frequency also limits the application of PZT ceramics, especially in high temperature applications such in nuclear reactors or jet engines. The other critical disadvantages of PZT piezoceramics are the lower voltage sensitivity ( $g_{33}$ ), the high density and the difficulty in fine tuning the acoustic impedance between the medium and the sensor itself, which restricts PZT ceramics from being used as a hydrophone material. Moreover, the high permittivity of PZT lowers its voltage coefficient values and also a smaller value for hydrostatic strain coefficient ( $d_h$ ), an important piezoelectric coefficient used to describe the charge generated from a

change in hydrostatic pressure [10]. Due to these reasons, the development of piezoelectric composites consisting of a polymer matrix containing PZT ceramics particles or fibers with reasonably good mechanical properties and an improved voltage sensitivity coefficient has become an important area of research. These composites possess a high voltage sensitivity, low acoustic impedance and moderate dielectric constant, along with a higher flexibility and a much improved shape freedom [11].

## 1.2 Piezoelectric composites

Very often, the technical specifications for electronic materials used in devices need combinations of desirable properties that often cannot be obtained in single phase materials. Sometimes, such intrinsic material imposed limitations can be overcome by combining two or more classes of materials in a single material product, i.e., by making a composite. In such composites, one of the material is responsible for providing one set of desirable properties, while the other material is responsible for providing another set of desirable (rather different) properties. Among these composites, the composites consisting of a polymer matrix containing piezoelectric particles or fibers are the focus of this study [12].

The piezocomposites are classified based on the 'Connectivity' between the individual phases. When a two-phase piezoelectric composite is considered, the connectivity of each phase is identified by two numbers. For example, if a phase is self-connected in all three directions (i.e. x, y and z directions), it is called '3' dimensional connectivity and if the other phase is connected only in the z-direction, then it has '1' dimensional connectivity [12] and hence the composite is designated as 1-3 composite. In general, a typical two phase piezoelectric composite can be classified into 10 types depending on the physical connectivity of each phase - 0-0, 0-1, 0-2, 0-3, 1-1, 1-2, 1-3, 2-2, 2-3 and 3-3 - with the first number denoting the connectivity of the

active phase (such as PZT) and the second number refers to the passive phase (in this case the polymer matrix) [12, 13]. A schematic representation of all possible connectivity types' of a two-phase piezoelectric composite material is shown in Figure 1.1.

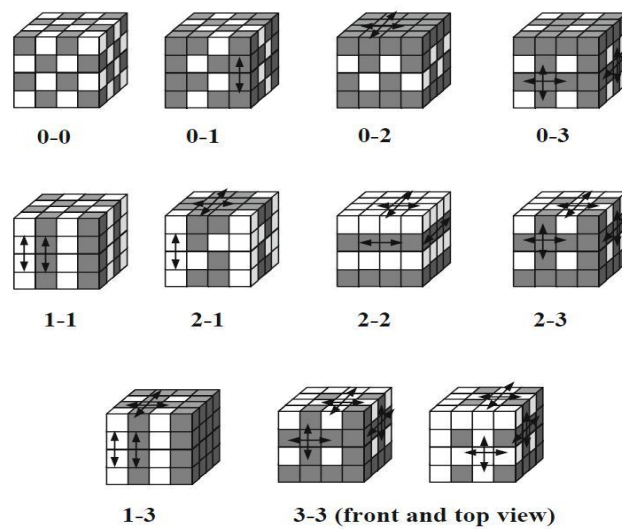


Figure 1.1: Schematic diagram of various types of piezocomposites based on different connectivity [12].

Among the various types of two-phase piezocomposites, 0-3 (the dilute granular approach) and 1-3 (the aligned fibrous approach) piezocomposites have received greater attention due to the simplicity in the processing of the former and relatively better piezoelectric properties of the latter. The reason for the relatively low piezoelectric properties of 0-3 type composite compared to 1-3 type is due to the random distribution of PZT particles in the polymer matrix of 0-3 type composites and the resulting deteriorating effect of the non-conductive polymer matrix separating the piezo active particles [12, 14]. Since in 1-3 composites, the active ceramic phase is fully connected from one electrode to the opposite electrode, these composites are being considered as direct replacements in the same applications as that of bulk ceramics. An ideal example for this replacement can be considered in the field of ultrasonic transducers, in which the lower permittivity of the polymer phase is used to

increase the sensitivity while at the same time the compliance of the polymer phase is used to reduce the lateral coupling [15].

Since 1980s, piezoelectric composites have been conceptualized, prototyped, fabricated and applied in lots of applications varying from medical imaging to military missions [16]. As far as aerospace engineering is considered, the piezoelectric composites can be used as a mean for in-situ damage detection of composite structures, a topic generally known as structural health monitoring. Piezoelectric elements, in particular 0-3 piezocomposites offer potential benefits as sensing elements for the structural health monitoring of composites structures due to their easy embedment within the advanced fiber composites together with their high voltage sensitivity and the ability to fine tune the mechanical impedance in order to make them comparable with the sensing medium. The ultrasonic Lamb waves send and received by the transducers made up of 0-3 piezocomposite can be used to detect large-area damage in composites [17]. In addition, piezocomposites patches can also be used as transducers for the purpose of structural health monitoring (SHM) using the same electromechanical impedance technique. This mode of damage detection approach can be used not only on aerospace components but also on a wide range of components varying from miniature precision machine to large civil structures [18].

Recently, there has been a continuous interest in high performance actuators suitable for control surfaces and active vibration control. The piezocomposites are seen as a solution to lightweight actuators for high performance smart structures such as control surface structures of aircraft, submarines and helicopter blades, which requires high specific force and displacement [19]. In addition, piezocomposites are seen as the preferred direction to actuate the trailing edges of the control surfaces of the biomimetic wing sections of small scaled unmanned aerial vehicles (UAVs) [20]. Piezoelectric composites have been identified as potentially interesting vibration controlling elements in space structures, which lack inertial grounding [21]. The voltage coefficient of different piezoelectric materials as a function of their Young's modulus is shown in Figure 1.2. Piezoelectric polymer films such as polyvinylidene

fluoride, PVDF and their various combinations are now relatively cheap and offer the possibility of developing transducers which would be inexpensive enough to be permanently attached to a structure. PVDF is being used in compression wave ultrasonic transducers for some years and has also been used in arrays. It has the advantage over piezo-electric ceramics of being flexible hence bonding it to curved structures does not cause engineering problems. Its internal damping is also higher than that of ceramics so the excitation of guided waves in the film is less likely to be a problem. However, such composites are less sensitive than ceramics and they cannot be used at high temperatures ( $>60$  °C) which may preclude its use in some structures [22]. Recently, with the advancement of mechatronics, an unprecedented demand for composites with adequate piezoelectric charge and voltage constants as well as good mechanical ductility has emerged for a variety of applications [23].

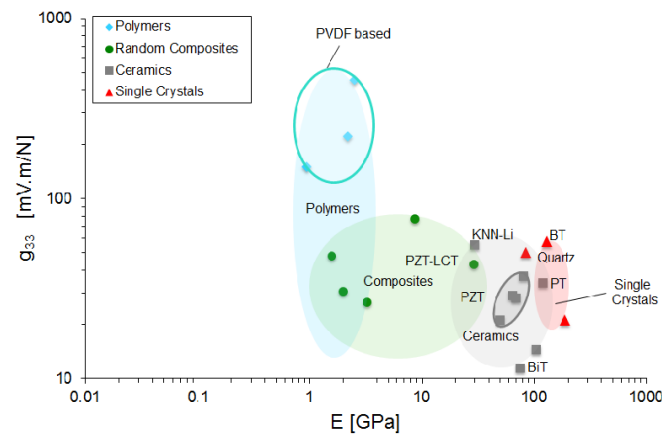


**Figure 1.2:** Piezoelectric voltage coefficient of various types of piezoelectric materials as a function of its Young's modulus.

The macroscopic piezoelectric properties of granular piezo ceramic-polymer composite are strongly dependent on the characteristics of the piezoceramic filler such as its composition, shape, volume fraction and its connectivity. The particle to particle connectivity of the piezo phase plays the crucial role on mechanical and the

final piezoelectric properties of the composites. Furthermore, the poling behavior of the piezoelectric ceramic phase in such composites is also very critical in determining the final microscopic properties of these composites. In this thesis, special focus has been devoted to develop new concepts to optimize piezoelectric composites while maintaining good mechanical properties and piezoelectric voltage sensitivity. In the development and screening of such concepts significant emphasis has been put on keeping the manufacturing technique as simple as possible, while at the same time making sure that the attractive and crucial properties of the piezo electric phase are optimally used by inducing a desired optimal topological alignment of the piezoelectric ceramic phase, different from that of a random distribution of a granular ceramic in a continuous polymer matrix.

For a long time the dominant piezoceramics has been based on lead zirconium titanate ( $\text{Pb}(\text{Zr}_{(1-x)}\text{Ti}_x)\text{O}_3$  or PZT). The increased usage of PZT releases more and more lead mainly in the form of either lead oxide or lead zirconium titanate into the environment. Hence, while the intrinsic properties of PZT ceramics, be it in granular or fibular form, are seen to offer the highest chance of being part of a successful piezoceramic-polymer composites, in this thesis new concepts are demonstrated to make use of environmentally friendly non-lead containing piezoceramic-polymer composites with a high load sensitivity [24].

### 1.3 Scope and outline of the thesis

The main objective of the thesis is to develop piezoelectric composite materials with good sensorial properties together with additional functionalities such as high mechanical flexibility, fatigue resistance and even self- healing properties. New sets of piezoelectric composites were developed based on the conventional PZT system and lead-free piezoelectric ceramics.

In chapter 2, the mechanical and piezoelectric properties of dielectrophoretically structured piezoelectric composites are investigated. Soft PZT ceramics are used as the filler material for the preparation of composites. The results

are compared with the corresponding unstructured 0–3 composites. The effect of poling voltage on the piezoelectric properties of the composites is also investigated. The mechanical properties of structured and 0–3 composites are analyzed using three-point bending tests.

In chapter 3, an ionomer is selected as the polymer matrix because of its high flexibility, good mechanical properties, good adhesion to the ceramic phase and self-healing additional functionality. The effective poling conditions for the PZT-Zn ionomer composites are investigated and the results are compared with the reference PZT-EMAA (ethylene methacrylic acid copolymer) composites and monolithic PZT ceramics. The static and high cycle fatigue properties of the composites are investigated to explore the potential of such composites for damage detection in tensile loaded composites.

The goal of chapter 4 is to further develop an approach to quantify the state of poling of the PZT granules embedded in a Zn-ionomer matrix using high energy synchrotron X-ray diffraction. The lattice strain and domain reorientation of the PZT particles are used as a tool to evaluate their poling state. The correlation between the poling induced structural changes and the macroscopic piezoelectric and dielectric properties is discussed.

In chapter 5, the piezoelectric and dielectric properties of the solid solution lead titanate – lead zirconate,  $\text{Pb}(\text{Zr}_x\text{Ti}_{1-x})\text{O}_3$ , ceramics and their 0-3 composites (using epoxy as the connecting polymer matrix) with  $x$  ranging from 0 to 0.8 are described. The possibility of exploring the use of compositions which are not in the morphotropic phase boundary, MPB, region in the phase diagram is investigated. Based on the results obtained, specific ceramic filler material selection criteria are proposed for piezoelectric ceramic-polymer composites in order to maximize the voltage sensitivity (i.e.  $g_{33}$ ) of the piezoelectric composites.

Based on the previous sections, in chapter 6, the production and properties of potassium sodium niobate (KNN) based lead-free piezoelectric composite are

described. The solid state calcination process is fine-tuned to obtain particles with a cubical morphology offering the potential of an improved alignment during dielectrophoretic processing. The structural, microstructural and piezoelectric properties are investigated and discussed in detail.

The main findings of the research as presented in this thesis are summarized towards the end of the thesis, in the Summary.

---

## References

- [1] B. Jaffe, W. Cook and H. Jaffe, "Piezoelectric Ceramics " *New York*, p. 115, 1971.
- [2] A. J. Moulson and J. M. Herbert, "Piezoelectric Ceramics," in *Electroceramics*, ed: John Wiley & Sons, Ltd, 2003, pp. 339-410.
- [3] J. Holterman and P. Groen, "*An Introduction to Piezoelectric Materials and Applications*", ed: Stichting Applied Piezo, 2013, pp. 19-66.
- [4] *Piezoelectric Ceramics: Principles and Applications* ed: APC International Ltd., 2011, pp. 13-33.
- [5] B. Jaffe, W. R. Cook Jr and H. Jaffe, "The Piezoelectric Effect in Ceramics," in *Piezoelectric Ceramics*, ed: Elsevier, 2012, pp. 7-22.
- [6] K. Uchino, "The Development of Piezoelectric Materials and the new Perspective," Woodhead Publishing, 2010.
- [7] J. Holterman and P. Groen, "Piezoelectric Materials," in *An Introduction to Piezoelectric Materials and Applications*, ed: Stichting Applied Piezo, 2013, pp. 67-102.
- [8] J. Li, R. Rogan, E. Üstündag and K. Bhattacharya, "Domain switching in polycrystalline ferroelectric ceramics," *Nature Materials*, vol. 4, pp. 776-781, 2005.
- [9] H. D. Stölting, E. Kallenbach and W. Amrhein, "Piezoelectric Drives," in *Handbook of fractional-horsepower drives*, ed: Springer, 2008, pp. 317-346.
- [10] A. Safari, G. Sa Gong, J. Giniewicz and R. E. Newnham, "Composite Piezoelectric Sensors," ed: Springer US, 1986, pp. 445-454.
- [11] J.G. Webster, "*The Measurement, Instrumentation, and Sensors, Handbook*," Springer, 1999.
- [12] R. E. Newnham, D. Skinner and L. E. Cross, "Connectivity and piezoelectric-pyroelectric composites," *Materials Research Bulletin*, vol. 13, pp. 525-536, 1978.
- [13] K. Uchino, "Piezoelectrci Composite Materials," in ed: Woodhead Publishing 2010, pp. 318-346.

- [14] D. A. van den Ende, "Structured Piezoelectric Composite: Materials and Applications," PhD, Aerospace Engineering, Technical University of Delft, 2012.
- [15] V. Y. Topolov and C. R. Bowen, "Effective Electromechanical Properties in Piezo-composites," *Electromechanical Properties in Composite Based on Ferroelectrics*, pp. 11-41, 2009.
- [16] E. K. Akdogan, M. Allahverdi and A. Safari, "Piezoelectric composites for sensor and actuator applications," *IEEE Transactions on Ultrasonics, Ferroelectrics and Frequency Control*, vol. 52, pp. 746-775, 2005.
- [17] R. Badcock and E. Birt, "The use of 0-3 piezocomposite embedded Lamb wave sensors for detection of damage in advanced fibre composites," *Smart Materials and Structures*, vol. 9, p. 291, 2000.
- [18] S. Bhalla and C. K. Soh, "Structural health monitoring by piezo-impedance transducers. I: Modeling," *Journal of Aerospace Engineering*, vol. 17, pp. 154-165, 2004.
- [19] K. J. Yoon S. Shin, H. C. Park and N. S. Goo, "Design and manufacture of a light weight piezo-composite curved actuator," *Smart Materials and Structures*, vol. 11, p. 163, 2002.
- [20] S. M. Lim, S. Lee, H. C. Park, K. J. Yoon and N. S. Goo, "Design and demonstration of a biomimetic wing section using a lightweight piezo-composite actuator (LIPCA)," *Smart Materials and Structures*, vol. 14, p. 496, 2005.
- [21] C. C. Won, J. L. Sulla, D. W. Sparks and W. K. Belvin, "Application of piezoelectric devices to vibration suppression," *Journal of guidance, control, and dynamics*, vol. 17, pp. 1333-1338, 1994.
- [22] T. Yamada, T. Ueda and T. Kitayama, "Ferroelectric-to-paraelectric phase transition of vinylidene fluoride-trifluoroethylene copolymer," *Journal of Applied Physics*, vol. 52, pp. 948-952, 1981.
- [23] E. K. Akdogan, M. Allahverdi and A. Safari, "Piezoelectric composites for sensor and actuator applications," *IEEE Transactions on Ultrasonics, Ferroelectrics and Frequency Control*, vol. 52, pp. 746-775, 2005.

---

## References

- [24] J. Rödel, W. Jo, K. T. Seifert, E. M. Anton, T. Granzow and D. Damjanovic, "Perspective on the Development of Lead-free Piezoceramics," *Journal of the American Ceramic Society*, vol. 92, pp. 1153-1177, 2009.



## CHAPTER 2

# **Piezoelectric and mechanical properties of structured PZT- epoxy composites**

---



## 2.1 Introduction

Piezoelectric ceramics exhibit excellent piezoelectric and dielectric properties, however their inherent properties, such as brittleness, non-ductility and poor shapeability limits their applications in areas such as vibration sensing, impact detection, structural health monitoring of wind turbines and fiber reinforced structures in aircrafts and energy harvesting [1-4]. In piezoelectric composite materials, the high piezoelectric and dielectric properties of PZT ceramics combined with the low density and the high flexibility of polymers [5] makes them suitable for aforementioned applications. Among these composites 0-3 and 1-3 type composites have received much attention. Because of random distribution of PZT particles in the polymer matrix, the 0-3 composites have relative low piezoelectric properties whereas in 1-3 composites the piezoelectric properties significantly improve [6-8]. The commonly used techniques to fabricate 1-3 composites like dice and fill, injection moulding, lost mould, tape casting, relic processing, laser or ultrasonic cutting are expensive and labour intensive, especially at low volume fractions and where a high degree of alignment is required for better voltage sensitivity [9-15].

It is demonstrated that dielectrophoresis can be used for structuring of PZT particles as columns in a polymer matrix, resulting in composites with quasi 1-3 connectivity [16-19]. This will keep the manufacturing process almost as simple as for 0-3 composites and consequently production costs can be kept low. In dielectrophoresis, when a moderate electric field is applied across a suspension of ferroelectric particles in an insulating medium, the particles orient themselves towards the direction of applied electric field. Under the optimum experimental parameters like electric field strength, frequency of the field, the particles attracts each other and bring together to form pearl chains parallel to the electric field direction.

The present chapter describes an investigation of piezoelectric and mechanical properties of structured soft PZT-epoxy composites prepared by dielectrophoresis. The results are compared with the corresponding unstructured 0-3 composites. The

effect of poling voltage on the piezoelectric properties of the composites is also investigated. The flexural properties of structured and 0-3 composites are analysed using three point bending tests.

## 2.2 Theory

Many analytical and numerical models have been proposed in literature for piezoelectric and dielectric properties of 0-3 and 1-3 piezoelectric composites by accounting the volume fractions of constituents, morphology, aspect ratio of the particles, polymer ceramic inter phase and particle to particle connectivity [16, 20-25]. Yamada et al. [20] proposed an analytical model in which the composite is treated as a spatially uniform distribution of equal sized ellipsoidal particles in an isotropic polymer matrix. The present experimental results of the 0-3 composites are compared with this model. The dielectric constant of the composite is given by Eq.2.1.

$$\varepsilon_c = \varepsilon_1 \left( 1 + \frac{n\varphi(\varepsilon_2 - \varepsilon_1)}{n\varepsilon_1 + (\varepsilon_2 - \varepsilon_1)(1 - \varphi)} \right) \quad (2.1)$$

where  $\varepsilon_c$  is the dielectric constant of the composite,  $\varepsilon_1$  and  $\varepsilon_2$  are that of the matrix and ceramic particles respectively,  $\varphi$  is the volume fraction of the ceramic and  $n$  is the inverse of the depolarization factor for an ellipsoidal particle in the direction of applied electric field. Bowen et al. [23] derived an expression for the dielectric constant of composites having particles aligned into chain like structures along a particular direction by considering the system as a collection of one dimensional chain of particles separated by polymer gaps. The expression is as follows,

$$\varepsilon_{DEP} = \varphi \left( \frac{R\varepsilon_1\varepsilon_2}{\varepsilon_2 + R\varepsilon_1} \right) + (1 - \varphi)\varepsilon_1 \quad (2.2)$$

$\varepsilon_{DEP}$  is the dielectric constant of dielectrophoretically structured 1-3 composites and  $R$  is the ratio of average particle size divided by the effective inter-particle distance.

Yamada's model for the piezoelectric charge constant in the poling direction of 0-3 composites yields

$$d_{33} = \frac{\varphi \alpha n \varepsilon_c d_{33_2}}{n \varepsilon_c + (\varepsilon_2 - \varepsilon_c)} \quad (2.3)$$

where  $\alpha$  is the poling ratio of the PZT particles and  $\varepsilon_c$  is the dielectric constant of the composite given by the Eq. 2.1. Van den Ende et al, [26] proposed an analytical equation for  $d_{33}$  of the structured composites by treating the particle - matrix stacking in the chains as two capacitors in series in the electrical domains and two springs in series in the mechanical domain. The resulting equation is given by Eq. 2.4.

$$d_{33_{DEP}} = \frac{(1+R)^2 \varepsilon_1 \varphi Y_{33_2} d_{33_2}}{(\varepsilon_2 + R \varepsilon_1)[(1+R\varphi)Y_{33_2} + (1-\varphi)RY_1]} \quad (2.4)$$

where  $Y_1$  and  $Y_{33_2}$  are elastic moduli of the polymer matrix and that of the ceramic in the direction of chains.

The flexural properties of the composites are determined according to the force - deflection curve of three point bending experiments. The flexural strength  $\sigma_f$  and modulus  $E_f$  are calculated according to the following equations,

$$\sigma_f = \frac{3P_f L}{2bh^2} \quad (2.5)$$

$$E_f = \frac{L^3 m}{4bd^3} \quad (2.6)$$

where  $P_f$  is the load at fracture,  $L$ ,  $b$  and  $h$  are distance between the supporting head, width and thickness of the sample respectively and  $m$  is the slope of the initial linear portion of the load deflection curve [27].

### 2.3 Experimental

The epoxy selected for present investigation, (Epotek 302-3M, Epoxy Technology Inc., Billerica, MA) is an optically clear two-component system. The resin, based on diglycidyl ether of bisphenol-A (DGEBA) (Figure 2.1(a)), is the prepolymer and the curing agent is based on the multi-functional aliphatic amine, poly (oxypropyl)-diamine (Figure 2.1(b)). As per the manufacturer's data sheet the system exhibit a viscosity of 0.8-1.6 Pa.s after mixing and at room temperature (25 °C). This relatively high viscosity of the matrix prevents quick settling of dense ceramic particles during dielectrophoresis. On the other hand the system has a low curing rate which make sure that the stage of low viscosity is sufficiently long to align the particles during dielectrophoresis [16, 19].

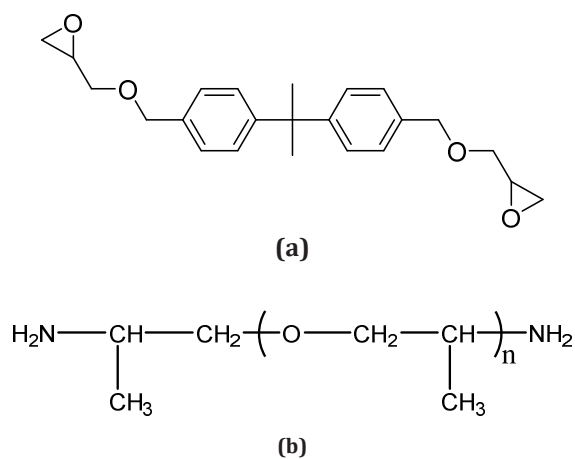


Figure 2.1: Chemical structure of (a) diglycidyl ether of bisphenol-A resin and (b) Poly (oxypropylene) diamine curing agent.

A donor-doped soft PZT powder (PZT507, Morgan Electro Ceramics, UK) is used for present study. This material is relatively easy to polarize and has a dielectric constant ( $\epsilon_{r33}$ ) of 4400, piezoelectric constant ( $d_{33}$ ) of 820 pC/N and a Curie temperature ( $T_c$ ) of 165 °C. In commercially available PZT powders, the compositional homogenization is completed only after the sintering, the process just before the final device fabrication. It has previously been reported that further calcination of commercial PZT powders improves the piezoelectric properties of the resulted composite [28, 29]. Hence it is decided to heat treat the as-received PZT 507 powder at 1200°C for 1 h in order to improve the crystal structure and compositional homogeneity. Further, to get rid of agglomeration of particles the calcined powder is ball milled with 5 mm zirconium balls for 48 hrs in cyclohexane. After ball milling the PZT powder is sieved using a 60  $\mu$ m mesh filter and the cyclohexane is evaporated at room temperature. The obtained PZT powder is heated at 150 °C for 1 h in order to remove absorbed moisture. The phase purity and compositional homogeneity is studied using a Bruker-AXS D5005 Diffractometer which uses  $\text{CuK}\alpha$  1 (0.15406 nm) X-rays.

The term dielectrophoresis (DEP) [15] stands for “the motion of suspension of particles relative to that of the solvent resulting from polarization forces produced by an inhomogeneous electric field”. It is different from the motion caused by the response to free charge on a body in an electric field (uniform or non-uniform). Under the influence of a non-uniform electric field polarises such that a negative charge is generated on the side nearer the positive electrode, and a positive one the side nearer to the negative electrode. Because the particle is neutral, the two charges on the body are in fact equal, but the fields operating on the two regions are unequal. This gives rise to a net force on the particle. The obvious result of such a polarization of a neutral body in a non-uniform field is to bring about a force impelling the particle toward the region of stronger field. But in the case of uniform field the neutral body will merely polarized. The result may produce a torque on the body but not a translational force, without which the body cannot move toward either of the electrode (Figure 2.2). The reported applications of DEP are directed toward areas such as biosensors, cell

therapeutics, drug discovery, medical diagnostics, micro-fluidics, nano-assembly and particle filtrations. The particles experience dielectrophoresis forces in a non-uniform electric field; the strength of the force depends on the medium and the particles electrical properties, shape, size as well as on the frequency, and amplitude of applied electric field.

The time averaged of dielectrophoretic force acting on a spherical particle of radius  $r$  is given by,

$$\langle f_{DEP} \rangle = 2\pi\epsilon_1' r^2 \text{Re}[K^*(\omega)] \nabla E^2 \quad (2.7)$$

where  $\epsilon_1'$  is the real part of the complex permittivity of the matrix and  $E$  is the applied electric field. The complex Clausius-Mossotti function  $K^*(\omega)$  is a function of complex dielectric and conductivities of both ceramic particles and the polymer matrix. A particle will be either attracted or repelled from a region of strong electric field intensity, depending on whether  $K^*(\omega) > 0$  (permittivity of ceramic is greater than the matrix) or  $K^*(\omega) < 0$  (permittivity of ceramic is less than that of the polymer matrix).

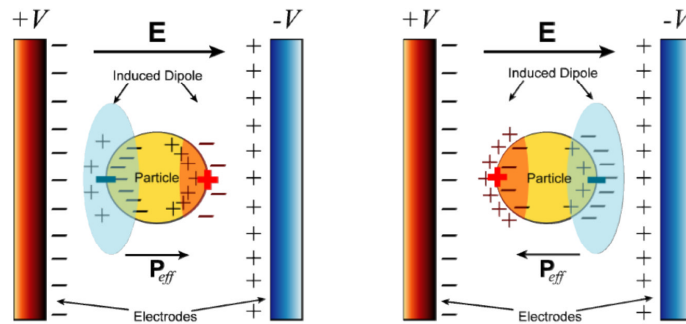


Figure 2.2: Electric field and polarization of a ferroelectric particle during dielectrophoresis [30].

The structured PZT- polymer composites were prepared by applying an alternating voltage with a frequency 1-4 kHz at 1 kV/mm across the suspension of ceramic particles in the epoxy matrix during the entire curing stage, although particle displacement only took place during the early stages of curing when the viscosity of the matrix polymer was still low. A schematic representation of different steps involved in the dielectrophoresis process for making structured PZT-epoxy composites has shown in Figure 2.3. The voltage was kept over the sample until the epoxy was cured. The completely cross linked circular disc shaped samples of dimension 16 mm x 0.5 mm were fine polished on both sides and post cured at 100 °C for 1h. Cross sections of the structured and 0-3 composites were analyzed using a JEOL JSM-7500F scanning electron micrograph.

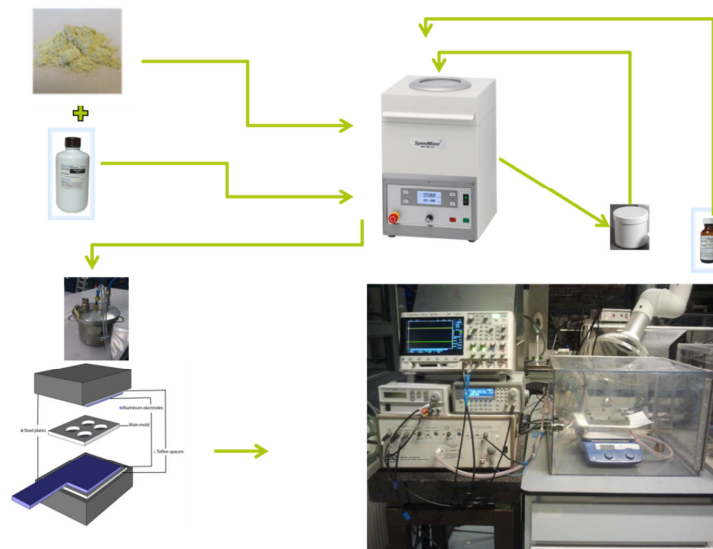


Figure 2.3: Schematic of the experimental set up used to align the PZT particles in epoxy resin using dielectrophoresis.

Four test samples were electroded on both sides by gold sputtering for electrical property measurements. The composite samples were then poled in an organic oil (rap seed oil) at 100 °C by keeping the field (10-17 kV/mm) for one hour, afterwards it was cooled down to room temperature while maintaining the poling field. The dielectric constant of the composites were measured using parallel plate capacitor method using an Agilent 4263B LCR meter at 1V and 1 kHz. The  $d_{33}$  of the composites were measured using a KCF technologies PM3001  $d_{33}$  meter.

Mechanical properties of the composites were determined in a three point bending test set up using ZwickRoell 20 kN tensile bench with 1kN load cell and a cross head speed of 0.5 mm/min at ambient temperature. Rectangular specimens with dimensions 10 mm x 5 mm x 2mm were tested and an average of four specimens of each composition was reported.

## 2.4 Results and discussion

X-ray diffraction was used to identify the phases present in the powder. The diffraction pattern could be indexed with a reference pattern for PZT (ICDD: 33-0784). PZT solid solution exhibit enhanced piezoelectric properties at the morphotropic phase boundary where tetragonal and rhombohedral phases coexist [31]. From the XRD pattern (Figure 2.4), it is clear that the present PZT powder indeed exhibits diffraction peaks belonging to the rhombohedral phase (200) and to the tetragonal phases (002), (200) together. The effect of calcination temperature on the piezoelectric properties of PZT5A4 powder was previously investigated and it has been reported that further calcinations of commercially available PZT powder improves the compositional homogeneity and thereby the piezoelectric properties [28]. From Figure 2.4 it is clear that the crystallinity of the powder calcined at 1200 °C is higher than that of the as-received PZT powder which will lead to better piezoelectric properties.

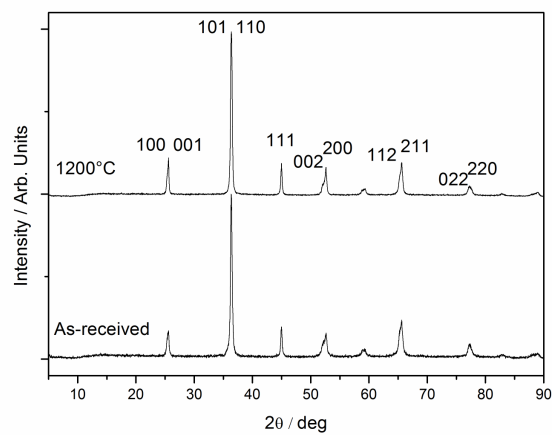
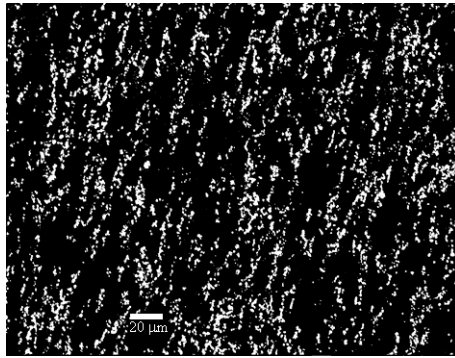
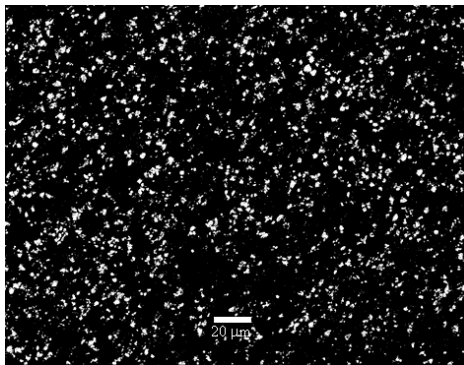


Figure 2.4: X-ray diffraction pattern of as received PZT powder and calcined at 1200°C.

Figure 2.5 shows the Scanning Electron Microscopy image of a 10 vol.% PZT composite of a dielectrophoretically structured quasi 1-3 composite (Figure 2.5(a)) and a 0-3 (Figure 2.5(b)) composite. It is evident from the micrograph that during dielectrophoresis PZT particles are oriented and do form short columns of particles along the electric field direction. The average particle size distribution of PZT powder is calculated using the software package ImageJ and was found to be around 0.5-2  $\mu\text{m}$  range [32].



(a)



(b)

Figure 2.5: Scanning Electron Micrographs of dielectrophoretically structured (a) and 0-3 (b) PZT-epoxy composites.

The piezoelectric properties of the composites depend on the poling state of the active PZT phase, as well as on the degree of connectivity of the PZT particles in the direction of the field lines. Figure 2.6 shows the variation of piezoelectric charge coefficient,  $d_{33}$ , of structured composites as a function of different poling fields for various volume fractions of PZT. The poling temperature and duration were fixed at 100 °C and 1 h for all the experiments. It can be seen that the  $d_{33}$  value increases with the poling field and saturation is obtained at a field of 15 kV/mm. Lee et al., investigated the effect of poling voltage and time on the piezoelectric properties of 70 volume percentage loaded  $\text{PbTiO}_3$  epoxy composites and they observed saturation of piezoelectric properties at a poling field of 8 kV/mm for a poling duration of 20 seconds [33].

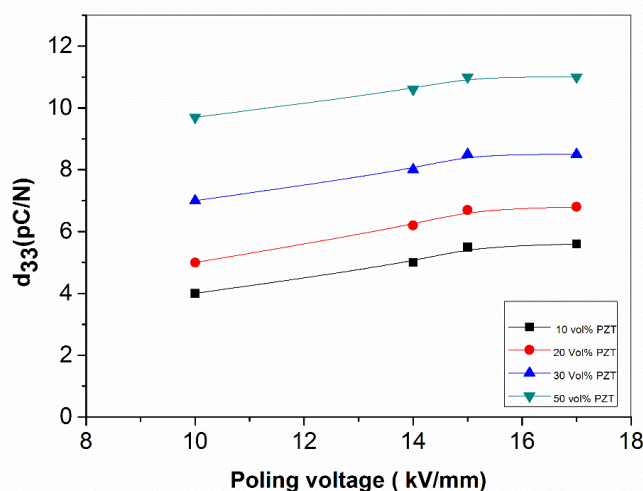
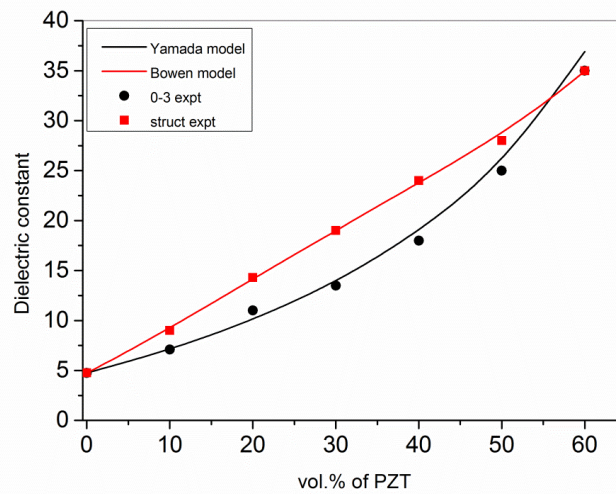


Figure 2.6: Effect of poling field on  $d_{33}$  of structured composites for different vol. % of PZT in epoxy matrix .

The effect of PZT particles volume fraction on the dielectric constant of the structured and unstructured composites is shown in Figure 2.7. The structured composites exhibit higher dielectric constants than those of the unaligned composites. During the dielectrophoresis process the PZT particles are redistributed to form fibrils

in the electric field direction and hence the properties are also enhanced in that direction. The experimental dielectric constants of the structured and randomly distributed ceramic polymer composites are compared with the models proposed by Bowen et al. and Yamada respectively (Eqs. 2.2 and 2.1).



**Figure 2.7:** Variations of dielectric constant of the composite compared with theoretical models as a function of PZT vol.% of in epoxy matrix.

It is to be noted that the experimental dielectric constants of the 0-3 composites match very well with the values predicted by Yamada's model for a shape parameter  $n = 4.56$ . Bowen et al. model treats the system as a one-dimensional chain of ceramic particles separated by polymer and the resulted expression for the structured composites is given by Eq. 2.2. The experimental dielectric constants of the structured composites are substituted in the Bowen's model and an interparticle distance in the range of  $0.40 \mu\text{m}$  is calculated. This is in the same range as the interparticle distances measured from SEM images using Image J software [32] of which the calculated distribution over fifty particle pairs is shown in Figure 2.8.

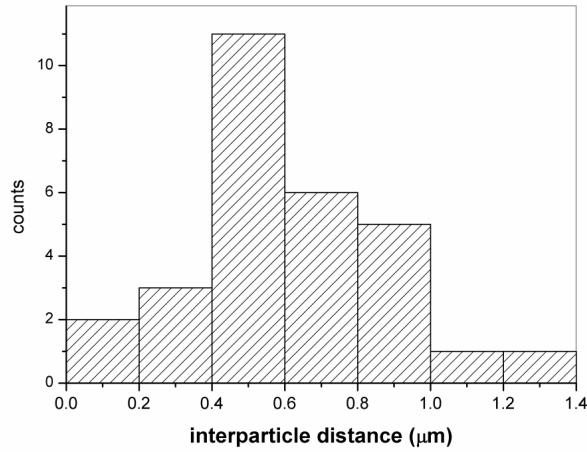


Figure 2.8: Inter particle distance from SEM micrograph of 10 vol. % filled structured composites.

In Figure 2.9, the experimentally observed  $d_{33}$  values of both structured and 0-3 composites are compared with Yamada's model [20] and the model proposed by Van den Ende et al., [16] (Eqs. 2.3 & 2.4) respectively. From the Figure it is clear that the structuring of PZT particles significantly improves the  $d_{33}$  values especially at lower PZT volume fractions. The inter particle distance was also calculated from Eq. 2.4 by fitting the experimental  $d_{33}$  values and it is found to be  $0.40 \mu\text{m}$ , in good agreement with the value obtained from the dielectric constants data.

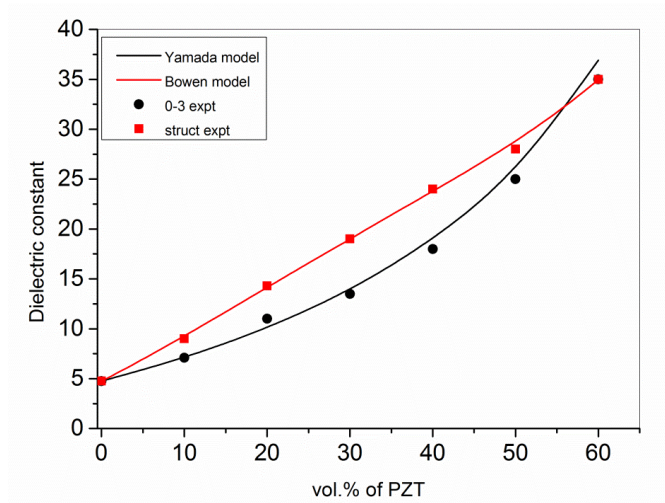


Figure 2.9: Variation of  $d_{33}$  of structured and 0-3 composites compared with theoretical models as a function of vol. % of PZT in epoxy matrix.

The piezoelectric voltage coefficient,  $g_{33}$  is defined as the ratio of  $d_{33}$  and  $\epsilon_{33}$ ;  $g_{33} = d_{33}/\epsilon_{33}$ . The change of  $g_{33}$  of the composites as a function of PZT volume fractions is depicted in Figure 2.10. The structured composites with 10 vol. % of PZT exhibit highest voltage coefficient value. For these composites, the increase in  $d_{33}$  is more rapid than the increase in dielectric constant especially at lower volume fractions. Therefore, the voltage coefficient of these composites exhibits a maximum at a low volume fraction.

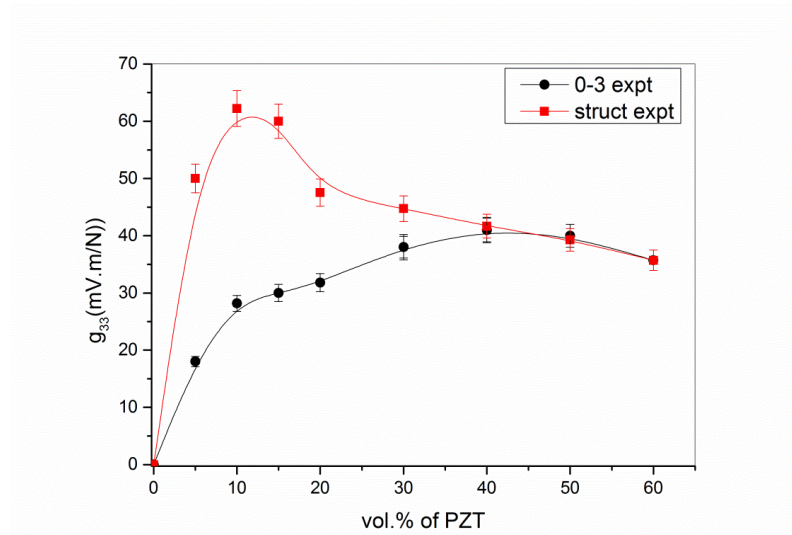


Figure 2.10: Variation of  $g_{33}$  of structured and 0-3 composites compared with theoretical models as a function of vol.% of PZT in epoxy matrix.

The flexural strengths and flexural moduli of structured quasi 1-3 composites and 0-3 composites are presented in Figure 2.11. From this figure it is clear that the flexural strength of the composite decreases with increasing amount of PZT loading in the polymer matrix for both structured and non-structured composite. It is mainly attributed to the fact that as the PZT content increases the ability of matrix to deform plasticity is reduced. Rashid et al. reported same kind of behaviour in alumina – epoxy composites for 0-3 composites [34]. The flexural modulus of the composite [Figure 2.11(b)] increases with increasing PZT content in the polymer matrix. This is mainly due to the higher stiffness of the PZT particles which contributes to the higher flexural modulus. Moreover structured composites exhibit higher flexural modulus than 0-3 composites. The PZT columns formed during the dielectrophoresis may restrict the mobility of polymer chains which increases the flexural modulus of the structured composites.

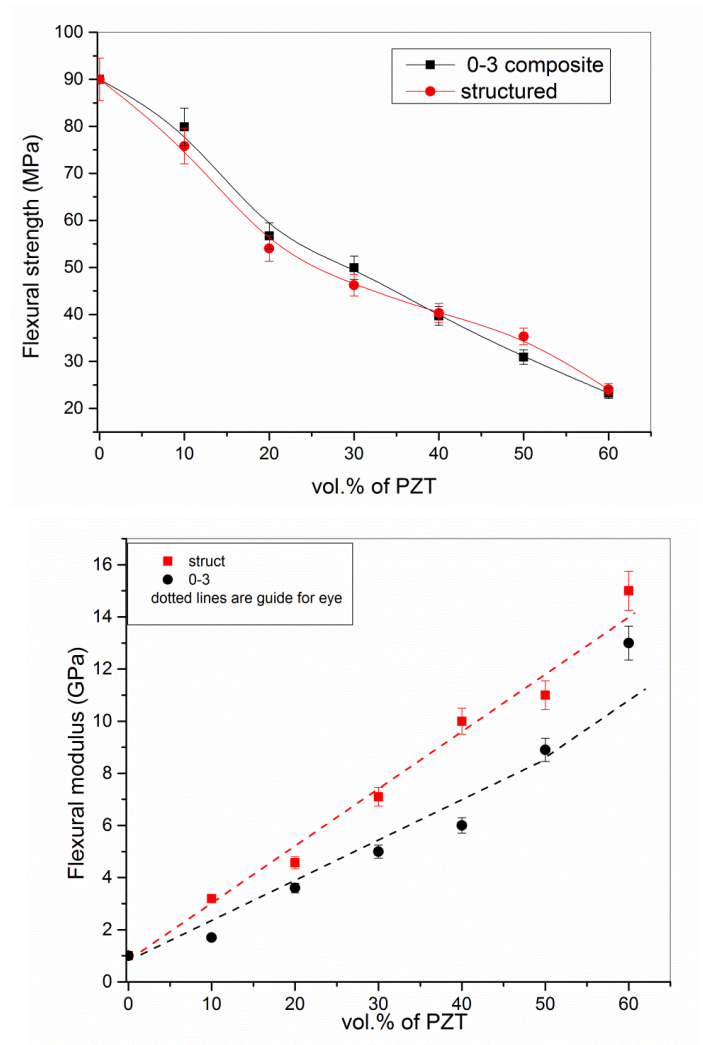


Figure 2.11: Variation of (a) flexural strength and (b) flexural modulus of structured and 0-3 composites as a function of PZT vol. %.

## 2.5 Conclusions

Structured (and reference random) PZT- epoxy composites were fabricated using dielectrophoresis. Piezoelectric and dielectric constants of the structured composites were found to be higher than those of the unstructured composites. The experimentally observed piezoelectric and dielectric constants of structured and 0-3 composites were well described by existing theoretical models. The structuring of PZT particles in the composite has been analyzed using scanning electron microscopy. The most attractive finding in this research is the high value of the piezoelectric voltage sensitivity at low fractions ( $\sim 10$  vol. %) leads to an attractive combination of high sensitivity, high flexibility and a lower density. Investigations of mechanical properties revealed that structuring of PZT particles increases the bending modulus of the composite compared to 0-3 composites whereas the flexural strength of the composite did not change much with structuring.

## References

- [1] T. R. Gururaja, W. A. Schulze, L. E. Cross, R. E. Newnham, B. A. Auld and Y. J. Wang, "Piezoelectric composite materials for ultrasonic transducer applications, Resonant modes of vibration of PZT rod polymer composites," *IEEE Transactions on Sonics and Ultrasonics*, vol. 32, pp. 481-498, 1985.
- [2] E. K. Akdogan, M. Allahverdi and A. Safari, "Piezoelectric composites for sensor and actuator applications," *IEEE Transactions on Ultrasonics Ferroelectrics and Frequency Control*, vol. 52, pp. 746-775, 2005.
- [3] R. E. Newnham, L. Bowen, K. Klicker and L. E. Cross, "Composite piezoelectric transducers," *Materials and Design*, vol. 2, pp. 93-106, 1980.
- [4] R. E. Newnham, D. P. Skinner and L. E. Cross, "Connectivity and piezoelectric-pyroelectric composites," *Materials Research Bulletin*, vol. 13, pp. 525-536, 1978.
- [5] T. F. McNulty, V. F. Janas, A. Safari, R. L. Loh and R. B. Cass, "Novel processing of 1-3-piezoelectric ceramic/polymer composites for transducer

- applications," *Journal of the American Ceramic Society*, vol. 78, pp. 2913-2916, 1995.
- [6] H. Taunaumang, I. L. Guy and H. L. W. Chan, "Electromechanical properties of 1-3 piezoelectric ceramic piezoelectric polymer composites," *Journal of Applied Physics*, vol. 76, pp. 484-489, 1994.
- [7] R. K. Panda, V. F. Janas and A. Safari, "Fabrication and properties of fine scale 1-3 piezocomposites by modified lost mold method," in *Applications of Ferroelectrics, ISAF '96., Proceedings of the Tenth IEEE International Symposium*, 1996, pp. 551-554.
- [8] C. J. Dias and D. K. DasGupta, "Inorganic ceramic/polymer ferroelectric composite electrets," *IEEE Transactions on Dielectrics and Electrical Insulation*, vol. 3, pp. 706-734, 1996.
- [9] K. A. Klicker, J. V. Biggers and R. E. Newnham, "Composites of pzt and epoxy for hydrostatic transducer applications," *Journal of the American Ceramic Society*, vol. 64, pp. 5-9, 1981.
- [10] S. Ayter, J. P. Mohr III and J. W. Sliwa Jr, "Method for making piezoelectric composites," US Patent:US5239736 A, 1993.
- [11] U. Bast, D. Cramer, H. Kaarmann, K. Lubitz, M. Vogt and W. Wersing, "Composite ultrasound transducer and method for manufacturing a structured component therefor of piezoelectric ceramic," ed: US Patent:US5164920 A, 1992.
- [12] S. S. Livneh, V. F. Janas and A. Safari, "Development of fine-scale PZT ceramic fiber/polymer shell composite transducers," *Journal of the American Ceramic Society*, vol. 78, pp. 1900-1906, 1995.
- [13] A. Safari, M. Allahverdi and E. K. Akdogan, "Solid freeform fabrication of piezoelectric sensors and actuators," *Journal of Materials Science*, vol. 41, pp. 177-198, 2006.
- [14] V. F. Janas and A. Safari, "Overview of Fine-Scale Piezoelectric Ceramic/Polymer Composite Processing," *Journal of the American Ceramic Society*, vol. 78, pp. 2945-2955, 1995.

- [15] C. P. Bowen, T. R. Shrout, R. E. Newnham and C. A. Randall, "Tunable electric-field processing of composite-materials," *Journal of Intelligent Material Systems and Structures*, vol. 6, pp. 159-168, 1995.
- [16] D. A. van den Ende, B. F. Bory, W. A. Groen and S. van der Zwaag, "Improving the  $d_{33}$  and  $g_{33}$  properties of 0-3 piezoelectric composites by dielectrophoresis," *Journal of Applied Physics*, vol. 107, pp. 024107,1-8, 2010.
- [17] C. Randall, D. Miller, J. Adair and A. Bhalla, "Processing of electroceramic-polymer composites using the electrorheological effect," *Journal of materials Research*, vol. 8, pp. 899-904, 1993.
- [18] S. A. Wilson, G. M. Maistros and R. W. Whatmore, "Structure modification of 0-3 piezoelectric ceramic/polymer composites through dielectrophoresis," *Journal of Physics D-Applied Physics*, vol. 38, pp. 175-182, 2005.
- [19] C. Park and R. E. Robertson, "Aligned microstructure of some particulate polymer composites obtained with an electric field," *Journal of Materials Science*, vol. 33, pp. 3541-3553, 1998.
- [20] T. Yamada, T. Ueda and T. Kitayama, "Piezoelectricity of a high-content lead zirconate titanate/polymer composite," *Journal of Applied Physics*, vol. 53, pp. 4328-4332, 1982.
- [21] T. Furukawa, K. Fujino and E. Fukada, "Electromechanical properties in composites of epoxy-resin and PZT ceramics," *Japanese Journal of Applied Physics*, vol. 15, pp. 2119-2129, 1976.
- [22] T. Furukawa, K. Ishida and E. Fukada, "Piezoelectric properties in the composite systems of polymers and PZT ceramics," *Journal of Applied Physics*, vol. 50, pp. 4904-4912, 1979.
- [23] C. P. Bowen, R. E. Newnham and C. A. Randall, "Dielectric properties of dielectrophoretically assembled particulate-polymer composites," *Journal of Materials Research*, vol. 13, pp. 205-210, 1998.
- [24] T. Zakri, J. P. Laurent and M. Vauclin, "Theoretical evidence for Lichtenecker's mixture formulae' based on the effective medium theory," *Journal of Physics D: Applied Physics*, vol. 31, p. 1589, 1998.
- [25] K. Lichtenecker, "Dielectric constant of natural and synthetic mixtures," *Phys. Z*, vol. 27, p. 115, 1926.

- [26] D. A. van den Ende, "Structured Piezoelectric Composite: Materials and Applications," PhD, Aerospace Engineering, Technical University of Delft, 2012.
- [27] N. E. Dowling, *Mechanical behavior of materials: engineering methods for deformation, fracture, and fatigue*: Prentice hall, 1993.
- [28] D. A. van den Ende, P. de Almeida and S. van der Zwaag, "Piezoelectric and mechanical properties of novel composites of PZT and a liquid crystalline thermosetting resin," *Journal of Materials Science*, vol. 42, pp. 6417-6425, 2007.
- [29] I. Babu, D. A. van den Ende and G. de With, "Processing and characterization of piezoelectric 0-3 PZT/LCT/PA composites," *Journal of Physics D: Applied Physics*, vol. 43, p. 425402, 2010.
- [30] T. B. Jones, *Electromechanics of particles*: Cambridge University Press, 2005.
- [31] B. V. Hiremath, A. I. Kingon, and J. V. Biggers, "Reaction sequence in the formation of lead zirconate-lead titanate solid-solution - role of raw-materials," *Journal of the American Ceramic Society*, vol. 66, pp. 790-793, 1983.
- [32] W. Rasband, "ImageJ, US National Institutes of Health," *Bethesda, Maryland, USA*, vol. 2012, 1997.
- [33] M. H. Lee, A. Halliyal and R. E. Newnham, "Poling of coprecipitated lead titanate-epoxy 0-3 piezoelectric composites," *Journal of the American Ceramic Society*, vol. 72, pp. 986-990, 1989.
- [34] E. S. A. Rashid, H. M. Akil, K. Ariffin and C. C. Kooi, "The mechanical and thermal properties of alumina filled epoxy," *Journal of Reinforced Plastics and Composites*, vol. 00, 2008, pp. 282-287.

## CHAPTER 3

### **Piezoelectric and mechanical properties of fatigue resistant, self- healing PZT-ionomer composites**

---



### 3.1 Introduction

Lead zirconium titanate (PZT) ceramics have good piezoelectric and pyroelectric properties and are widely used in transducers, actuators and sensors. However, their poor mechanical properties, limited freedom in creating sensors with complex curved surfaces and the acoustic impedance mismatch between ceramics and transmitting media limit their use in many applications [1-6]. Moreover, piezoelectric ceramics have a relatively low hydrostatic piezoelectric coefficient and piezoelectric voltage coefficient ( $g_{33}$ ) because of their negative  $d_{31}$  and high dielectric constant respectively. In order to overcome the aforementioned limitations, piezoelectric composite materials were developed in which piezoelectric ceramic particles are embedded in a polymeric matrix. These composites bring together the required properties such as a high piezoelectric voltage constant, a low acoustic impedance and mechanical flexibility [7, 8].

The mechanical and electrical properties of the composite materials can be tailored by the selection of the constituents, the volume fractions of constituent phases and the way in which the individual phases are connected. Newnham et al. described ten possible connectivity patterns between particles in diphasic composite systems [3]. The inter particle connectivity has a large influence on the final electrical and mechanical properties of such composites. Composites with 0-3 connectivity are obtained by distributing the ceramic particles in a polymer matrix in such a way that the particles are not in contact with one another while the polymer phase is connected in all three dimensions. The 0-3 composites are considered to be the least complicated in terms of manufacturing and ease of molding in complex, predesigned shapes. Although there have been many reports about piezoelectric-polymer composites with 0-3 connectivity, only a handful of investigations have been carried out on the effect of poling conditions on the piezoelectric properties of the composites for polymer matrices with different electrical conductivities [9-15].

In the present chapter an ionomer has been selected as the polymer matrix because of its high flexibility, good mechanical properties, excellent adhesion to the ceramic phase and self-healing potential [16, 17]. The effective poling conditions for PZT-Zn ionomer composites were investigated and the results were compared with

the reference PZT-EMAA (ethylene methacrylic acid copolymer) composites and PZT ceramics. The experimentally observed dielectric and piezoelectric coefficient are compared with Yamada's model [18]. Furthermore, to investigate the suitability of potential applications of such composites, the tensile properties and high cycle fatigue behaviour of the composites for large strain levels has been studied. Finally, for the first time ever it is demonstrated that for a well-chosen self-healing polymer matrix the loss of sensorial functionality of the composites after high cyclic tensile fatigue can be partially recovered by thermal healing.

### 3.2 Theory

One of the major factors influencing the macroscopic piezoelectric properties of a polymer-piezoelectric ceramic composite is the degree of poling of the ceramic phase. A fine grained piezoelectric particle in a polymeric matrix requires high poling fields to achieve sufficient poling efficiency. The electric field  $E_1$  acting on an isolated spherical grain in a polymer matrix is given by Eq. 3.1.

$$E_1 = \frac{3\varepsilon_p}{\varepsilon_c + 3\varepsilon_p} E_0 \quad (3.1)$$

where  $\varepsilon_c$  and  $\varepsilon_p$  are the dielectric constants of the spherical piezoelectric grains and polymer matrix respectively, and  $E_0$  is the applied electric field [12]. The effective electric field experienced by the ceramic phase is generally low due to the low dielectric constant of the polymer phase. While applying a DC poling electric field to the sample for a time longer than the sample relaxation time, the field distribution is also controlled by  $\sigma_p/\sigma_c$ , the ratio of the electrical conductivity of the polymer to that of the ceramics. During the poling process, the mobility of charges in the polymer matrix plays an important role. It has been theoretically shown that the poling time should be sufficiently longer than the relaxation time  $\tau$ , which is defined as [19]:

$$\tau = \frac{\phi 3\varepsilon_p + (1-\phi)(\varepsilon_c + 2\varepsilon_p)}{\phi 3\sigma_p + (1-\phi)(\sigma_c + 2\sigma_p)} \quad (3.2)$$

where  $\phi$  is the volume fraction of the ceramic. The poling process can be accelerated and optimized by using a polymer matrix with high electrical conductivity and piezoelectric ceramic particles with a low dielectric constant. Different approaches have been taken to increase the poling efficiency, for example the use of piezoelectrically active polymers, the use of various conductive additives such as carbon black or graphite and the use of functionalized PZT ceramics by a silane coupling agent to enhance the binding between PZT and the polymer matrix [13, 19-21].

Yamada et al., proposed a model to predict the piezoelectric charge constant and dielectric constant of a composite by assuming a perfect degree of poling of individual ellipsoidal piezoelectric particles which are dispersed in a continuous low dielectric polymer matrix [18]. The final equations are given below.

$$\varepsilon = \varepsilon_p \left( 1 + \frac{n\phi(\varepsilon_c - \varepsilon_p)}{n\varepsilon_p + (\varepsilon_c - \varepsilon_p)(1-\phi)} \right) \quad (3.3)$$

$$d_{33} = \phi \frac{n\varepsilon}{(n\varepsilon + (\varepsilon_c - \varepsilon))} d_{33c} \quad (3.4)$$

where  $n$  is a parameter reflecting the aspect ratio of the ferroelectric particle and  $d_{33}$  and  $d_{33c}$  are the piezoelectric charge constant of the composite and ceramic phase respectively [19]. The piezoelectric voltage constant of the composite,  $g_{33}$ , can be calculated according to the following equation:

$$g_{33} = \frac{d_{33}}{\epsilon_0 \epsilon} \quad (3.5)$$

where  $d_{33}$  is the piezoelectric charge constant in  $\text{pC}\cdot\text{N}^{-1}$  and  $\epsilon_0$  is the permittivity of vacuum.

### 3.3 Experimental

The piezoelectric ceramic powder used for manufacturing the composites was a soft doped  $\text{Pb}(\text{Zr,Ti})\text{O}_3$  (PZT507) (Morgan Electroceramics, Ruabon, UK). In order to improve its piezoelectric properties the as-received powder was calcined at  $1200^\circ\text{C}$  for 2h in a closed alumina crucible in a Nabertherm furnace with a heating rate of 5 K/min. The calcined powder was ball milled using yttria stabilized zirconia balls of 5 mm diameter in cyclohexane for 4 hrs. Subsequently, the powder was dried at  $150^\circ\text{C}$  and stored in a closed container to avoid moisture absorption. The average particle size ( $d_{50}$ ) of the milled powder is  $4.26\ \mu\text{m}$  as measured by laser scattering with a Horiba LA950. The particle size measured with SEM is about 3-5  $\mu\text{m}$ , which is in good agreement particle size measured by laser scattering. The phase purity and compositional homogeneity are studied by X-ray powder diffraction using a Bruker-AXS D5005 diffractometer [11, 15]. The calcined powder crystallizes in a perovskite structure with the coexistence of rhombohedral and tetragonal phases.

Zn based ionomer (Surlyn 9320 DuPont) and ethylene methacrylic acid (EMAA) copolymer were used as the polymer matrix materials. In EMMA based ionomers, the ethylene methacrylic acid copolymer (see Figure 3.1(a)) is neutralized such that a certain percentage of metallic cations such as zinc (Zn), sodium (Na) or lithium (Li) are retained along the polymer back bone (Figure 3.1(b)) [16]. Self-healing behavior of ionomers has been well reported [16, 17, 22], in which the self-healing phenomena was either initiated by high energy impact or a puncture test, such as bullet penetration or by more controlled quasi-static penetration experiments [23] or by mild thermal treatments and looking at the healing of surface scratches [24]. As shown elsewhere [17], the Zn based ionomers show the highest degree of self-healing (i.e. the

ability to close cracks or other local mechanical damage upon application of a modest temperature well below the melting point of the polymer). An additional desirable characteristic of the ionomeric polymer is the relaxation of the ionic species at elevated temperatures which increases the electrical conductivity significantly, which should be beneficial to the poling efficiency.

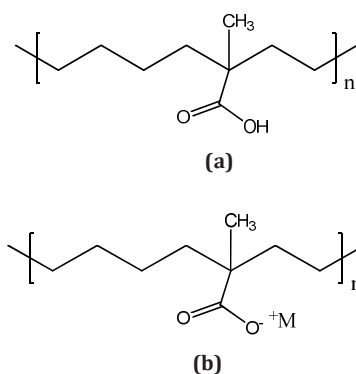


Figure 3.1: Molecular structure of (a) EMAA (b) Zn ionomer.

The composites were prepared by mixing a defined ratio of polymeric matrix and PZT powder in a lab-scale counter rotating twin screw extruder (DSM Xplore Research Netherlands). The processing temperature was kept at 170 °C for both the PZT-Zn ionomer and the PZT-EMAA composites. The rotating force was set to 4.5 kN. In order to get a homogeneous distribution of PZT ceramic particles in the polymer matrix, the residence time was forest to 5 minutes, which ensured multiple passes of the material through the mixing section of the extruder. The composites were finally extruded through a 2 mm diameter outlet. In order to get planar sheets of composites, the extruded wire-shaped materials were hot pressed at temperature of 150 °C with a pressure of 1 MPa for 5 minutes, yielding flexible planar sheets with a thickness of about 1 mm. Gold electrodes on the samples were made by sputtering. The samples

were poled in an organic oil (rape seed oil) bath under different poling conditions (electric field strength, temperature and time). The dielectric constants of the composites were measured using the parallel plate capacitor method using an Agilent 4263B LCR meter at 1V AC signal and 1 kHz. The  $d_{33}$  of the composites was measured using a Berlincourt type  $d_{33}$  meter (KCF technology PM3001). The static tensile properties of the composite at room temperature were investigated using a ZwickRoell 20 kN tensile bench with a 1 kN load cell and a cross-head speed of 0.5 mm/min. Rectangular specimens with dimensions 50 x 5 x 1 mm were tested. The average values over four samples are reported. Fatigue tests were conducted at room temperature on an MTS 831 Elastomer test system. Rectangular specimens with dimensions 50 x 5 x 1 mm were prepared and within these samples two circular regions were metalized and poled at 15 kVmm<sup>-1</sup> prior to the fatigue test. The  $d_{33}$  values of both the as produced composites and cyclically loaded composites were measured. The specimens were fatigue tested under different strain levels, by properly selecting the stress ratio defined as the ratio of the minimum stress to the maximum stress. The shape of the loading waveform was sinusoidal and the employed frequency was restricted to 1 Hz to avoid sample heating.

Finally, to measure the functional healing, the degraded tensile fatigue loaded composites were stepwise annealed at 70 °C in a conventional circulating hot air oven while the piezoelectric properties at room temperature were measured at appropriate intervals.

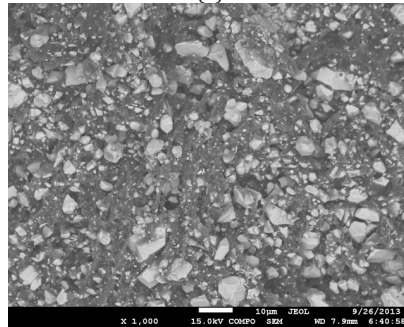
## 3.4 Results and discussion

### 3.4.1 Microstructure

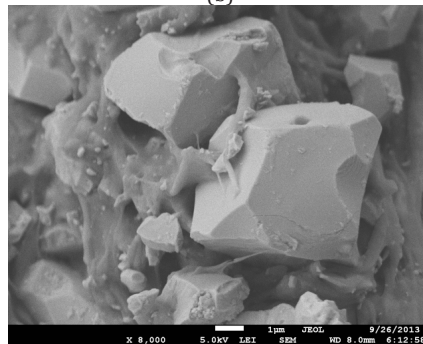
The as-produced composites are in the form of opaque whitish flexible sheets of about 1 mm thickness. An SEM micrograph of the cross-sectional view of a 30% volume percent filled PZT-Zn ionomer composite is shown in Figure 3.2(a). The micrograph confirms as shown in Figure 3.2(b) that fully dense PZT-Zn ionomer composites with a spatially uniform distribution of the PZT particles were created. The PZT particles are well distributed, show limited agglomeration (hence a 0-3 configuration) and adhere well to the polymer matrix which is a key requirement for optimal piezoelectric and mechanical properties. A higher magnification SEM micrograph showing the primary particles inside the composite is given in Figure 3.2(c).



(a)



(b)



(c)

Figure 3.2: (a) Macro photograph of 30 vol.% PZT filled ionomer composite (b) SEM micrograph of cross-sectional view of 30 vol.% filled PZT-Zn ionomer composite (c) SEM micrograph showing the primary particles.

### 3.4.2 Poling behaviour

The effect of poling temperature on the  $d_{33}$  of 30 volume percent filled PZT-Zn ionomer and PZT-EMAA composites is shown in Figure 3.3 for a poling field of  $15 \text{ kV}\cdot\text{mm}^{-1}$  and a time of 60 min. The results are also compared with those for bulk PZT sintered ceramics. It is evident that for the PZT-polymer composites the poling temperature has a marked effect on the  $d_{33}$ , especially around 50-80 °C, whereas the  $d_{33}$  of the bulk PZT ceramics remains more or less constant. The dielectric breakdown of the composites prevents higher poling temperatures being applied. It is clear that PZT-Zn ionomer composites show significantly better piezoelectric properties than the corresponding PZT-EMAA composites. The increase of  $d_{33}$  with poling temperature observed for the PZT-Zn ionomer composite can be attributed to the relaxation of the ion clusters of the polymer chain at elevated temperatures which increases the electrical conductivity of the polymer matrix, which in turn increases the effective electric field experienced by the ceramic phase. This promotes an easier polarization of the ceramic phase in the ionomer matrix. The temperature at which the poling efficiency increases sharply (between 50 and 60 °C) is in agreement with the de-clustering temperature of this ionomer [16, 17].

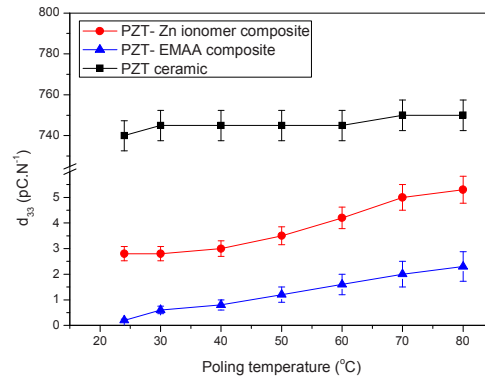


Figure 3. 3: Variation of the piezoelectric charge coefficient ( $d_{33}$ ) as a function of poling temperature with an electric field of  $15 \text{ kV}\cdot\text{mm}^{-1}$  for 1 h.

The effect of poling time on the  $d_{33}$  of 30 volume percent filled PZT-Zn ionomer and PZT-EMAA composites is shown in Figure 3.4 for a poling field of  $15 \text{ kV}\cdot\text{mm}^{-1}$  and at a poling temperature of  $60^\circ\text{C}$ . It is clear that the  $d_{33}$  of the composites increases considerably with poling time during the first 60 min and reaches a stable value thereafter. This increase and subsequent saturation is attributed to two separate effects. In a polymer-ceramic composite the effective electric field experienced by the ceramic phase is controlled by the electrical conductivity and dielectric constants of both the polymer and the ceramic phase. The effective electric field is always much lower than the actual applied electric field [22, 25]. This results in a longer poling time requirement for composites as compared to bulk PZT ceramics. In addition to this, while the reversal of  $180^\circ$  ferroelectric domains takes place mainly at the initial stage of poling,  $90^\circ$  domain rotation is accompanied by local stress and strain which requires a longer amount of time. Therefore, the degree of poling in composites can be improved by increasing the poling time, but after a poling time exceeding 60 min the composite  $d_{33}$  reaches its maximum value indicating the reorientation of ferroelectric domains to be near to completion. It is observed that the  $d_{33}$  of the PZT-Zn ionomer composites increases more rapidly than the PZT-EMAA composites which again can be attributed to the Zn ion cluster relaxation and the higher dielectric constant of the ionomer polymer matrix.

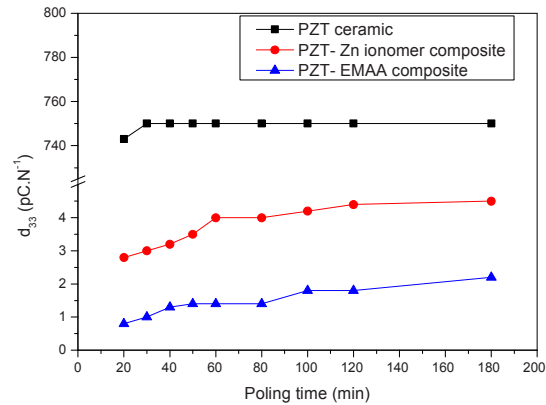


Figure 3.4: Variation of the piezoelectric charge coefficient as a function of poling time with an electric field of  $15 \text{ kV}\cdot\text{mm}^{-1}$  and poling temperature of  $60^\circ\text{C}$ .

The dependence of the piezoelectric charge coefficient on the poling electric field is shown in Figure 3.5 for a poling temperature of 60 °C and a time of 60 min. As expected, the piezoelectric charge coefficient of the composites increases with the poling field for both PZT-Zn ionomer and PZT-EMAA composites and reaches a constant level at about 17 kV.mm<sup>-1</sup>. In PZT ceramics, the maximum is already observed at 4 kV.mm<sup>-1</sup>. The poling field is the driving force for the reversal of domains. The higher the field, the faster and more complete the reorientation of the domains in the direction of the poling field. In a 0-3 polymer-ceramic composite, a large part of the applied electric field during poling is obscured by the polymer phase. According to eq. 1, the effective electric field experienced by the ceramic phase is of the order of 1.7-28 V.mm<sup>-1</sup> for the range of applied electric fields of 1-15 kV.mm<sup>-1</sup>. Hence, a polymer-ceramic composite requires a high electric field for effective poling of the piezoelectric phase. From these results, the optimum poling conditions for the described composites are observed to be an electric field of 17 kV.mm<sup>-1</sup> applied at a temperature of 60 °C for 60 min.

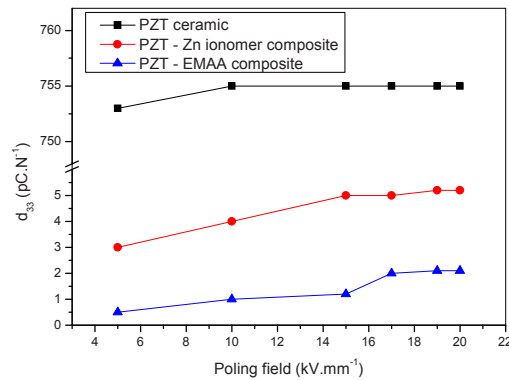


Figure 3.5: Variation of the piezoelectric charge coefficient ( $d_{33}$ ) as a function of poling field.

Figure 3.6 (a) and (b) compare the variation of the dielectric constant and loss tangent of 30 vol.% PZT-EMAA and PZT-ionomer composites as a function of frequency and temperature. It is seen that in all cases the dielectric constant shows nearly a frequency independent behavior even though a small decrease is observed in

the low frequency region. The loss tangent spectrum is characterized by a peak appearing in the low frequency region of PZT-ionomer composites especially at a temperature of 60 °C. The strength and frequency of relaxation depend on characteristic property of molecular and dipolar relaxation [26]. In PZT-ionomer composites, the relaxation and mobility of ionic clusters is evident by the peak shifting towards higher frequency side, thereby reducing the relaxation time. The relatively high mobility at higher temperatures enhances the transport properties which increases the loss tangent of PZT-ionomer composites at higher temperatures.

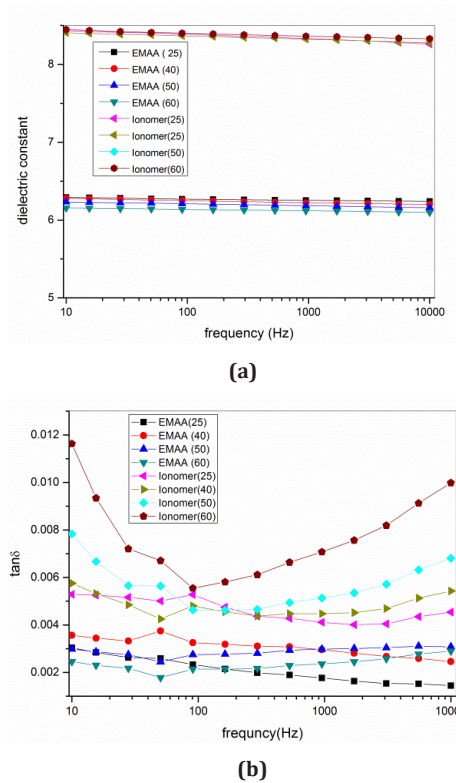
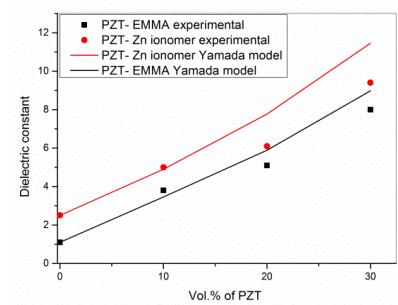


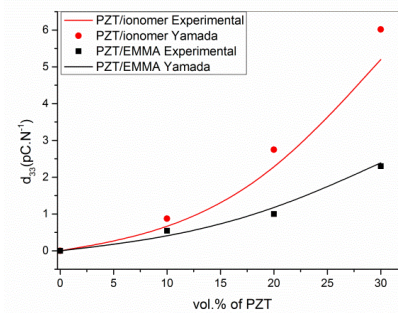
Figure 3.6: (a) The dielectric constant and (b) loss tangent of 30 vol.% PZT-EMAA and PZT-ionomer composites as a function of frequency and temperature ( the number inside brackets in the legend indicates the temperature in °C ).

### 3.4.3 Piezoelectric and dielectric properties

In Figure 3.7 the measured dielectric constant and piezoelectric charge coefficient of the composites are compared to the values predicted using Yamada's model. This model predicts that these properties mainly depend on the volume fraction of PZT and the aspect ratio of the particles. The dielectric constant and piezoelectric charge coefficient increases significantly with increasing PZT volume fraction. The theoretically predicted values match well with the experimentally observed data for the composites. The  $d_{33}$  and dielectric constant of the composite follow the same trend as reported for other 0-3 hot pressed composites [8, 11, 18].



(a)



(b)

Figure 3.7: (a) The dielectric constant and (b) piezoelectric charge coefficient of the composites as a function of PZT volume percentage.

The variation of piezoelectric voltage coefficient of the composites as a function of PZT volume fraction is shown in Figure 3.8. The piezoelectric voltage coefficient of ionomer-PZT composites increases with increasing PZT volume fraction in the composite. A maximum value for  $g_{33}$  of  $52 \text{ mV.m.N}^{-1}$  is obtained for a 30% volume fraction of PZT-Zn ionomer composite. Compared to the ionomer-based composites, the voltage coefficient of EMAA-PZT composites increases linearly up to 20% volume percent of PZT and reaches a maximum the plateau at around  $18 \text{ mV.m.N}^{-1}$ . The voltage sensitivity obtained for the PZT-Zn ionomer composites is reasonably good compared to other 0-3 composites [15, 26, 27].

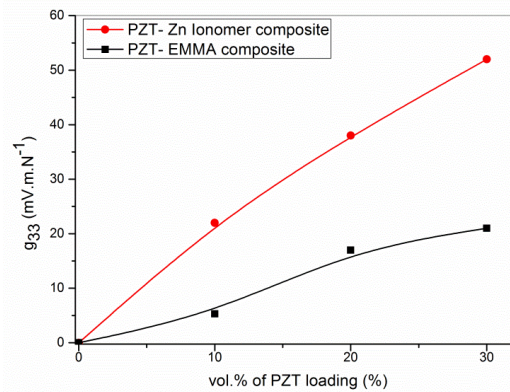


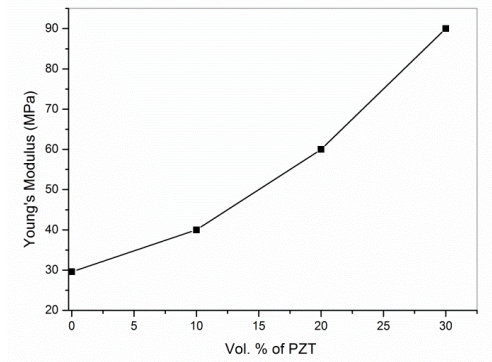
Figure 3. 8: Variation of piezoelectric voltage coefficient  $g_{33}$  of the composites as a function of PZT volume percentage.

#### 3.4.4 Mechanical properties

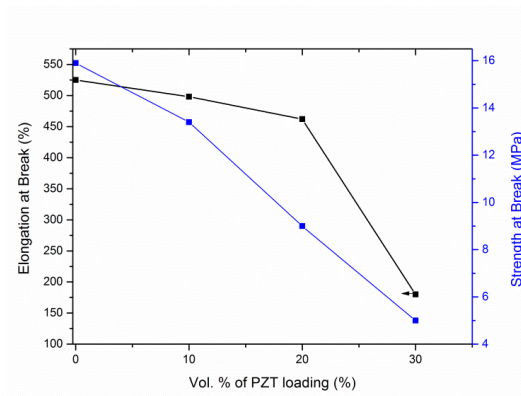
The results described above indicate that 30 vol.% PZT filled ionomer composites attain a reasonably good voltage coefficient at the optimized poling conditions. Hence, the static and dynamic mechanical properties of such composites were studied in more detail.

### **Tensile properties**

Changes in Young's modulus, elongation and strength at break as a function of PZT loading are shown in Figures 3.9(a) and (b). The results indicate that as the PZT filler loading content increases, the Young's modulus of the composite increases which is a common trend for any 0-3 polymer -ceramic composites. The 30 vol.% filled PZT-Zn ionomer composite exhibits a relatively low Young's modulus of 90 MPa, a tensile strength of 5 MPa and an elongation at break of 150%. Few 0-3 composites have been reported with a comparable low modulus and good piezoelectric voltage coefficient [11, 25]. It has been reported that the filler particle size, morphology, volume fraction and adhesion between the particles and polymer can have a detrimental effect on the mechanical properties of the composite [28]. The good adhesion between PZT ceramic particles and the ionomer matrix leads to high strength and elongation at break. Both tensile strength and elongation at break of the composite decreases as the PZT filler loading increases in the polymer matrix, which is a normal behavior for any polymer ceramic composite.



(a)



(b)

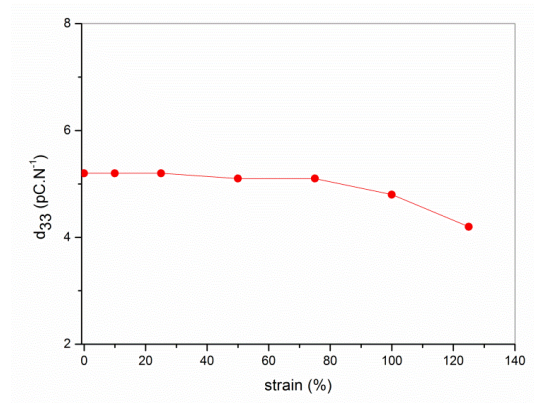
Figure 3.9: Variation of (a) Young's modulus (b) elongation and strength at break as a function of PZT volume percentage in a Zn ionomer based composite.

#### Fatigue lifetime

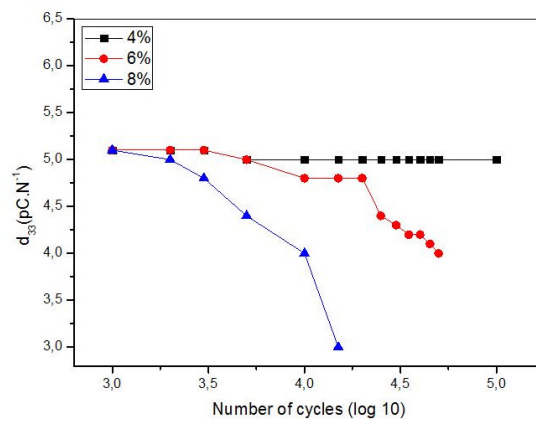
The effect of single and cyclic tensile loading to specific strain values on the piezoelectric properties of the 30 vol.% filled PZT-Zn ionomer composite is shown in Figure 3.10(a) and (b) respectively. It is clear that a significant degradation of piezoelectric properties only occurs upon straining the composites above 80%. Just before failure, at 125% of elongation, the  $d_{33}$  value has decreased with 20% as

compared to the initial  $d_{33}$  value for the un-stressed composites. Figure 3.10(b) shows that no degradation of piezoelectric properties is observed for strain levels of 4% up to  $10^5$  cycles. At higher strain levels, a decrease of piezoelectric properties is observed. The  $d_{33}$  of the PZT-Zn ionomer composites was measured to be  $5.2 \text{ pC.N}^{-1}$  before the fatigue test, and it dropped by 57% after  $10^3$  cycles for a strain of 8%.

At higher strain levels, and larger number of cycles a decrease in sensorial properties is observed. It is most likely that such a drop in  $d_{33}$  is caused by delamination between PZT particles and the polymer matrix as there are no intrinsic changes in the properties of the constituent phases are to be expected at room temperature testing. The de-bonding is evident from SEM micrographs [Figure 3.12(a)] of the cross-sectional view of the PZT-Zn ionomer composite.



(a)



(b)

Figure 3.10: Piezoelectric charge coefficient of the 30 vol.% filled PZT-Zn ionomer composite (a) after strain the composite at different % (b) after cyclic loading.

### 3.4.5 Self-healing properties

The piezoelectric charge coefficient recovery of the degraded composites which endured tensile cyclic loading at 6 and 8% strain levels for 50,000 and 15,000 cycles, upon annealing at 70 °C is shown in Figure 3.11 as function of healing time.

The results indicate that the 6% strain level fatigued composites recovered their properties much faster than the composites strained at 8%. This is due to the fact that fewer and smaller voids are formed in the composites strained at 6% than at 8%, which in turn will also require a shorter time to be healed. A high magnification SEM micrograph as shown in Figure 3.12 (b) of the composites healed at 70 °C for 1 hour reveals that the debonded interfaces areas indeed are healed, contributing to the recovery of the piezoelectric properties. The fact that the  $d_{33}$  properties were not fully restored to their original properties suggest that for the loading condition explored the healing was imperfect and not all interphases were reformed.

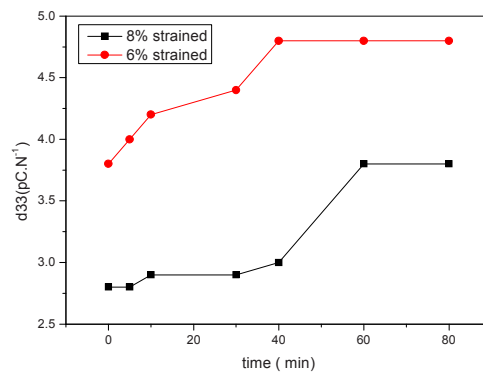
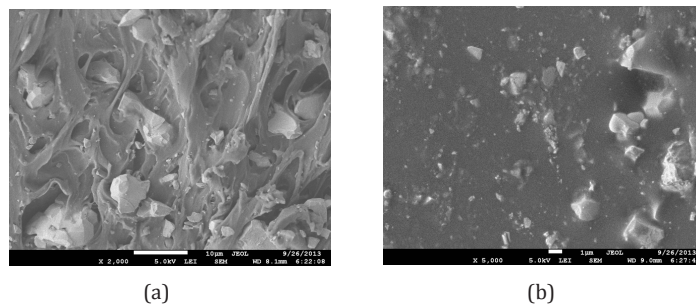


Figure 3.11: Self-healing of the PZT- Zn ionomer composite piezoelectric charge coefficient at 70 °C.



(a)

(b)

Figure 3.12: SEM micrographs of 8% strained and fatigued PZT- Zn ionomer composite (a) before and (b) after healing.

### 3.5 Conclusion

A highly flexible PZT-Zn ionomer piezoelectric composite has been developed which can be used for sensor or transducer applications in high strain applications. The manufacturing process of such composites is straightforward and can be easily up-scaled. At optimized poling conditions, the 30 vol.% filled PZT-Zn ionomer composites exhibit a  $d_{33}$  and  $g_{33}$  of 5.2 pC.N<sup>-1</sup> and 52 mV.m.N<sup>-1</sup> respectively. The measured dielectric and piezoelectric properties are in good agreement with theoretical models. The tensile fatigue loading has shown that PZT-Zn ionomer composites exhibit minimal degradation in performance at lower strain levels and with 4% strain PZT-Zn ionomer composites has a useful life of more than 10<sup>5</sup> cycles. The self-healing experiments demonstrated that, the degraded piezoelectric properties after high strain tensile cyclic loading, can be recovered to significant degrees due to the thermal healing capability of Zn based ionomer matrix.

### References

- [1] B. Jaffe, W. Cook and H. Jaffe, "Piezoelectric Ceramics Academic," *New York*, p. 115, 1971.
- [2] T. R. Gururaja, "Piezoelectrics for medical ultrasonic-imaging," *American Ceramic Society Bulletin*, vol. 73, pp. 50-55, 1994.
- [3] R. E. Newnham, D. Skinner and L. E. Cross, "Connectivity and piezoelectric-pyroelectric composites," *Materials Research Bulletin*, vol. 13, pp. 525-536, 1978.
- [4] E. Fukada, "History and recent progress in piezoelectric polymers," *IEEE Transactions on Ultrasonics Ferroelectrics and Frequency Control*, vol. 47, pp. 1277-1290, 2000.
- [5] X. Qiu, "Patterned piezo-, pyro-, and ferroelectricity of poled polymer electrets," *Journal of Applied Physics*, vol. 108, pp. 011101,1-19, 2010.
- [6] T. Furukawa, K. Ishida and E. Fukada, "Piezoelectric properties in the composite systems of polymers and PZT ceramics," *Journal of Applied Physics*, vol. 50, pp. 4904-4912, 1979.

- [7] C. J. Dias and D. K. Das Gupta, "Inorganic ceramic/polymer ferroelectric composite electrets," *IEEE Transactions on Dielectrics and Electrical Insulation*, vol. 3, pp. 706-734, 1996.
- [8] E. Venkatragavaraj, B. Satish, P. R. Vinod and M. S. Vijaya, "Piezoelectric properties of ferroelectric PZT-polymer composites," *Journal of Physics D-Applied Physics*, vol. 34, pp. 487-492, 2001.
- [9] K. H. Lam and H. L. W. Chan, "Piezoelectric and pyroelectric properties of 65PMN-35PT/P(VDF-TrFE) 0-3 composites," *Composites Science and Technology*, vol. 65, pp. 1107-1111, 2005.
- [10] M. Wegener and K. Arlt, "PZT/P(VDF-HFP) 0-3 composites as solvent-cast thin films: preparation, structure and piezoelectric properties," *Journal of Physics D-Applied Physics*, vol. 41, 2008.
- [11] D. A. van den Ende, W. A. Groen and S. van der Zwaag, "The effect of calcining temperature on the properties of 0-3 piezoelectric composites of PZT and a liquid crystalline thermosetting polymer," *Journal of Electroceramics*, vol. 27, pp. 13-19, 2011.
- [12] G. Sa Gong, A. Safari, S. Jang and R. E. Newnham, "Poling flexible piezoelectric composites," *Ferroelectrics Letters Section*, vol. 5, pp. 131-142, 1986.
- [13] S. T. Lau, K. W. Kwok, F. G. Shin and S. Kopf, "A poling study of lead zirconate titanate/polyurethane 0-3 composites," *Journal of Applied Physics*, vol. 102, pp. 200-205, 2007.
- [14] M. Lee, A. Halliyal and R. E. Newnham, "Poling studies of piezoelectric composites prepared by coprecipitated PbTiO<sub>3</sub> powder," *Ferroelectrics*, vol. 87, pp. 71-80, 1988.
- [15] N. K. James, D. A. van den Ende, U. Lafont, S. van der Zwaag and W. A. Groen, "Piezoelectric and mechanical properties of structured PZT-epoxy composites," *Journal of Materials Research*, vol. 28, pp. 635-641, 2013.
- [16] R. Rees and D. Vaughan, "Physical structure of ionomers," *Polymer preprints. American Chemical Society. Division of Polymer Chemistry*, vol. 6, p. 287, 1965.
- [17] K. Tadano, E. Hirasawa, H. Yamamoto and S. Yano, "Order-disorder transition of ionic clusters in ionomers," *Macromolecules*, vol. 22, pp. 226-233, 1989.

- [18] T. Yamada, T. Ueda and T. Kitayama, "Piezoelectricity of a high-content lead zirconate titanate/polymer composite," *Journal of Applied Physics*, vol. 53, pp. 4328-4332, 1982.
- [19] C. K. Wong, Y. W. Wong and F. G. Shin, "Effect of interfacial charge on polarization switching of lead zirconate titanate particles in lead zirconate titanate/polyurethane composites," *Journal of Applied Physics*, vol. 92, pp. 3974-3978, 2002.
- [20] W. K. Sakamoto, E. D. Souza and D. K. Das-Gupta, "Electroactive properties of flexible piezoelectric composites," *Materials Research*, vol. 4, pp. 201-204, 2001.
- [21] J. F. Capsal, E. Dantras, L. Laffont, J. Dandurand and C. Lacabanne, "Nano texture influence of BaTiO<sub>3</sub> particles on piezoelectric behaviour of PA 11/BaTiO<sub>3</sub> nanocomposites," *Journal of Non-Crystalline Solids*, vol. 356, pp. 629-634, 2010.
- [22] J. Mendiola, C. Alemany, B. Jiménez and E. Maurer, "Poling of (Pb, La)(Zr, Ti) O<sub>3</sub> ferroelectric composite," *Journal of Materials Science Letters*, vol. 4, pp. 1383-1386, 1985.
- [23] R. J. Varley and S. van der Zwaag, "Autonomous damage initiated healing in a thermo-responsive ionomer," *Polymer International*, vol. 59, pp. 1031-1038, 2010.
- [24] S. van der Zwaag, "*Self-healing materials: an alternative approach to 20 centuries of materials science*," Springer Science and Business Media BV, 2008.
- [25] M. C. Chure, P. C. Chen, L. Wu, B. H. Chen and K. K. Wu, "Influence of Poling Conditions on the Characteristics of PZT Ceramics." vol. 284, pp. 1375-1380, 2011.
- [26] K. Uchino, "Piezoelectric Composites," *Comprehensive Composite Materials*, vol. 5, ed: Elsevier Science Ltd., 2000, pp. 523-532.
- [27] I. H. Tavman, "Thermal and mechanical properties of aluminum powder-filled high-density polyethylene composites," *Journal of Applied Polymer Science*, vol. 62, pp. 2161-2167, 1996.

---

## References

- [28] F. Kremer and A. Schönhals, *Broadband dielectric spectroscopy*: Springer, 2003.



## CHAPTER 4

### **Analysis of the state of poling in granular PZT-polymer composites by High Energy Synchrotron X-ray diffraction**

---



## 4.1 Introduction

Lead zirconium titanate (PZT) ceramics exhibit a high piezoelectric charge constant ( $d_{33}$ ), making them a suitable choice for actuators, but their high dielectric permittivity drastically reduces the voltage sensitivity for force sensing applications [1, 2]. On the other hand, piezoelectric polymers exhibit a high sensitivity ( $g_{33}$ ) but a much poorer actuator performance and this contrast in properties led to the development of piezoelectric composites, in which a piezoelectric ceramic material either in a granular or fibrous form is embedded in a polymeric matrix. This hybrid nature leads amongst others, to a lower density and the freedom to fine tune the acoustic impedance of transducers made out of such composites. As for piezoceramics, piezoelectric composites need to be poled by applying a high dc electric field during a late stage of the manufacturing process. However, poling of such composites, in particular for the case of the piezoceramic particles all being surrounded by the continuous polymer matrix the so called 0-3 composites [3], is difficult since a large part of the externally applied electric field may be shielded by the polymer matrix having a low dielectric constant and a low electrical conductivity. As a result, very large electric fields are required to pole the ceramic fraction [4]. Such large electric fields often cause dielectric breakdown of the composites. In addition, the presence of local weak points, such as pinholes or bubbles, short-circuits the electrodes and prevents thorough poling [5].

In chapter 3, the attractive properties of PZT-ionomer composites, which include a good value for the load sensitivity,  $g_{33}$ , a high flexibility, good mechanical strength, excellent ceramic-polymer adhesion and a self-healing functionality were reported [6]. The piezoelectric properties of ceramic-polymer composites depend on the poling state of the active PZT phase, as well as the dielectric properties of both phases and the type of connectivity present. The optimum poling conditions for soft PZT-ionomer composites were analysed by systematically studying the piezoelectric properties after poling under various conditions. In that work, it was shown that the piezoelectric properties saturate at longer poling times, higher electric fields and elevated poling temperatures suggesting that the PZT phase is then relatively well

poled. However, the actual state of poling of the particles in such composites has never been measured or compared to the state of poling in the fully dense ceramic reference state.

The electromechanical response in ferroelectric materials is comprised of both intrinsic (piezoelectric lattice strain) and extrinsic (domain wall motion) components. The non-180° domain switching and lattice strain that occurs during poling under an electric field above the coercive field can be determined from the changes in crystal structure as measured by X-ray diffraction as has been reported in detail for bulk ceramics [7]. However, using conventional X-ray diffraction studies on bulk ceramics provide information only for the near-surface [8]. Guo et al. reported that the penetration depth in their study was in the region of 2  $\mu\text{m}$ , for an X-ray wavelength of 0.8  $\text{\AA}$ . The problems associated with studying the near surface region can be overcome by exploiting the intensity and penetration of high energy synchrotron X-rays, which is very much needed to probe the change in crystal structure of PZT particles in a polymer matrix due to poling [9].

The goal of this investigation is to further develop an approach to quantify the poling state of the PZT particles inside the polymer matrix by using high energy synchrotron X-ray diffraction. The results obtained from the diffraction experiment are correlated with the macroscopic property measurements.

## 4.2 Experimental procedure

The piezoelectric ceramic powder used for manufacturing the composites was a *soft* PZT type (PZT507, Morgan Electroceramics, Ruabon, UK). In order to improve its piezoelectric properties the as-received powder was calcined at 1200 °C for 2h in a closed alumina crucible in a Nabertherm furnace applying a heating rate of 5 °C/min. The calcined powder was ball milled using yttria stabilized zirconia balls of 5 mm diameter in cyclohexane for 4 hrs [10]. Subsequently, the powder was dried at 150° C and stored in a closed container to avoid moisture absorption. The average particle size ( $d_{50}$ ) of the milled powder is 4.3  $\mu\text{m}$  as measured by light scattering with a Horiba

LA950DLA. The particle size measured with SEM was about 3-5  $\mu\text{m}$ , which is in good agreement with the laser scattering results. Prior to making the composites, laboratory X-ray diffractometer (Bruker D8, Berlin, Germany) was used to identify the phases present in the PZT powder with a scanning speed of 2°/min using  $\text{CoK}\alpha 1$  X-rays.

The polymer selected for the experiments is a commercial Zn-based ionomer (Surlyn 9320 DuPont), which is a partially ( $\text{Zn}^{2+}$ ) neutralized ethylene methacrylic acid copolymer. Apart from its excellent chemical resistance, good mechanical properties and its temperature stimulated self-healing capability, the ionomer has the desirable characteristic that the relaxation of the ionic species at elevated temperatures increases the electrical conductivity significantly, which should be beneficial to the poling efficiency. The electrical conductivity of the ionomer at the selected poling temperature of 60 °C is  $3.96 \times 10^{-12}$  S/m.

The composites were prepared by mixing the polymeric matrix and PZT powder (30 volume %) in a lab-scale counter rotating twin screw extruder (DSM Xplore Research Netherlands). The processing temperature was kept at 170 °C. In order to get a homogeneous distribution of PZT ceramic particles in the polymer matrix, the residence time was forest at 5 minutes, which ensured multiple passes of the material through the mixing section of the extruder. The composites were finally extruded through a 2 mm diameter outlet. In order to get planar sheets of composites, the extruded wire-shaped materials were hot pressed at a temperature of 150 °C and a pressure of 1 MPa for 5 min, yielding flexible planar sheets with a thickness of about 1 mm. Gold electrodes on both sides of the samples were made by sputtering. The samples were poled in organic oil (rap seed oil) at an electric field of 15  $\text{kVmm}^{-1}$  and a temperature of 60°C for 60 min.

The dielectric properties of the composites were measured using the parallel plate capacitor method using an Agilent 4263B LCR meter at 1V AC signal and a frequency of 1 kHz. The  $d_{33}$  of the composites was measured using a Berlincourt-type  $d_{33}$  meter (KCF technology PM3001, State college, PA, USA). The P-E (polarisation-

electric field) hysteresis loops of the composites were measured at room temperature using a Radiant hysteresis loop measurement system (RT 6000 HVS-2, Radiant Technologies In., Germany).

The synchrotron X-ray diffraction experiments were performed on Beamline I15 at the Diamond Light Source, UK. A schematic diagram of the high energy synchrotron X-ray diffraction experimental set up is shown in Figure 4.1. A synchrotron X-ray beam with a cross-section of 100 x 100 microns and a photon energy of 67 KeV was used (wavelength =  $0.1839 \times 10^{-10}$  m), with the diffraction patterns being recorded in transmission. A 2D detector (Perkin Elmer 1621 AN) was located about 1 m away from the sample, from which Debye-Scherrer rings (Figure 4.1) were collected. In order to generate 2-theta - Intensity plots, the data was caked into  $10^\circ$  slices centered around the poling direction ( $\Psi = 0^\circ$ ), using Fit2D software [11].

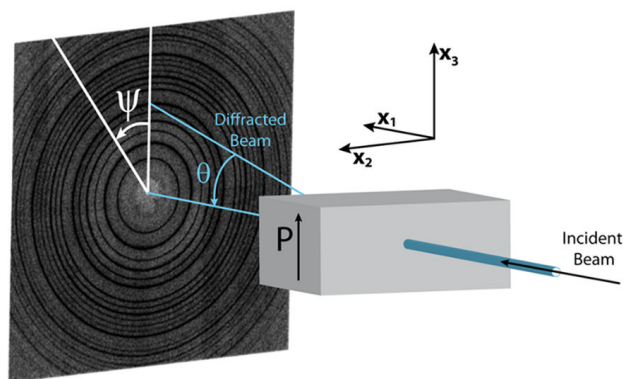


Figure 4.1: Experimental set up for time resolved high energy X-ray diffraction and the 2D diffraction image shows the Debye-Scherrer rings.

### 4.3 Results and Discussion

X-ray diffraction was used to identify the phases present in the calcined powder. The X-ray diffraction patterns were indexed with the reference pattern for tetragonal  $\text{PbZr}_{0.52}\text{Ti}_{0.48}\text{O}_3$  (ICDD: 33-0784). From the XRD pattern (Figure 4.2), it is clear that the present calcined PZT powder crystallizes in a tetragonal crystal structure, due to the presence of a single (111) peak and the splitting of the (002)/(200) peaks.

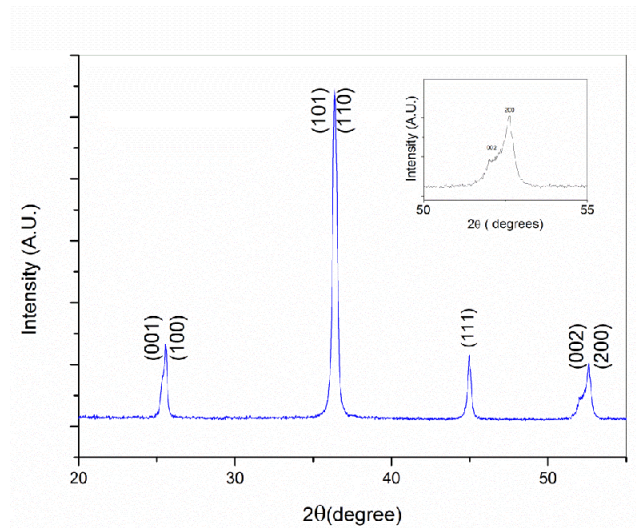


Figure 4.2: XRD diffraction pattern of PZT 507 powder used for fabrication of 0-3 ionomer composites.

The microstructure of the PZT-ionomer composites with 30 vol.% PZT is shown in the SEM micrographs of a sample fractured at room temperature presented in Figure 4.3. All the composites had a pore free nature and PZT particles were uniformly distributed in the polymer matrix. The high resolution image (Figure 4.3(b)) shows the good adhesion between polymer matrix and the ceramic particles. As shown in Figure 4.3(b) the PZT particles retained their equiaxed morphology after the multiple extrusion steps.

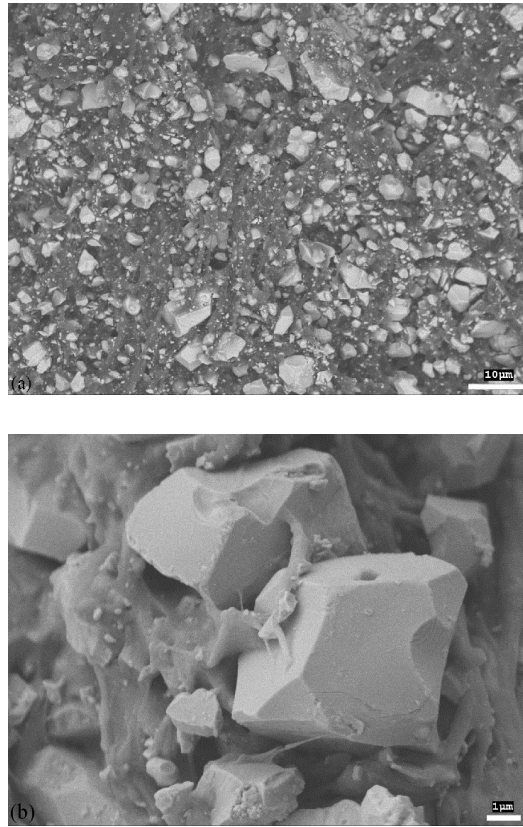
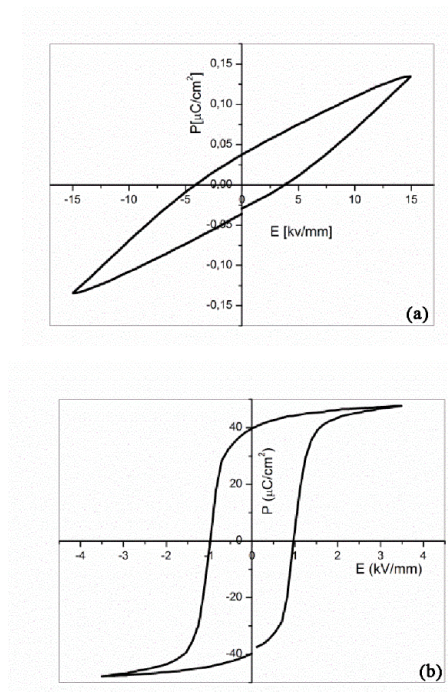


Figure 4.3: SEM micrographs PZT-ionomer composites (a) overview of the cross section and (b) the primary particles.

By comparing the P-E hysteresis loops, shown in Figure. 4.4, it is clear that the remnant polarization,  $P_r$ , of the PZT-ionomer composite is far lower than that of the bulk PZT ceramics while the coercive field,  $E_c$ , of the composite is higher than that of the PZT ceramics. For the fully dense PZT ceramic, when the external electric field reaches  $1 \text{ kV}\cdot\text{mm}^{-1}$ , the hysteresis loop is completely open and saturated, whereas for the composites, when the external field reach as high as  $15 \text{ kV}\cdot\text{mm}^{-1}$ , the loop only

starts to open up but is not saturated. This is mainly due to the presence of a low dielectric, non-piezoelectric polymer layer between the PZT particles, shielding the particles from the applied electric field and significantly lowering the resulting polarization of the PZT particle. A further increment of the applied driving voltage led to electric arcing between the electrodes, making it impossible to apply higher electric fields than  $15 \text{ kV}\cdot\text{mm}^{-1}$ .



**Figure 4.4:** P-E hysteresis loops of (a) PZT-ionomer composites and (b) PZT ceramics at room temperature.

In contrast to the P-E hysteresis measurements reported above, poling of the composites was carried out at elevated temperatures and the electric field was maintained for a long time (up to 1 hour) to obtain an optimal more-saturated polarization level. In ceramic-polymer composites, the effective electric field

experienced by the ceramic phase is controlled by the electrical conductivity and dielectric constant of both ceramic and polymer phases. If the timescale for poling is greater than the dielectric relaxation time constant of each of both phase, it is expected that the distribution of electric field within the PZT and polymer phases is controlled by their electrical resistivity rather than their dielectric properties. Hence we expect to achieve a significantly higher degree of poling of the PZT phase in the poled composites than was evident from the P-E hysteresis measurements, which were conducted over a relatively short timescale.

A detailed study of the piezoelectric and dielectric properties of PZT-ionomer composites has been reported in the previous chapter showing that poling for longer times at elevated temperatures leads to saturation of the piezoelectric properties, as shown in Table 1. Reversal of 180° ferroelectric domains takes place at the initial stages of poling, while 90° domain reorientation involving local stresses and strains demands longer time poling. The measured piezoelectric charge coefficient of the PZT-ionomer composites is in agreement with the values predicted by Yamada's model [6]. In this model, it is assumed that the PZT phase is completely poled and hence the poling efficiency factor, ' $\alpha$ ' is taken as 1. The actual state of poling was determined using synchrotron X-ray diffraction results.

**Table 1. Piezoelectric charge coefficients of the PZT-ionomer composites, obtained after poling under an electric field of  $15 \text{ kV}\cdot\text{mm}^{-1}$  with various temperatures and time [Chapter 3] [6].**

Temperature ( °C )	Time (hrs.)	$d_{33}$ (pC.N <sup>-1</sup> )
25	2	2.8
60	0.5	3.0
60	1	4.5
80	1	4.5

The high energy synchrotron XRD patterns of PZT-ionomer composites in the unpoled and poled conditions are compared in Figure. 4.5, for an azimuthal angle  $\psi = 0^\circ$ . The crystallographic analysis of the phases present in the composite shows that the PZT powder is phase pure and consistent with a tetragonal PZT perovskite structure, as reported previously [12]. It is known that stress due to non  $180^\circ$  domain reorientation and inter-granular strains in polycrystalline ferroelectrics can lead to changes in the intensities and positions of specific diffraction peaks [11, 13-15]. The structural changes of the PZT particles inside the polymer matrix were subsequently investigated by analysing and comparing the diffraction peak profiles obtained for the unpoled and poled composites.

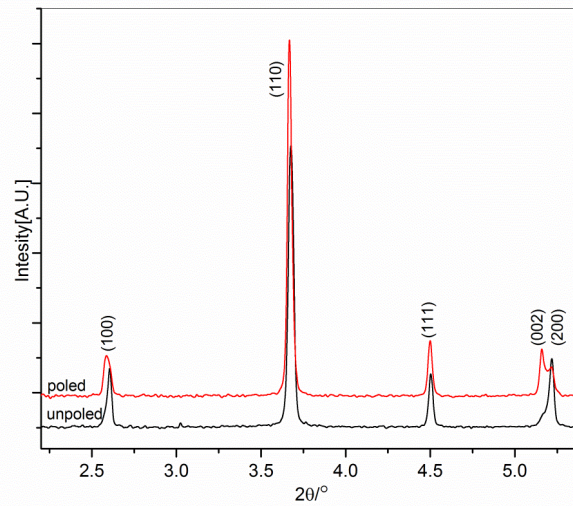


Figure 4.5: Integrated high energy synchrotron XRD patterns of PZT-ionomer composite, for  $\psi = 0^\circ$ .

Figure 4.6 illustrates schematically the evolution of domain reorientation and overall strain developed during the poling process. The family of grains or particles having their  $\{001\}$  planes oriented perpendicular to the applied electric field direction ( $\psi = 0^\circ$ ) experience a tensile (positive) elongation in this direction and a compressive (negative) elongation in the transverse direction ( $\psi = 90^\circ$ ) due to the combination of the intrinsic piezoelectric effect and extrinsic non  $-180^\circ$  ferroelectric domain switching during poling. Although the piezoelectric strain disappears when the electric field is removed, the transformation strain due to domain switching remains as a result of the non-zero remnant polarization. In contrast, ferroelectric domain switching within a  $\{111\}$ -oriented grain causes zero elongation along the poling direction, provided that there is no significant elastic constraint. Therefore, the  $\{111\}$  grain family can serve as a convenient sensor to detect the influence of elastic constraint and the associated residual stress due to poling [12].

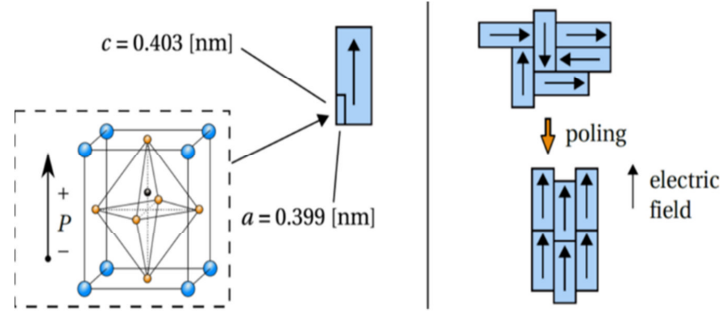


Figure 4.6: Schematic representation of strain development due to ferroelectric domain reorientation during the poling process [16].

The lattice strain during poling results in a shift in the d-values as determined from the diffraction pattern and can be calculated by the following equation:

$$\varepsilon_{hkl} = \frac{d_{hkl(\text{poled})} - d_{hkl(\text{unpoled})}}{d_{hkl(\text{unpoled})}} \quad (4.1)$$

where  $d_{hkl(\text{poled})}$  and  $d_{hkl(\text{unpoled})}$  are the lattice spacing of a given (hkl) plane in the poled and unpoled conditions respectively [14]. The {111} diffraction peaks were used to calculate the lattice strain since the {111}-oriented grains respond to tensile or compressive inter-granular stresses caused by ferroelectric domain reorientation within neighbouring grains [14]. Changes in the {111} peak position as a function of the azimuthal angle  $\psi$  for the poled composite are illustrated in Figure 4.7. It is evident that the {111} peak shifts to lower angles and hence larger d-spacing as  $\psi$  reduces, indicating the presence of a tensile residual stress along the poling direction ( $\psi = 0^\circ$ ) in the PZT particles. In contrast, for the unpoled composite (not shown) it was found that the {111} peak positions showed no systematic change with  $\psi$ , confirming

that the PZT particles in the unpoled composite were not subjected to any significant residual stresses.

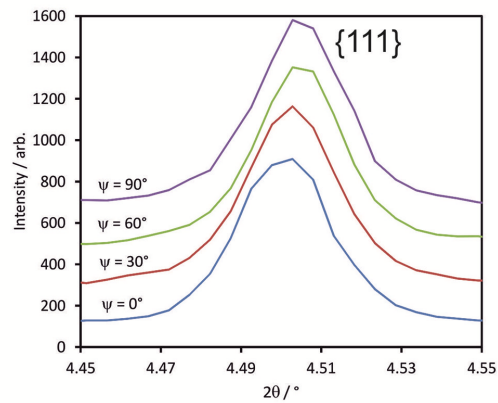


Figure 4.7: Changes in {111} peak position as a function of azimuthal angle  $\Psi$  for poled composite.

The positions of the {111} diffraction peaks were determined by fitting the peak profiles to a pseudo-Voigt function and hence calculating the lattice spacings using the Bragg equation. Subsequently the lattice strain,  $\epsilon_{\{111\}}$ , was calculated according to Eq. 4.1. The results of these calculations are presented in Figure. 4.8. It is evident that the  $\epsilon_{\{111\}}$  values for the unpoled composite were essentially independent of  $\psi$  and were scattered about the zero level. For the poled composite, an approximately linear relationship was obtained between  $\epsilon_{\{111\}}$  and  $\cos^2\psi$ , similar to that observed in poled tetragonal PZT ceramics [12]. The maximum strain of approximately 0.6% is lower than the value of 1% reported previously for a poled tetragonal PZT ceramic, but it does indicate that the PZT particles in the composite are subject to a significant level of elastic constraint and that this gives rise to residual stresses during poling. This result was unexpected, since it was anticipated that the difference between the elastic moduli of the ceramic and polymer phases should result in a relatively free (unconstrained) state for the PZT particles. This behavior could possibly be caused by elastic particle-particle interactions, since the volume fraction of the ceramic phase is relatively high, or the presence of hard particle

agglomerates. Further work is required to establish whether any of these mechanisms could give rise to the observed level of residual stress in the poled composite.

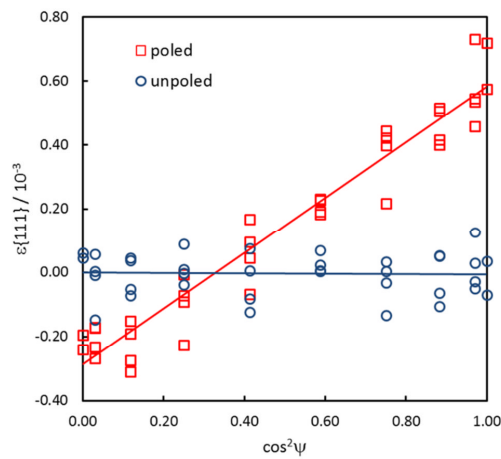


Figure 4.8: Lattice strain  $\varepsilon\{111\} - \cos^2 \Psi$  plots for unpoled and poled composites.

The changes in the {002} peak profiles of the poled composite as a function of the azimuthal angle,  $\psi$ , are presented in Figure 4.9. Poling of a polycrystalline ferroelectric material is achieved by domain reorientation within the grains and thus by a local change of domain fractions. This reorientation of domains towards the direction of the applied electric field ( $\psi = 0^\circ$ ) is clearly reflected in the relative intensities of the (002) and (200) diffraction peaks. More specifically, the intensity of the (002) peak increases while that of the (200) peak decreases with decreasing  $\psi$ . This indicates that a greater proportion of c-axis domains, with their spontaneous polarisation directed along  $\langle 001 \rangle$ , are evident in the XRD pattern obtained at  $\psi = 0^\circ$ , while the opposite occurs at  $\psi = 90^\circ$ .

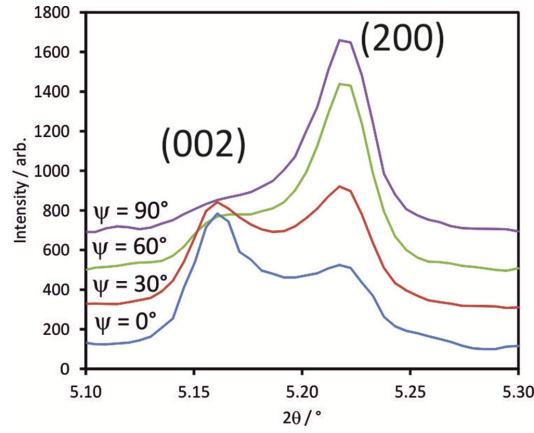


Figure 4.9: Changes in {200} peak profiles as a function of azimuthal angle,  $\Psi$ , for the poled composite.

The volume fraction of *c*-axis domains oriented along any given direction can be calculated from the intensities of the (002) and (200) diffraction peaks as

$$v_{002} = \frac{\frac{I_{002}}{I'_{002}}}{\frac{I_{002}}{I'_{002}} + 2 \frac{I_{200}}{I'_{200}}} \quad (4.2)$$

where  $I_{hkl}$  and  $I'_{hkl}$  denote the integrated area of a given plane for the poled (oriented) and unpoled (randomly oriented) conditions respectively [15]. The value of  $v_{002}$  should be equal to 1/3 in the unpoled state and 1 in the fully poled state, for  $\psi = 0^\circ$ .

The dependence of  $v_{002}$  on  $\psi$  for both the unpoled and poled composites is illustrated in Figure 4.10. It is evident that the value of  $v_{002}$  for the unpoled composite is scattered around the fixed value of 1/3, as defined by Eq. 4.2. In contrast,  $v_{002}$  for the poled composite exhibits a linear dependence on  $\cos^2\psi$ , which reflects the macroscopic strain state induced by poling and leads to a similar relationship for the

lattice strain  $\varepsilon\{111\}$  through the occurrence of residual stress [12]. The maximum value of  $v_{002}$ , obtained for  $\psi = 0^\circ$ , was approximately 0.70; this is considerably larger than the value of approximately 0.47 observed previously in a tetragonal PZT ceramic by Hall [12].

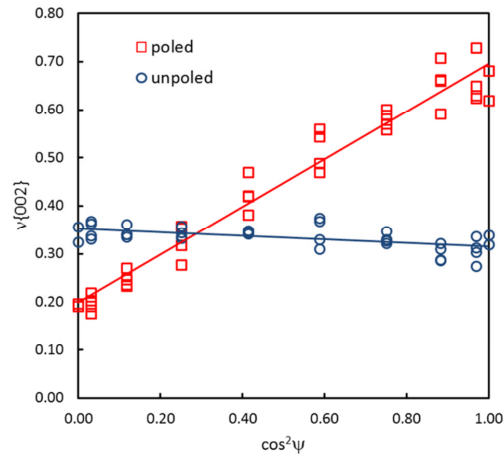


Figure 4.10: Variation in fraction of c-axis oriented domains,  $v(002)$ , as a function of  $\cos^2 \Psi$  for unpoled and poled composites.

Jones employed a different indicator,  $\eta_{002}$ , to describe the crystallographic texture in poled PZT ceramics [15]. This texture indicator was used to quantify the volume fraction of switched domains and is related to  $v_{002}$  by

$$\eta_{002} = v_{002} - \frac{1}{3} \quad (4.3)$$

It was reported that  $\eta_{002}$  values for poled tetragonal PZT ceramics in the literature varied from 0.13 to 0.46, corresponding to  $v_{002}$  values in the range 0.46 to 0.79. In comparison with these values, it is evident that the degree of poling achieved

for the PZT-ionomer composites in the present study is relatively high, in accordance with the bulk piezoceramic results. In the present case, the 2-3  $\mu\text{m}$  size PZT particles are big enough to accommodate the domains and the poling conditions employed were adequate to materialize the maximum piezoelectric properties out of the composite.

#### 4.4 Conclusions

The poling behaviour of the tetragonal PZT particles in a Zn based ionomer polymer matrix has been analysed using high energy synchrotron X-ray diffraction. The reorientation of ferroelectric domains during poling was quantified in terms of the parameter  $v_{002}$ , which represents the volume fraction of c-axis domains oriented in any given direction,  $\psi$ , relative to that of the applied electric field. It was shown that the highest value of  $v_{002}$ , equal to 0.70, was obtained for domains oriented along the poling direction ( $\psi = 0^\circ$ ), demonstrating that a relatively high degree of poling could be achieved using this polymer matrix with a moderate electrical conduction, a high field and a long poling time. An approximately linear  $v_{002}\text{-cos}^2\psi$  relationship was observed, in agreement with previous studies of poled tetragonal PZT ceramics. Unexpectedly, it was also found that the lattice strain,  $\epsilon\{111\}$ , exhibited a linear dependence on  $\text{cos}^2\psi$ , reaching a maximum value around  $0.6 \times 10^{-3}$  for  $\psi = 0^\circ$ . This result indicates that the PZT particles in the composite are subject to considerable elastic constraint, even though the elastic moduli of the two constituent phases differ by several orders of magnitude. Clearly the strain evolution is due to domain reorientation and not so much due to mechanical constraints of the polymer matrix surrounding the particle.

## References

- [1] A. J. Moulson and J. M. Herbert, "Piezoelectric Ceramics," in *Electroceramics*, ed: John Wiley & Sons, Ltd, 2003, pp. 339-410.
- [2] B. Jaffe, W. Cook and H. Jaffe, "Piezoelectric Ceramics Academic," *New York*, p. 115, 1971.
- [3] R. E. Newnham, D. Skinner and L. E. Cross, "Connectivity and piezoelectric-pyroelectric composites," *Materials Research Bulletin*, vol. 13, pp. 525-536, 1978.
- [4] G. Sa Gong, A. Safari, S. Jang and R. E. Newnham, "Poling flexible piezoelectric composites," *Ferroelectrics Letters Section*, vol. 5, pp. 131-142, 1986.
- [5] D. Waller, T. Iqbal and A. Safari, "Poling of lead zirconate titanate ceramics and flexible piezoelectric composites by the corona discharge technique," *Journal of the American Ceramic Society*, vol. 72, pp. 322-324, 1989.
- [6] N. K. James, U. Lafont, S. van der Zwaag and W. A. Groen, "Piezoelectric and mechanical properties of fatigue resistant, self-healing PZT-ionomer composites," *Smart Materials and Structures*, vol. 23, p. 055001, 2014.
- [7] A. Pramanick, D. Damjanovic, J. C. Nino and J. L. Jones, "Subcoercive cyclic electrical loading of lead zirconate titanate ceramics I: nonlinearities and losses in the converse piezoelectric effect," *Journal of the American Ceramic Society*, vol. 92, pp. 2291-2299, 2009.
- [8] J. L. Jones, B. J. Iverson and K. J. Bowman, "Texture and anisotropy of polycrystalline piezoelectrics," *Journal of the American Ceramic Society*, vol. 90, pp. 2297-2314, 2007.
- [9] R. Guo, L. E. Cross, S. E. Park, B. Noheda, D. E. Cox and G. Shirane, "Origin of the high piezoelectric response in  $\text{PbZr}_{1-x}\text{Ti}_x\text{O}_3$ ," *Physical Review Letters*, vol. 84, p. 5423, 2000.
- [10] D. A. van den Ende, W. A. Groen and S. van der Zwaag, "The effect of calcining temperature on the properties of 0-3 piezoelectric composites of PZT and a liquid crystalline thermosetting polymer," *Journal of Electroceramics*, vol. 27, pp. 13-19, 2011.

- [11] A. Hammersley, S. Svensson, M. Hanfland, A. Fitch and D. Hausermann, "Two-dimensional detector software: from real detector to idealised image or two-theta scan," *International Journal of High Pressure Research*, vol. 14, pp. 235-248, 1996.
- [12] D. Hall, A. Steuwer, B. Cherdhirunkorn, P. Withers and T. Mori, "Micromechanics of residual stress and texture development due to poling in polycrystalline ferroelectric ceramics," *Journal of the Mechanics and Physics of Solids*, vol. 53, pp. 249-260, 2005.
- [13] J. L. Jones, A. Pramanick, J. C. Nino, S. M. Motahari, E. Üstündag and M. R. Daymond, "Time-resolved and orientation-dependent electric-field-induced strains in lead zirconate titanate ceramics," *Applied Physics Letters*, vol. 90, p. 172909, 2007.
- [14] A. Pramanick and J. L. Jones, "Measurement of structural changes in tetragonal PZT ceramics under static and cyclic electric fields using a laboratory X-ray diffractometer," *Ultrasonics, Ferroelectrics and Frequency Control, IEEE Transactions on*, vol. 56, pp. 1546-1554, 2009.
- [15] J. L. Jones, E. B. Slamovich and K. J. Bowman, "Domain texture distributions in tetragonal lead zirconate titanate by X-ray and neutron diffraction," *Journal of Applied Physics*, vol. 97, p. 034113, 2005.
- [16] J. Holterman and P. Groen, "An Introduction to Piezoelectric Materials and Applications" ed: Stichting Applied Piezo, 2013, pp. 18-66.

## CHAPTER 5

**Exploring the Lead Zirconium Titanate (PZT) phase diagram for high sensorial properties in piezoelectric ceramic-polymer composites**

---



## 5.1 Introduction

PZT ceramics based on solid solutions of lead zirconate titanate (PZT) are well known piezoelectric materials with widespread technological applications [1]. The compositional dependence of the structure and the electrical properties of PZT ceramics has been investigated extensively. In this system rhombohedral and tetragonal phases coexist in a region which is a strong function of composition,  $\text{Pb}(\text{Zr}_{0.52}\text{Ti}_{0.48})\text{O}_3$  and a weak function of temperature known as the morphotropic boundary, or MPB [1, 2]. In 1999, Noheda discovered a monoclinic phase, sandwiched between rhombohedral and tetragonal phases near the MPB in PZT ceramics and this monoclinic symmetry allows the polarisation direction to continuously rotate in a plane and contributes to enhanced piezoelectric and dielectric properties at the MPB and nearby MPB region [3]. Such PZT ceramics with compositions at MPB or near this region are much easier to pole and exhibits improved piezoelectric and dielectric properties compared to their rhombohedral and tetragonal counterparts. MPB based PZT ceramics and its compositionally modified variants with soft and hard dopants have been exploited in many sensor and transducer applications for their high electromechanical properties [4, 5]. However, it is also noteworthy to point out that the piezoelectric and dielectric properties for the entire range of PZT compositions has not yet been systematically reported. B. Jaffe et al., partially showed the ceramic piezoelectric and dielectric properties with respect to Zr and Ti levels ranging from 0.48 to 0.60 [1].

Furthermore, in order to be usable in sensors and energy harvesting applications, not only the piezoelectric charge constant ( $d_{33}$ ) but also the piezoelectric voltage coefficient ( $g_{33}$ ) must be taken into account [6]. The good electro-mechanical properties of ceramics with MPB compositions are due to the fact that for this composition there are 14 polarisation direction to accommodate electromechanically induced strains leading to good actuation properties but non-MPB composition have fewer polarisation directions which ends up in higher inter-granular strains and hence lower piezoelectric and dielectric properties. Unlike bulk ceramics, in which the ceramic grains are in contact with each other in all direction, in 0-3 piezoelectric-

polymer composites, the high dielectric constant ( $\epsilon_r$ ) PZT ceramic filler particles having a particle size of 2-4  $\mu\text{m}$  range are surrounded by a low dielectric constant and poorly conductive polymer phase. Due to this, the piezoelectric ceramics in composites will exhibit entirely different poling behaviour and polarization mechanisms [7]. Consequently, it is not necessary that the MPB or near MPB compositions of ceramic filler particles will result in higher dielectric and piezoelectric properties in composites. Even though the lack of particle-particle connectivity will result in low piezoelectric charge coefficient ( $d_{33}$ ), at the same time the significantly lower effective dielectric constant results in an enhanced piezoelectric voltage coefficient ( $g_{33}$ ) in composites, which enable these composites to be used for various potential applications such as pressure sensors and strain-energy harvesting.

The present chapter describes a study of the piezoelectric and dielectric properties for the complete set of PZT ceramic  $[\text{PbNb}_{0.01}[\text{Zr}_x\text{Ti}_{(0.99-x)}]\text{O}_3]$  compositions ranging from pure  $\text{PbTiO}_3$  to  $\text{PbZrO}_3$ . The piezoelectric properties of PZT ceramics are improved by the addition of donor dopants, the popular one being Niobium (Nb) ions, resulting in the formation of Nb-doped PZT (PNZT) ceramics.  $\text{Nb}^{5+}$  ions substitutes  $\text{Zr}^{4+}/\text{Ti}^{4+}$  ions at B-site and thereby promote domain wall motion in PZT ceramics. Apart from providing superior piezoelectric and dielectric properties, Nb-oxide is also a good sintering aid for PZT-based materials resulting in higher density and smaller grain size with 1 mol % doping in the system [8]. Hence, 1 mol% Nb was added in the base system in order to make the poling and sintering process easier. In addition a detailed investigation has been carried out exploring the possibility of using non-MPB PZT compositions as fillers for 0-3 composites to maximize their voltage sensitivity composites by using a well-studied epoxy as polymer matrix.

## 5.2 Theory

Major factors which determine the dielectric and piezoelectric properties of polymer-ceramic composites are volume fractions, connectivity and the intrinsic properties of constituent phases. Apart from above mentioned dominant factors, the

inter-phase interaction between the ceramic particles and polymer matrix, percolation and porosity also have an influence of the final dielectric and piezoelectric properties of the composites. Rule of mixtures and Yamada's model based on different theories and assumptions are used to compare and validate the experimental results [9, 10].

The mixture rule is based on the assumption that the filler particles are uniformly distributed in a continuous matrix and no interactions between these constituents are taken into account. Using these assumptions, the effective dielectric constant of composite containing dielectric fillers embedded in a polymer matrix can be expressed as:

$$(\epsilon_c)^k = V_f(\epsilon_f)^k + (1-V_f)(\epsilon_m)^k \quad (5.1)$$

where  $\epsilon_c$ ,  $\epsilon_f$  and  $\epsilon_m$  are the dielectric constants of the composite, pure ceramic filler and polymer matrix respectively,  $k$  is an empirical parameter that depends on shape and orientation of the filler particles and  $V_f$  is the volume fraction of the filler medium. In general, the value of  $k$  corresponds to -1 (series model) or 1 (parallel model), with the former being derived by considering the total capacitance (which is later on used to derive dielectric constant) of the composite as the sum of two capacitances in series connection whereas  $k=1$  corresponds to parallel connection. In addition, for randomly dispersed ceramic filler particles the value of  $k$  corresponds to 1/3 and is termed as random model.

Yamada considered the composite system as a ellipsoidal particles dispersed in a continuous polymer medium. In this model the composite dielectric constant ( $\epsilon_c$ ) and piezoelectric charge coefficient ( $d_{33,c}$ ) of the composite was derived to be given by:

$$\varepsilon_c = \varepsilon_m \left( 1 + \frac{nV_f(\varepsilon_f - \varepsilon_m)}{n\varepsilon_m + (\varepsilon_f - \varepsilon_m)(1 - V_f)} \right) \quad (5.2)$$

$$(d_{33,c}) = \frac{V_f \varphi \alpha n \varepsilon_c (d_{33,f})}{n\varepsilon_c + \varepsilon_f - \varepsilon_c} \quad (5.3)$$

where  $n$  is the shape factor (depends on the geometry of the filler particles and its orientation with respect to the surface of the composite) and  $\varphi$  is the ceramic volume fraction and  $\alpha$  is the state of poling of the piezoelectric particles compared to that achievable in a fully dense monolithic ceramics.

### 5.3 Experimental

Conventional solid state reaction chemistry methods were used to synthesize the  $\text{PbNb}_{0.01}[\text{Zr}_x\text{Ti}_{(0.99-x)}]\text{O}_3$  ceramic powder with various Zr and Ti levels. The lead oxide (PbO), zirconia ( $\text{ZrO}_2$ ), titania ( $\text{TiO}_2$ ) and niobium pentoxide ( $\text{Nb}_2\text{O}_5$ ), with 99.9% purity, were used as the raw materials. The raw materials were mixed according to the stoichiometric proportions based on the desired ceramic composition. In order to attain homogeneity, the raw materials were thoroughly ball milled with 5-mm zirconium balls for 7 hrs in distilled water. The mixture was then dried in a hot air oven in order to remove the distilled water. The dried powder was calcined in a furnace at 750 °C for 2 hrs at a heating rate of 2 °C/min in order to initiate the formation of perovskite phase. The crystallographic structure of the calcined powders was measured for phase formation by X-ray diffraction using a Bruker D8 diffractometer and  $\text{CoK}\alpha 1$ ,  $\lambda = 1.78901 \text{ \AA}$ . Once the phase formation was observed the powder was milled again as mentioned above for 3 hrs and was dried in a hot air oven for overnight at 120 °C. The dried powder was calcined again at 1150 °C for 2 hrs at a heating rate of 2 °C/min. The crystal structure, phase formation and lattice parameters of the ceramic powders were again determined using X-ray diffraction technique. The XRD results were further analyzed using PAN analytical X'Pert HighScore Plus, Version 2.0, to determine the lattice parameters of each compositions. The particle size distribution of the calcined  $\text{PbNb}_{0.01}[\text{Zr}_x\text{Ti}_{(0.99-x)}]\text{O}_3$

ceramic powders, for  $x = 0$  to 0.8, were measured using laser diffractometer. The pure lead zirconate, which is an antiferroelectric and  $x=0.9$  compositions were excluded from the present study since the former composition does not any piezoelectric properties and the latter one expected to have very low piezoelectric properties. Densities were measured using the Archimedes principle in distilled water. In order to investigate the dielectric and piezoelectric properties of ceramics, four to five sintered ceramic disks were prepared by pellet-pressing. Prior to the pressing of ceramic disk, polyvinyl alcohol (PVA) was used as a binder in order to reduce the brittleness of the disks. The fine and homogeneous ceramic powder was pressed into cylindrical disks of 6.5 mm diameter and 1.5-2.5 mm thickness under an uniaxial pressure of  $5 \times 10^5$  N/m<sup>2</sup> using a hydraulic press. The pressed ceramic disks were sintered for 2 hrs at 1250 °C on a bed of commercial PZT powder using a high temperature furnace. Gold electrodes on both sides of the ceramics were made by sputtering. The ceramics were poled at 2-5 kV/mm at 100 °C in silicon oil bath for 30 min.

The 20 and 40 vol. % 0-3 epoxy-ceramic composites with desired ceramic compositions were prepared by tape-casting method. 20 and 40 vol % ceramic loading fractions were chosen to get a dilute system and one in the higher particle to particle connectivity regime. The ceramic filler particles were first dispersed in the resin component of the epoxy and mixed at 3000 rpm for 5 min. using a planetary mixer (Speed Mixer DAC 150.1 FVZ). The slurry was degassed for 5 min. and subsequently, the curing agent was added to the mix of resin and ceramic particles. Hereafter, it was mixed at 2000 rpm for 5 min. This slurry was degassed for 5 min. in order to remove air bubbles. Subsequently, the slurry was poured on a thin aluminum foil and tape-casted using a movable doctor blade at a speed of 2 mm/s, resulting in the formation of 200 micron thin sheets of 0-3 PZT Epoxy composites. The composites thus formed were cured at room temperature for 24 hrs. After curing, the composites were cut into thin circular disks of 12 mm diameter. Gold electrodes on both sides of the composites were made by sputtering. The composites were poled at 15 kV/mm at 80 °C in silicon oil bath for 1 hr. The oil bath containing the composites was then cooled down to 30 °C while applying the poling field. Initially saturation of piezoelectric and dielectric properties of lead titanate-epoxy composites were optimized with various poling

conditions and the above mentioned poling condition were used for the rest of the composites. In order to further improve the poling efficiency, the poling temperature was chosen close to the  $T_g - 80$  °C of the epoxy matrix where it exhibits higher electrical conductivity [11-13]. The composites were allowed to age for at least 24 hrs before measuring the dielectric and piezoelectric properties. The dielectric constant of the ceramics and composites were measured by parallel plate capacitor method using an Agilent 4263B LCR meter at 1 V and 1 kHz. The piezoelectric charge constant ( $d_{33}$ ) of the composites was measured using a Berlincourt type  $d_{33}$  meter and the measurements were carried out at a standard force of 10 N and frequency of 110 Hz. P-E and strain hysteresis loop measurements were carried out to determine the remnant polarization ( $P_r$ ), spontaneous polarization ( $P_s$ ) and coercive field ( $E_c$ ) of the 0-3 composites prepared. The measurements were carried out at room temperature and at an applied field range of 5 - 40 kV/mm, using a standardized ferroelectric measurement test system of Radiant Technology.

## 5.4 Results and Discussion

### 5.4.1 Crystallographic phase analysis and Microstructure characterization

#### XRD Analysis

The room temperature X-ray diffraction patterns of prepared  $\text{PbNb}_{0.01}[\text{Zr}_x\text{Ti}_{(0.99-x)}]\text{O}_3$  as a function of Zr-compositions are shown in Figure 5.1. The sharp and well defined diffraction peaks confirm the formation of a single phase perovskite structure in all compositions. The phases were identified by analysing the diffraction patterns within the two theta ( $2\theta$ ) range of  $20^\circ$  and  $60^\circ$ . Within this range (100), (110), (111) and (200) peaks showed a systematic shift in the  $2\theta$  position with varying Zr/Ti ratio. This systematic shift in the position of  $2\theta$  indicates the transition from rhombohedral (PZT-70) to the tetragonal (PZT-0) phases of the ceramic powder. The splitting of (002) into (002) and (200) peaks at PZT-52 (MPB i.e.  $x=0.52$ ) reflects the morphotropic phase boundary (MPB) region, where the

tetragonal and rhombohedral phases coexist. The reason behind this splitting of reflections in the MPB region can be attributed to the local compositional fluctuations, leading to the coexistence of the rhombohedral and tetragonal phases [14-16]. It can also be seen that when  $Zr/Ti < 52/48$ , the diffraction patterns exhibit distinct (101) and (110) peaks at  $2\theta=36^\circ$ , which denotes the tetragonal phase. In addition, with the increase in the tetragonal phase, the (111) peak becomes more distinct.

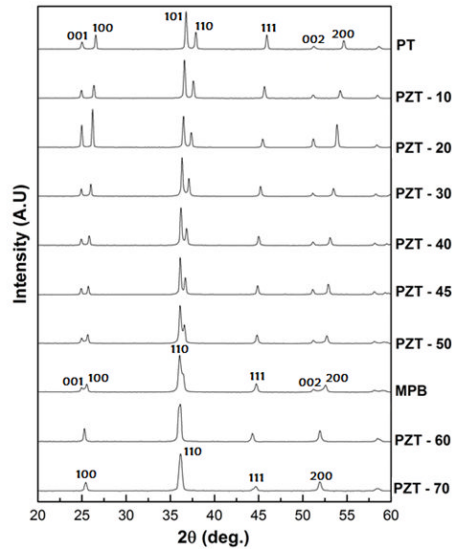


Figure 5.1: X-ray diffraction pattern of calcined  $PbNb_{0.01}[Zr_xTi_{(0.99-x)}]O_3$  ceramic powder.

### Lattice Parameter

Figure 5.2 shows the variation of lattice parameters 'a' and 'c' and  $c/a$  ratio as a function of the Zr mol%. The  $c/a$  ratio for MPB composition is found to be 1.025 whereas that of  $PbTiO_3$  is 1.062. Even though the lattice constant 'c' remains almost constant, an increase in lattice constant 'a' is observed, thereby leading to a reduction in  $c/a$  ratio with increase in Zr content. This reduction in  $c/a$  ratio indicates that the tetragonality of PZT ceramics decreases with increase in Zr content. The values of the lattice parameters were found to be close to those reported previously [17].

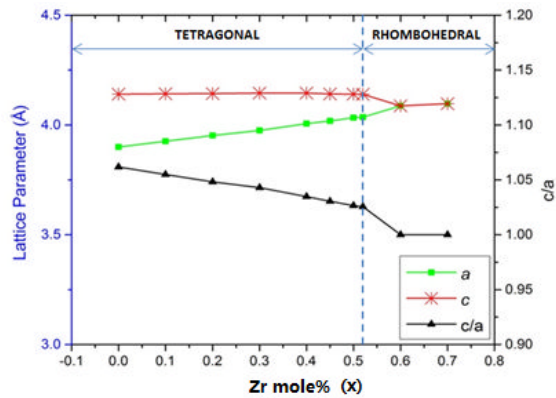


Figure 5.2: Lattice parameters and  $c/a$  ratio of calcined  $\text{PbNb}_{0.01}[\text{Zr}_x\text{Ti}_{(0.99-x)}]\text{O}_3$  ceramic powder.

### *Particle and Morphology*

Figure 5.3(a-c) shows the SEM micrographs of the calcined ceramic powder with Zr mol% corresponding to 0 (tetragonal), 0.52 (MPB) and 0.80 (rhombohedral) respectively. The particle size of the calcined powder was found to increase with Zr content, which was well supported by the results from particle size analysis of the ceramic powders. The calcined PT powder appears to have a more or less spherical morphology whereas the other powders have a polyhedral morphology.

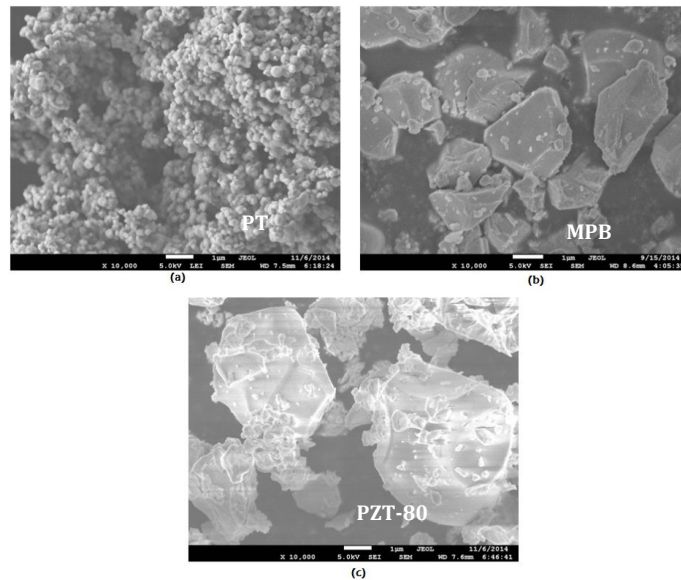


Figure 5.3: Microstructure of ceramic powder for compositions corresponding to (a) PT-0, (b) PZT-52 (MPB) and (c) PZT-80 [scale:1 $\mu$ m].

#### *Microstructure of sintered ceramics and composites*

Figure 5.4 (a-c) shows the SEM micrographs of ceramics sintered at 1250 °C for different Zr mol% corresponding to 0 (PZT-0), 0.52 (MPB) (PZT-52) and 0.80 (PZT-80) respectively. It can be seen that the MPB and rhombohedral composition have a densely packed microstructure whereas PT has a porous microstructure, which reflects the poor sinterability of tetragonal PZT ceramics. The reason behind the poor sinterability of lead titanate (PZT-0) ceramics is the large spontaneous strain and thermal expansion anisotropy of the tetragonal phase of lead titanate (PZT-0), which results in local interfacial (see Figure 5.4 (d)) upon cooling from sintering temperature through the cubic to the tetragonal phase transition temperature of 490 °C [18]. In addition, the formation of an impurity phase (identified as pyrochlore) is observed in ceramics with a rhombohedral composition, which became less notable

with increasing Ti. The presence of non-ferroelectric pyrochlore phase will have a detrimental effect on the piezoelectric properties of the ceramics and thus needs to be avoided [19]. The formation of pyrochlore phase was not observed in the calcined ceramic powder where a two-stage calcination process applied [20]. The lead oxide loss during the sintering process of Zr-rich compositions at 1250 °C, results in the formation of this undesirable Zr-rich phase whereas in double step calcination process has been done at 1150 °C.

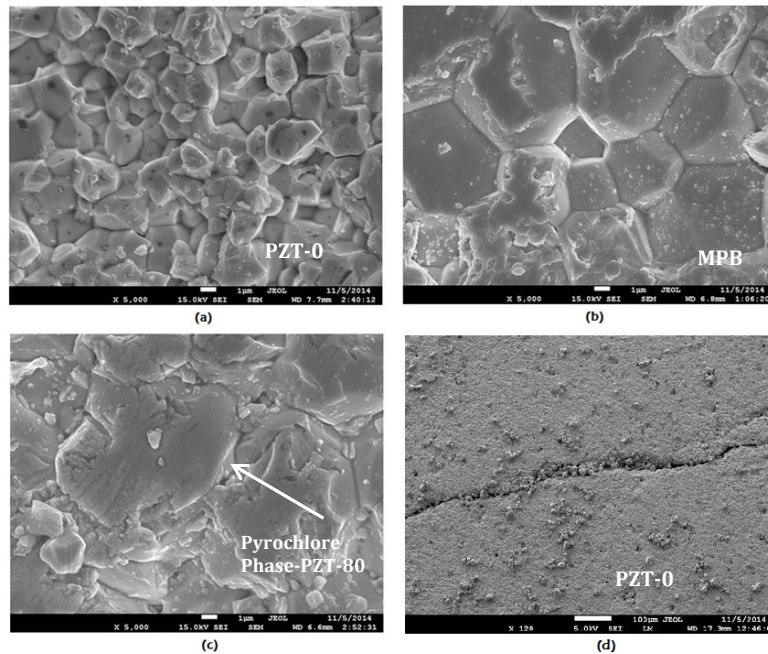


Figure 5.4: Microstructure of ceramic disks sintered at 1250 °C for compositions corresponding to (a) PZT-0, (b) PZT-52 (MPB), (c) PZT-80 (i.e.  $x = 0.80$ ) and (d) crack on surface of PT ceramics after sintering process: [scale for figure (a), (b), (c):1 $\mu$ m (d) 10  $\mu$ m].

Figure 5.5 shows the SEM micrographs of the cross-sections of 0-3 PZT-Epoxy composites for 20 and 40 vol. % of ceramic filler of lead titanate (PZT-0) or MPB (PZT-52) composition. It can be seen that for 20 vol. % composite, there is barely any particle to particle connectivity resulting in a 'dilute' system. On the other hand, 40

vol. % composite have a better particle to particle connectivity which can expect higher piezoelectric and dielectric properties.

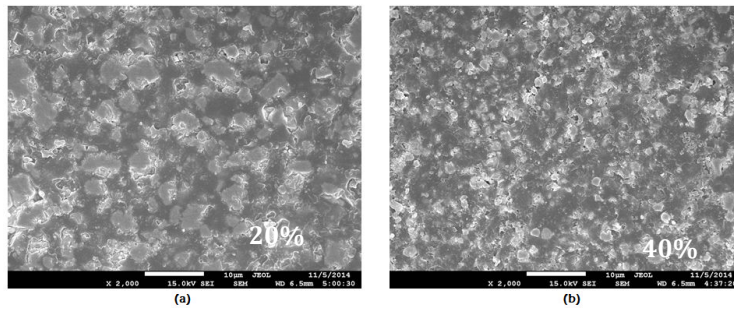


Figure 5. 5: Cross-sectional micrographs of composites prepared with 20 vol. % (a) and 40 vol. % (b) of  $\text{PbNb}_{0.01}[\text{Zr}_x\text{Ti}_{(0.99-x)}]\text{O}_3$  ceramic powder with  $x = 0.52$  (MPB).

#### 5.4.2 Dielectric and Piezoelectric Properties

##### Ceramics

Table 5.1 reports the densities of the sintered  $\text{PbNb}_{0.01}(\text{Zr}_x\text{Ti}_{(0.99-x)})\text{O}_3$  ceramics measured. The densities of the sintered ceramics are in the range of 7.12 to 7.49 g/cc (90-93 % of theoretical density) depending on Zr composition. From the specific density values, it is evident that all the ceramic specimens prepared are sufficiently dense to allow reliable for piezoelectric and dielectric characterization except for the PZT-0 which has achieved only 89% relative density.

**Table 5.1: Density of the sintered  $\text{PbNb}_{0.01}(\text{Zr}_x\text{Ti}_{(0.99-x)})\text{O}_3$  ceramics for x ranging from 0 to 0.80**

Composition	Density ( $\text{g}/\text{cm}^3$ )	Relative density (%)
PZT-0	7.12	89
PZT-10	7.18	90
PZT-20	7.20	90
PZT-30	7.25	90
PZT-40	7.30	91
PZT-45	7.35	92
PZT-50	7.41	92
PZT-52 (MPB)	7.49	93
PZT-60	7.41	93
PZT-70	7.41	92
PZT-80	7.39	92

Figure 5.6 shows the electric-field induced polarization hysteresis of  $\text{PbNb}_{0.01}(\text{Zr}_x\text{Ti}_{(0.99-x)})\text{O}_3$  ceramics, for  $x = 0.0, 0.52$  and  $0.80$ , measured at an applied field ranging from  $4.5$  to  $7.5$   $\text{kV}/\text{mm}$  and at room temperature. The P-E hysteresis loop clearly shows that for all compositions the polarisation attains a saturation level all at different electric fields. The P-E hysteresis displays significantly higher remnant polarization ( $P_r$ ) at lower electric fields for MPB ceramics than that of its tetragonal and rhombohedral counter parts. The remnant polarisation increases from  $\text{PbTiO}_3$  with increasing Zr content till MPB composition ( $x = 0.52$ ) and then decreases for Zr-rich compositions. The presence of 14 polarisation directions contributes the highest remnant polarisation with low electric fields for the PZT ceramics at MPB ceramics.

On the other hand, the decrease in remnant polarisation of PZT-80 composition is due to the high content of antiferroelectric rhombohedral phase [21].

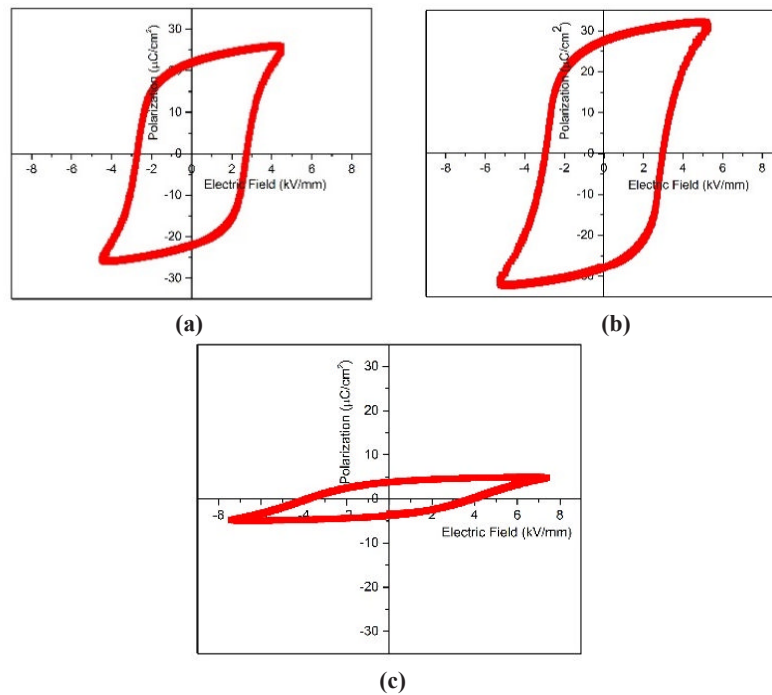
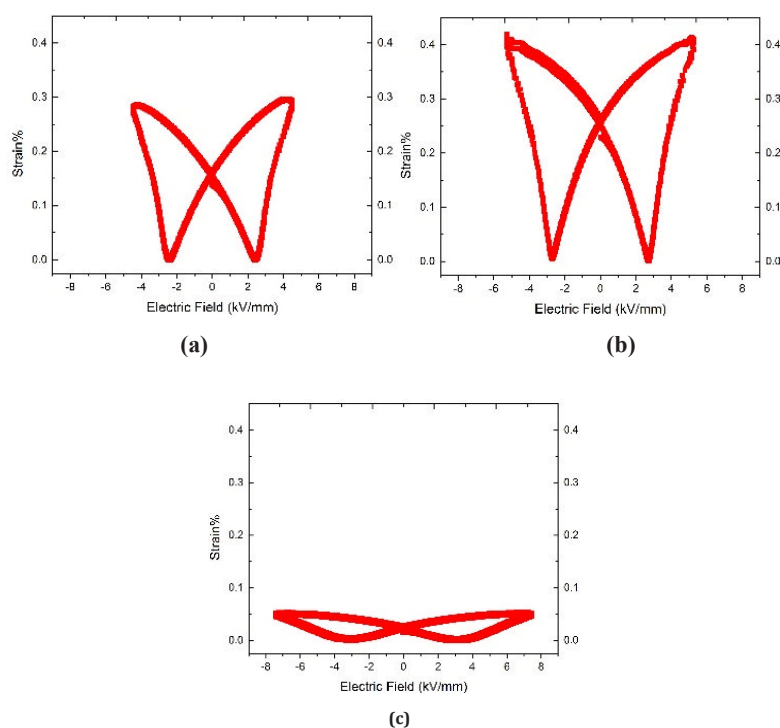


Figure 5.6: P-E Hysteresis loop for  $\text{PbNb}_{0.01}(\text{Zr}_x\text{Ti}_{(0.99-x)})\text{O}_3$  ceramics for (a)  $x = 0$  (PZT-0), (b) 0.52 (PZT-52, MPB) and (c) 0.80 (PZT-80).

Figure 5.7 shows the electric-field induced strain curves of  $\text{PbNb}_{0.01}(\text{Zr}_x\text{Ti}_{(0.99-x)})\text{O}_3$  ceramics, for  $x = 0, 0.52$  (MPB) and  $0.80$ , measured at a frequency of 1 Hz and at room temperature. It can be seen that each composition exhibits classical butterfly strain loops irrespective of their Zr/Ti ratio. The well-defined strain loop of PT and MPB ceramics suggests that these ceramics possess excellent actuation properties compared to that of rhombohedral PZT ceramics. In general, the electric-field-induced strain in ceramics is caused by the domain switching, number of polarisation states, electrostriction and the applied electric field. As a result, MPB composition displays the maximum strain in ceramics due to the

coexistence of rhombohedral and tetragonal phases, which in turn leads to enhanced polarization and piezoelectric properties [22].



**Figure 5.7: The electric-field induced strain hysteresis loop for  $\text{PbNb}_{0.01}(\text{Zr}_x\text{Ti}_{(0.99-x)})\text{O}_3$  ceramics for  $x = 0$  (PZT-0),  $0.52$  (PZT-52,MPB) and  $0.80$  (PZT-80).**

Figure 5.8(a) and (b) shows the values of dielectric constant and piezoelectric charge constant of ceramics as a function of Zr mol% respectively. Since it is difficult to perform the poling process of tetragonal PZT ceramic, including PT, the piezoelectric charge constant ( $d_{33}$ ) of the ceramics were deduced by substituting the experimental values of the dielectric constant of corresponding composites in Yamada's model (See Figure 5.9(b)). The reason behind the difficulty in the poling process of tetragonal ceramics is due to the large coercive field of these ceramics [18]. In addition, it is also difficult to completely sinter the tetragonal ceramics to high

densities due to the high vapour pressure of PbO, thereby resulting in a fragile and porous ceramics [Figure 5.4(b)]. Also the large tetragonal distortion (c/a ratio of pure PT is 1.062) results in cracking of the ceramics when cooled after sintering.

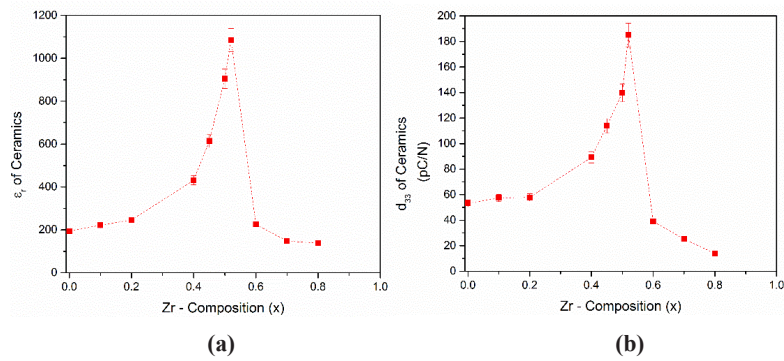


**Figure 5.8:** Variation of room temperature (a) dielectric constant ( $\epsilon_r$ ) and (b) piezoelectric charge constant ( $d_{33}$ ) of  $\text{PbNb}_{0.01}[\text{Zr}_x\text{Ti}_{(0.99-x)}]\text{O}_3$  as a function of Zr mol%.

As for the dielectric constant, the maximum value of the piezoelectric charge constant is also observed a maximum at the MPB composition (See Figure 5.8(b)). The reason for this sharp increase in the dielectric and piezoelectric properties is attributed to the presence of 14 polarisation directions, originating from the co-existence of tetragonal and rhombohedral phases at the MPB, which have nearly equivalent free energy. This provides a high polarisation for MPB compositions, which in turn favours strong dielectric and piezoelectric effects [23-25]. As mentioned previously, when  $x > 0.52$ , the composition has only the rhombohedral phase whereas when  $x < 0.52$ , the composition is dominated by the tetragonal phase. In either case, the number of orientations for the polarisations less than that of MPB composition, which in turn decreases the piezoelectric response. In addition, as mentioned earlier, the porous nature of tetragonal ceramics also contributes towards the decrease in piezoelectric charge constant since the porosity reduces the polarization per unit volume [23, 26].

The piezoelectric voltage coefficient ( $g_{33}$ ) of PZT ceramics as a function of Zr mol% is shown in Figure 5.9 and it can be seen that the highest  $g_{33}$  is exhibited by  $\text{PbTiO}_3$  (PZT=0) ceramics, in spite of its lower  $d_{33}$  than that of MPB ceramics. The significantly low dielectric constant of PT ( $\epsilon_r = 194$ ) compared to that of MPB ceramics ( $\epsilon_r = 1085$ ) is responsible for this difference in the voltage coefficient. The piezoelectric voltage coefficients ( $g_{33}$ ) increases towards the tetragonal side while it remains almost constant in the rhombohedral field until the antiferroelectric nature of the rhombohedral phase gains over the ferroelectric properties, after which the  $g_{33}$  drops significantly.

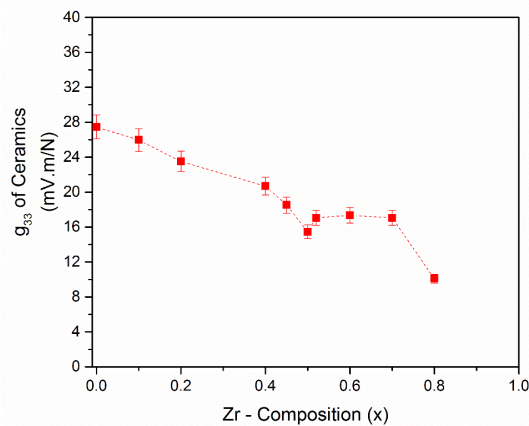


Figure 5.9 Variation of room temperature piezoelectric voltage coefficient ( $g_{33}$ ) of  $\text{PbNb}_{0.01}[\text{Zr}_x\text{Ti}_{(0.99-x)}]\text{O}_3$  ceramics.

### Composites

The polarization hysteresis for 0-3 composites are carried out for different applied fields (5 – 40 kV/mm) at room temperature and the loops are shown in Figure 5.10. The development of hysteresis loop confirms the ferroelectric nature of the 0-3 PZT-Epoxy composites prepared. With the increase in the electric field, the composites exhibited higher polarization due to the reorientation of the dipoles within the ceramic granules, resulting in an increase in the area of the P-E loops.

However, the remnant polarization ( $P_r$ ) is much lower than that of bulk ceramics due to the influence of the non-ferroelectric polymer phase. It can also be seen that the poling efficiency of composites with 40 vol. % of ceramic filler is much higher than that of the ones with 20 vol. %. This is due to the better connectivity of the ceramic filler particles in 40 vol. % loaded composites. The strain loops of composites do not have any observable butterfly nature.

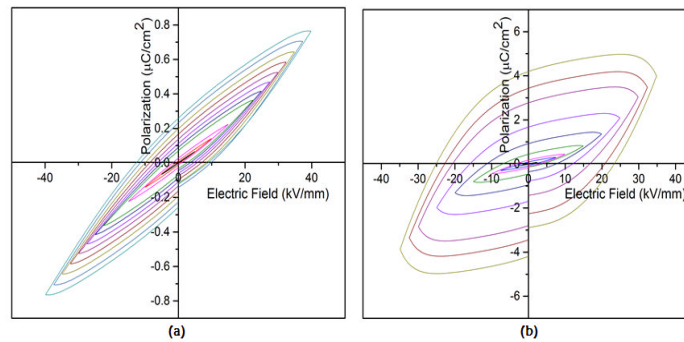


Figure 5.10: Polarization hysteresis loops for (a) 20 vol. % and (b) 40 vol. % of 0-3 PZT (MPB)-Epoxy Composite.

It is clear from Figure 5.11 that, even though there is a large difference between dielectric constants of  $\text{PbTiO}_3$  (PZT-0) and MPB (PZT-52) ceramics (see Figure 5.8(a)), when these compositions are used as a filler material in composites, the effective dielectric constant of the composite varies less and does not show the peak value at the composite with MPB ceramic filler. From Figure 5.7(a), it can be seen that the difference between the dielectric constant of PT and MPB ceramics is about 885 whereas in 0-3 composites, this difference is drastically reduced and both the composites possess about same dielectric constant. The reason behind this anomaly between bulk ceramics and composites is related to the difference in the dielectric constant of each constituent (i.e. PZT ceramic filler and epoxy matrix) [27]. Considering 0-3 composite, which contains ceramic particles with MPB composition, the difference in the dielectric constant of epoxy matrix ( $\epsilon_{r, \text{epoxy}} = 4.2$ ) and the ceramic filler ( $\epsilon_{r, \text{filler}} = 1085$ ) is about 1081. At the same time, for PT ceramic filler ( $\epsilon_{r, \text{filler}} = 200$ ), the difference is only 196. This low difference between the dielectric constant of the polymer and ceramic phase has resulted in a better dielectric homogenization

between the PT ceramic filler and epoxy matrix in 0-3 composites and thus resulted in a dielectric constants, which is comparable to that of MPB composites. This is well supported by the theoretical prediction based on the Yamada model as shown in Figure 5.12. Series and parallel mixing rules give lower and upper limits of the dielectric constant respectively. It is clearly evident that, the analytical model for the particular polymer matrix, the dielectric constant of composites attains saturation after a sharp increase with the dielectric constant of constituent ceramic fillers in the initial stage. Once saturated, the increase in the dielectric constant of ceramic filler particles does not have any significant impact on the dielectric constant of its composites. This observation is consistent with the experimental results.

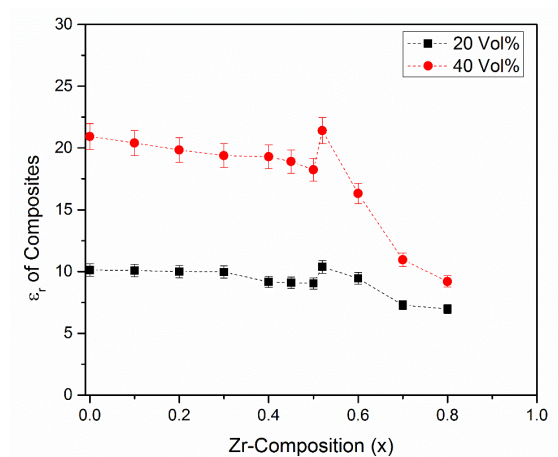


Figure 5.11: Dielectric constant ( $\epsilon_r$ ) of the composites as a function of Zr composition in 0-3 composites with 20 and 40 vol. % of  $\text{PbNb}_{0.01}[\text{Zr}_x\text{Ti}_{(0.99-x)}]\text{O}_3$  ceramic filler.

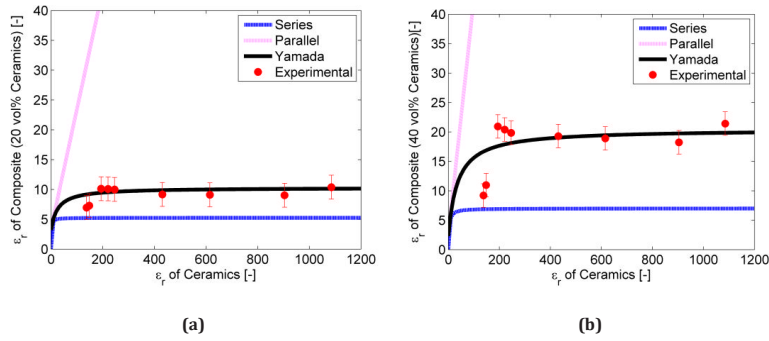


Figure 5.12: Comparison of variation of dielectric constant of (a) 20 vol. % and (b) 40 vol. % composite as a function of the dielectric constant of corresponding  $\text{PbNb}_{0.01}[\text{Zr}_x\text{Ti}_{(0.99-x)}]\text{O}_3$  ceramic compositions.

Figure 5.13 shows the variation of piezoelectric charge constant ( $d_{33}$ ) as a function of Zr composition for 0-3 PZT-Epoxy composites. As reported elsewhere [30, 40], composites with 40 vol. % of ceramic filler show higher  $d_{33}$  than those with 20 vol. % of filler due to the presence of higher content of active ceramic phase and low inter particle distance. Similar to that of bulk PZT ceramics [1], an increase in the  $d_{33}$  of composites is observed, for compositions close to the MPB, attaining its maxima at  $x=0.52$  (i.e. MPB composition). For higher Zr content (i.e.  $x > 0.52$ ), the antiferroelectric rhombohedral phase dominates, resulting a sharp decline in the  $d_{33}$  of ceramic filler and consequently its composites. Figure 5.14 shows the results of theoretical predictions of  $d_{33}$  of composites using Yamada's model as a function of dielectric constant of ceramic fillers used [Figure 5.143(a)&(b)]. Similar to the observation made for the effective dielectric constant of composites, the  $d_{33}$  of the composites also attained saturation after a sharp increase with the dielectric constant of constituent ceramic fillers in the initial stage. This can be correlated to large difference in dielectric constant between the ceramic phase and polymer phase make the system dilute which in turn reduces the overall effect drastically. In addition to that, the higher depolarization factor of higher dielectric constant filler material also deteriorates the effective piezoelectric and dielectric properties of the composites made out of it.

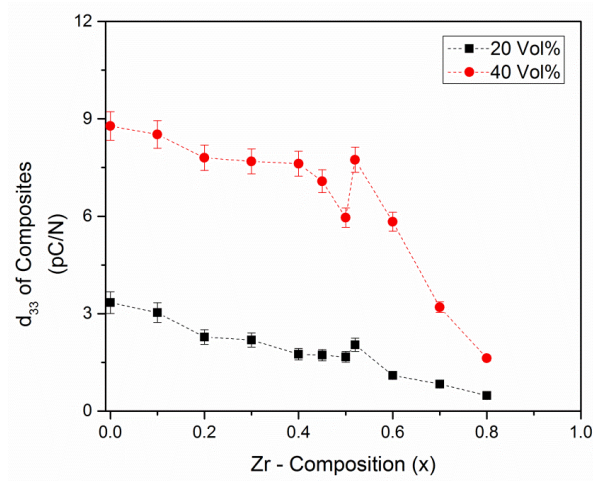


Figure 5.13: Variation of room temperature piezoelectric charge coefficient ( $d_{33}$ ) of 0-3 composites for 20 and 40 vol. % of  $\text{PbNb}_{0.01}[\text{Zr}_x\text{Ti}_{(0.99-x)}]\text{O}_3$  ceramic filler.

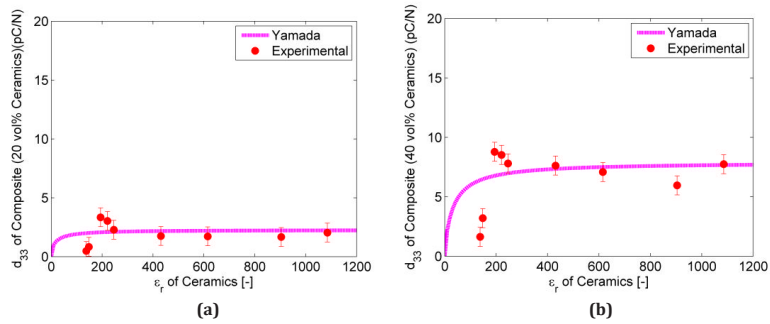


Figure 5.7: Variation of room temperature piezoelectric charge constant ( $d_{33}$ ) of 0-3 composites as a function of filler dielectric constant for (a) 20 vol. % and (b) 40 vol. % of  $\text{PbNb}_{0.01}[\text{Zr}_x\text{Ti}_{(0.99-x)}]\text{O}_3$  ceramic filler.

The piezoelectric voltage constant ( $g_{33}$ ) of the composites as a function of Zr mol% in PZT filler material is shown in Figure 5.15. The  $g_{33}$  values were obtained by taking the ratio of  $d_{33}$  and  $\epsilon_{r33}$  and it range from 11 to 42 mV.m/N, depending on the

vol. % of ceramic filler and composition. The highest value of 42 mV.m/N was obtained or the composite with 40 vol. % of PT ceramic filler. The reason behind the highest voltage sensitivity for PT composites can be attributed to the moderately high  $d_{33}$  and relatively lower dielectric constant of PT ceramic filler compared to that of its MPB counterpart.

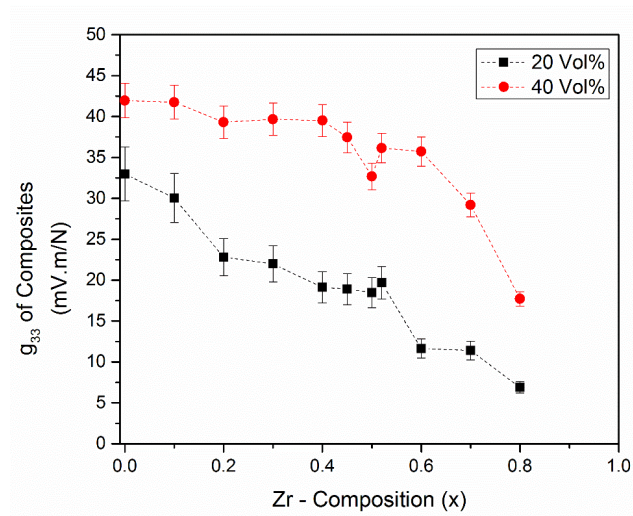


Figure 5.15: Variation of room temperature piezoelectric voltage coefficient ( $g_{33}$ ) of 0-3 Composites for 20 and 40 vol. % of  $\text{PbNb}_{0.01}[\text{Zr}_x\text{Ti}_{(0.99-x)}]\text{O}_3$  ceramic filler.

Finally we report the effect of large number of cyclic electric field loading on the polarisation behaviour of 40 vol. % PZT-0 and 40 vol. % MPB composites. The Figure 5.16 shows that for both systems the polarisation remains more or less constant with number of cycles.

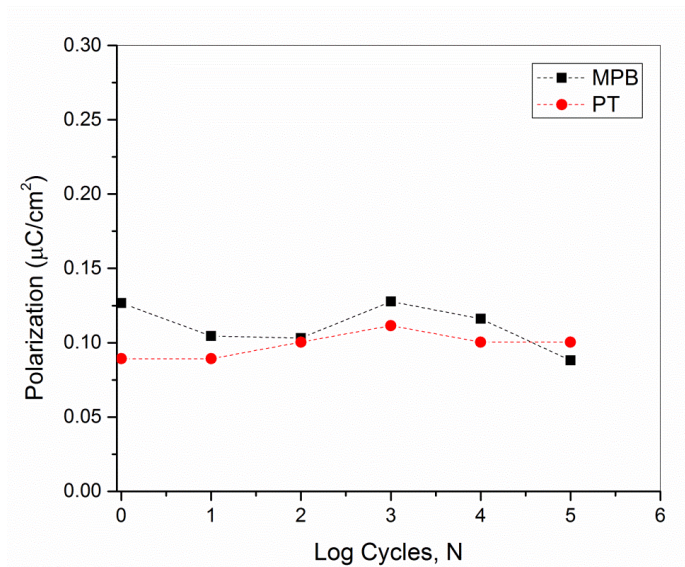


Figure 5. 16: Polarization fatigue of 0-3 composites with 40 vol. % of PT and MPB based ceramic filler.

As shown in Figure 5.11 and 5.13, the difference between the dielectric and piezoelectric properties of MPB and non-MPB based composites were not as significant as their sintered ceramics as shown in Figure 5.7. With the unique combination of low dielectric constant and moderately high  $d_{33}$ , composites with PT ceramic fillers exhibited a higher  $g_{33}$  than that of its MPB and close to MPB counterparts (see Figure 5.15). In addition, the poor sinterability associated with sintered ceramics was not an area of concern in case of composites, since the composites made of calcined ceramic filler particles. Based on this investigation, it can be concluded that composites with non PZT ceramic particulates (tetragonal side of the phase diagram) composites exhibit better piezoelectric charge constant and voltage coefficient together with superior electric fatigue properties.

## 5.4 Conclusions

The piezoelectric and dielectric properties of the ceramics for the complete set of the PZT compositions in their phase diagram has been reported systematically. The processing window of PZT based piezoelectric composites has been opened to the Non-MPB region of the phase diagram and a material selection criteria for developing high  $g_{33}$  composites has been proposed. The effect of filler properties of PZT compositions on the effective properties of the composites has been studied using theoretical models. Furthermore, the unique combination of low dielectric constant and moderately high  $d_{33}$  ceramic filler selection criteria can be also applied to lead-free piezoelectric composites for having composites with high sensorial properties.

## References

- [1] B. Jaffe, W. R. Cook Jr and H. Jaffe, "*Piezoelectric ceramics*" vol. 3: Elsevier, 2012.
- [2] A. J. Moulson and J. M. Herbert, "Piezoelectric ceramics," *Electroceramics: Materials, Properties, Applications, Second Edition*, pp. 339-410, 2003.
- [3] B. Noheda, D. Cox, G. Shirane, J. Gonzalo, L. Cross, and S. E. Park, "A monoclinic ferroelectric phase in the Pb (Zr<sub>1-x</sub>Ti<sub>x</sub>)O<sub>3</sub> solid solution," *Applied Physics Letters*, vol. 74, pp. 2059-2061, 1999.
- [4] J. F. Tressler, S. Alkoy and R. E. Newnham, "Piezoelectric sensors and sensor materials," *Journal of Electroceramics*, vol. 2, pp. 257-272, 1998.
- [5] S. Y. Chu, T. Y. Chen, I. T. Tsai, and W. Water, "Doping effects of Nb additives on the piezoelectric and dielectric properties of PZT ceramics and its application on SAW device," *Sensors and Actuators A: Physical*, vol. 113, pp. 198-203, 2004.
- [6] C. Bowen and V. Y. Topolov, "Piezoelectric sensitivity of PbTiO<sub>3</sub> based ceramic/polymer composites with 0-3 and 3-3 connectivity," *Acta Materialia*, vol. 51, pp. 4965-4976, 2003.
- [7] R. E. Newnham, "Composite electroceramics," *Ferroelectrics*, vol. 68, pp. 1-32, 1986.

- [8] S. Y. Chu, T. Y. Chen, I. T. Tsai and W. Water, "Doping effects of Nb additives on the piezoelectric and dielectric properties of PZT ceramics and its application on SAW device," *Sensors and Actuators A: Physical*, vol. 113, pp. 198-203, 2004.
- [9] M. C. Araújo, C. Costa and S. Lanceros-Méndez, "Evaluation of dielectric models for ceramic/polymer composites: Effect of filler size and concentration," *Journal of Non-Crystalline Solids*, vol. 387, pp. 6-15, 2014.
- [10] T. Yamada, T. Ueda and T. Kitayama, "Piezoelectricity of a high-content lead zirconate titanate/polymer composite," *Journal of Applied Physics*, vol. 53, pp. 4328-4332, 1982.
- [11] N. K. James, D. A. van den Ende, U. Lafont, S. van der Zwaag and W. A. Groen, "Piezoelectric and mechanical properties of structured PZT-epoxy composites," *Journal of Materials Research*, vol. 28, pp. 635-641, 2013.
- [12] N. K. James, U. Lafont, S. van der Zwaag and W. A. Groen, "Piezoelectric and mechanical properties of fatigue resistant, self-healing PZT-ionomer composites," *Smart Materials and Structures*, vol. 23, p. 055001, 2014.
- [13] H. Khanbareh, S. van der Zwaag and W. A. Groen, "Effect of dielectrophoretic structuring on piezoelectric and pyroelectric properties of lead titanate-epoxy composites," *Smart Materials and Structures*, vol. 23, p. 105030, 2014.
- [14] A. Boutarfaia, "Investigations of co-existence region in lead zirconate-titanate solid solutions: X-ray diffraction studies," *Ceramics International*, vol. 26, pp. 583-587, 2000.
- [15] A. Boutarfaia, C. Boudaren, A. Mousser and S. Bouaoud, "Study of phase transition line of PZT ceramics by X-ray diffraction," *Ceramics International*, vol. 21, pp. 391-394, 1995.
- [16] A. Boutarfaia, "Study of the solid state reaction and the morphotropic phase boundary in  $\text{Pb}(\text{Zr,Ti})\text{O}_3\text{-Pb}(\text{Fe}_{1/5},\text{Ni}_{1/5},\text{Sb}_{3/5})\text{O}_3$  ceramics," *Ceramics International*, vol. 27, pp. 91-97, 2001.
- [17] S. Fushimi and T. Ikeda, "Phase equilibrium in the system  $\text{PbO-TiO}_2\text{-ZrO}_2$ ," *Journal of the American Ceramic Society*, vol. 50, pp. 129-132, 1967.
- [18] A. Safari and E. K. Akdogan, "Piezoelectric and acoustic materials for transducer applications," Springer, 2008.

- [19] N. Vittayakorn, G. Rujijanagul, T. Tunkasiri, X. Tan and D. P. Cann, "Perovskite phase formation and ferroelectric properties of the lead nickel niobate–lead zinc niobate–lead zirconate titanate ternary system," *Journal of Materials Research*, vol. 18, pp. 2882-2889, 2003.
- [20] D. S. Lee, C. W. Ahn, I. W. Kim, H. Y. Choi and Y. H. Jeong, "The sintering behavior and piezoelectric properties of  $\text{Pb}(\text{Ni}_{1/3}\text{Nb}_{2/3})\text{O}_3\text{-PbTiO}_3\text{-PbZrO}_3$  ceramics using two-step calcination," *Journal of Korean Physics Society*, p. S1215, 2003.
- [21] A. Prasatkhetragarn, N. Triamnak, R. Yimnirun and D. Cann, "Morphotropic Phase Boundary of  $0.875\text{Pb}(\text{Zr}_x\text{Ti}_{1-x})\text{O}_3\text{-}0.125\text{Pb}(\text{Mg}_{1/3}\text{Nb}_{2/3})\text{O}_3$  Ceramics," *Ferroelectrics*, vol. 470, pp. 280-286, 2014.
- [22] K. H. Yoon and H. R. Lee, "Electric-field induced strain and piezoelectric properties near the morphotropic phase boundary of  $\text{Pb}(\text{Mg}_{1/3}\text{Nb}_{2/3})\text{O}_3\text{-PbZrO}_3\text{-PbTiO}_3$  ceramics," *Journal of Applied Physics*, vol. 89, pp. 3915-3919, 2001.
- [23] J. Holterman and P. Groen, "*Piezoelectric Materials and Applications*," Apeldoorn (The Netherlands): Stichting Applied Piezo, 2012.
- [24] Y. Cao, G. Sheng, J. X. Zhang, S. Choudhury, Y. L. Li and Randall, "Piezoelectric response of single-crystal  $\text{PbZr}_{1-x}\text{Ti}_x\text{O}_3$  near morphotropic phase boundary predicted by phase-field simulation," *Applied Physics Letters*, vol. 97, pp. 252904:1-3, 2010.
- [25] R. Waser, *Nanoelectronics and information technology*: John Wiley & Sons, 2012.
- [26] M. Wang, M. Huang, T. Wong and N. Wu, "Sintering and piezoelectric properties of  $\text{Pb}(\text{Ni}_{1/3}\text{Sb}_{2/3})\text{O}_3\text{-PbZrO}_3\text{-PbTiO}_3$  ceramics," *Journal of Materials Science*, vol. 37, pp. 663-668, 2002.
- [27] B. Chambion, L. Goujon, L. Badie, Y. Mugnier, C. Barthod and C. Galez, "Optimization of the piezoelectric response of 0–3 composites: a modeling approach," *Smart Materials and Structures*, vol. 20, p. 115006, 2011.



## CHAPTER 6

### **Structured and unstructured Lead-free (K, Na)<sub>x</sub>Li<sub>1-x</sub>NbO<sub>3</sub> (KNN) piezoelectric ceramic – epoxy composites with a high piezoelectric voltage coefficient**

---



## 6.1 Introduction

Piezoelectric materials are an indispensable part of ultrasonic sensors utilized in medical diagnostics, industrial automation, defence and communication systems. Piezoelectric materials are also used in emerging fields such as micro motors, self-powered sensors and high power transformers. Lead zirconate titanate (PZT) based ceramics dominate the market of piezoelectric materials because of their excellent piezoelectric properties, their flexibility in terms of compositional modifications to fine tune the properties depending on the applications and finally the fact that they can be produced on a large scale [1, 2]. However, the high lead content (60 wt. % of PbO) in PZT materials has generated environmental concerns and PZT is therefore mentioned in governmental regulations dealing with hazardous substances [3]. Extensive research has been conducted on the development of lead-free piezoelectric materials with an adequate piezoelectric coefficient and an electromechanical coupling factor [3-6]. Among various possible material choices, the most widely investigated lead-free systems are  $K_{1-x}Na_xNbO_3$  (KNN),  $Na_{0.5}Bi_{0.5}TiO_3$  (BNT) and  $BaTiO_3$  (BT) based materials [3, 4, 6]. Among these,  $K_{1-x}Na_xNbO_3$  (KNN) is considered to be the best suitable lead-free candidate to replace PZT [7, 8] notwithstanding its properties being somewhat lower. The Curie temperature ( $T_c \sim 350-400$  °C) of KNN based lead-free piezoelectric ceramics are comparable with PZT ceramics.

The piezoelectric and dielectric properties of KNN ceramics as a function of its composition have been investigated extensively [7, 9]. The composition near  $x=0.6$  is of great interest because of optimal piezoelectric and dielectric properties due to the composition being on the polymorphic phase boundary between two orthorhombic phases. The biggest problem towards commercial application is its poor sinterability. The high volatility of alkali metals at temperatures higher than 1100 °C leads to sintered ceramics with a relatively low density and hence rather poor piezoelectric and dielectric properties. The natural cubical shape of KNN grains also contributes to this problem as a high packing density is difficult to achieve with such a particle shape [10]. A significant number of dopants on both A and B sites as well as different solid solutions have been studied in order to improve the piezoelectric properties of KNN.

Among this, Li doped KNN  $(\text{K, Na})_{x}\text{Li}_{1-x}\text{NbO}_3$  ceramics shows a significant improvement in piezoelectric properties ( $d_{33} - 235 \text{ pC/N}$ ) at the phase boundary of orthogonal and tetragonal crystal structure within the range of  $0.05 < x < 0.07$  [11]. In the remainder of this work we will focus on the Li-doped KNN only.

Monolithic piezoceramics are vulnerable to breakage during handling and bonding process due to their inherent brittle nature and are difficult to conform to curved surfaces. Their relatively high density and low failure strain are another factor limiting their applications in light weight flexible structures. Piezoelectric polymers on the other hand are flexible and relatively insensitive to mechanical damage. However, their poor thermal stability and poor actuation capability limit their application [12]. Sheets of composites consisting of granular (typical particle size  $1\text{-}5\mu\text{m}$ ) piezoelectric ceramics in a piezoelectrically inert yet mechanically optimized polymer matrix have been suggested as an alternative material concept to overcome these problems. While the piezoelectric charge coefficient ( $d_{33}$ ), which is a measure for its actuation potential, of such composites will be small in comparison to that of a monolithic ceramic, the piezoelectric voltage coefficient ( $g_{33}$  or  $d_{33}/\epsilon$ ), which is a measure of the sensorial potential, can be high and even higher than that of a monolithic ceramic. This inversion in relative performance is due to the very low dielectric constant of the polymer matrix.

The primary parameter to optimize the combination of the sensorial and mechanical properties for a given set of selected component materials is of course the volume fraction of the piezoelectric granulates. However, at a fixed volume fraction of granulate, the piezoelectric properties can be improved further by structuring, i.e. creating 'chain-like' assemblies in the composite perpendicular to the sheet surface as discussed in chapter 2 [13]. The improvement in sensorial behaviour is due to the reduction in interparticle spacing (and hence increase in charge transfer) in the direction of the applied load or electrical field [13]. For well developed 'chains' the topology of such composites approaches that of very expensive composites based on perfectly aligned fibres with a length equal to the electrode distance [12]. While the piezoelectric properties of such 'quasi' 1-3 composites will remain below those of

'real' 1-3 fibrous composites, the bending and stretching fatigue behaviour of the quasi- 1-3 composites is far superior [13, 14].

In chapter 2 it was shown that dielectrophoresis (DEP), i.e. the application of an alternating frequency electrical field on the composite while the (thermoset) polymer is still in its uncured, low-viscosity stage, is a very suitable and cost effective technique to generate such 'structured' composites containing chain-like assemblies of functional granular ceramics. To date, such DEP structured (PZT-epoxy) composites have always been based on rough, more or less equiaxed particles, which, on the micro scale, have a rather poor stacking potential in comparison to cubic particles.

In the present work we will therefore study the structuring behaviour of almost perfect cubic KNN particles produced via a new processing route in a well-studied epoxy system [the same epoxy used in chapters 2 & 5] with the intention of making optimal use of the attractive properties and shape of the KNN piezoceramic particles in order to obtain structured composites with outstanding sensorial properties.

## 6.2 Theory

The ceramic-particle polymer-matrix composites can be regarded as a heterogeneous system of two different constituents and many theoretical models have been proposed to predict the effective dielectric constant by accounting the morphology of the constituents and its volume fraction. Also factors like polymer-ceramic interface and ceramic-to-ceramic connectivity significantly affect the dielectric properties of the composites. Yamada et al., proposed a model to explain the behaviour of the permittivity, piezoelectric constant and elastic constant of a composite in which ellipsoidal particles are dispersed in a continuous medium aligned along the electric field [15]. Their model shows excellent agreement with experimental data reported in the literature. The key equations in the Yamada model

for the dielectric constant and the piezoelectric charge coefficient are given by Eq. 6.1 and 6.2 respectively.

$$\varepsilon_c = \varepsilon_1 \left( 1 + \frac{n\varphi(\varepsilon_2 - \varepsilon_1)}{n\varepsilon_1 + (\varepsilon_2 - \varepsilon_1)(1 - \varphi)} \right) \quad (6.1)$$

$$d_{33} = \frac{\varphi \alpha n \varepsilon_c d_{33_2}}{n\varepsilon_c + (\varepsilon_2 - \varepsilon_c)} \quad (6.2)$$

where  $\varepsilon_c$  and  $d_{33}$  are the dielectric constant and piezoelectric charge constant of the composite (subscript c) and the matrix (subscript 1) and the ceramic filler fraction (subscript 2) respectively,  $\varphi$  is the volume fraction of the ceramic and  $n$  is the inverse of the depolarization factor for an ellipsoidal particle in the direction of the applied electric field.

Bowen et al., [16] proposed an analytical model (6.3) to predict the effective dielectric constant of dielectrophoretically fully structured composites by assuming the system as a collection of one dimensional chains of particles separated by polymer gaps and the final equation is given by,

$$\varepsilon_{DEP} = \varphi \left( \frac{R\varepsilon_1\varepsilon_2}{\varepsilon_2 + R\varepsilon_1} \right) + (1 - \varphi)\varepsilon_1 \quad (6.3)$$

where  $R$  is the average particle size divided by interparticle distance and the other parameter have the just defined meaning [16].

In a similar way, Van den Ende et al. [13], analysed the electromechanical representation of structured piezoelectric materials as that of two capacitors in series in the electrical domain and two springs in the mechanical domain leading to an effective piezoelectric charge coefficient for the composite  $d_{33DEP}$  given by

$$d_{33_{DEF}}^d = \frac{(1+R)^2 \varepsilon_1 \varphi Y_{33_2} d_{33_2}}{(\varepsilon_2 + R\varepsilon_1)[(1+R\varphi)Y_{33_2} + (1-\varphi)RY_1]} \quad (6.4)$$

where  $Y_1$  and  $Y_{33_2}$  are the elastic moduli of the polymer matrix and that of the ceramic in the direction of chains.

### 6.3 Experimental

The KNN ceramic powder was prepared through a conventional solid state reaction route. Stoichiometric proportions of  $K_2CO_3$ ,  $Na_2CO_3$ ,  $Li_2CO_3$  and  $Nb_2O_5$  (>99.9%) powders were mixed in a polypropylene jar with zirconia balls of 5 mm diameter in cyclohexane for 3 h. The slurry was then dried in a hot air oven for 24 hrs and the homogeneously mixed powder was calcined at either 1000 or 1050 °C for three hours in a programmable Nabertherm muffle furnace with an heating rate of 5 °C/min and furnace cooling . After the first calcination at the higher temperature, the powder was ball milled for 3 hrs to refine the particle size and a second calcination treatment was performed at 900, 925, 950 or 975 °C for times of 10, 20, 30 or 40 hrs with the heating rate was 1°C/min. After the second calcination the powder was ultrasonicated for 1h in cyclohexane medium to break up agglomerates. Such powder was dried at 150 °C for 24 hrs and kept in an air ventilated drying oven to avoid moisture absorption. The crystal structure and the phase purity of the double-calcined powder were investigated with a Bruker D8 diffractometer (Germany) using  $CoK\alpha_1$  X-rays. The particle size distribution and particle morphology of  $(K, Na)_xLi_{1-x}NbO_3$  ;  $x=0.06$  calcined powders prepared by different processing route were analysed using Particle size analyzer (Beckman Coulter) and scanning electron microscopy (JEOL JSM-7500F).

For the polymer matrix a two component epoxy system, (Epotek 302-3M, Epoxy Technology Inc., Billerica, MA, USA) based on diglycidyl ether bisphenol-A (DGEBA) resin and poly (oxypropyl) -diamine (POPD) multifunctional aliphatic amine curing agent was used. The chemical structures of the components were depicted in

chapter 2 (Figure 2.1). As per the manufactures' data sheet the system exhibit a viscosity of 0.8-1.6 Pa.s after mixing and at room temperature (25 °C). This relatively high viscosity of the matrix prevents quick settling of dense ceramic particles during dielectrophoresis. The epoxy resin and ceramic particles were mixed together using a high speed mixer (Speed Mixer DAC 150 FVZ) at 3000 rpm for 3 min after which the hardener was added and the composite resin was mixed again at 3000 rpm for 5 min followed by degassing in vacuum for 10 min. The structured KNN- polymer composite were prepared by applying an alternating (1 kV/mm) voltage at 1.5 kHz across the suspension of ceramic particles in the epoxy matrix during the entire pre-curing stage at room temperature. Unstructured (0-3) reference samples were also prepared from the same batch of composite slurry and cured in a different mould without any structuring field being applied. The room temperature cured circular disc shaped samples of dimension 16 mm x 0.5 mm were fine polished on both sides and post cured at 100 °C for 1h. The cross-sections of the structured and 0-3 composites were analysed using a scanning electron microscope and computed X-ray tomography. Test samples were electroded on both sides by gold sputtering for electrical property measurements. The samples were poled at 80 °C in a circulating oil bath. The dielectric constant of the composites was measured using the using an Agilent 4263B LCR meter based on the parallel plate capacitor method at 1V and 1 kHz. The thickness mode piezoelectric charge constant,  $d_{33}$ , was measured using a Berlincourt type  $d_{33}$  meter (PM300, PiezoTest), set to 110Hz. The piezoelectric voltage constant,  $g_{33}$ , was calculated via the relation:  $g_{33} = d_{33}/\epsilon_r \cdot \epsilon_0$ .

## 6.4 Results and discussion

### 6.4.1 Optimization of calcination process

The two-step calcination procedure was optimized to form phase pure  $(K, Na)_xLi_{1-x}NbO_3$  ceramic particle having a cubic particle morphology. Figure 6.1 shows the optimized calcination profile. The first high temperature calcination step was used to form the crystal structure without any secondary phases. During the

second crystallization at a slightly lower temperature and a longer time, the sub-micron size particles crystallize together and form micron size cubical particles. This route was based on the earlier double calcination treatment developed by Gao et al. which only optimized the morphology [9]. In their process route crystallization and phase formation of KNN powder took place in the final sintering step at the higher temperature and hence the piezoelectric properties and crystal structure were inferior to those of bulk sintered ceramics using conventionally calcined powder. In the present study, the prolonged second calcination at the lower temperature leads to a complete phase formation and well-defined cubical particles.

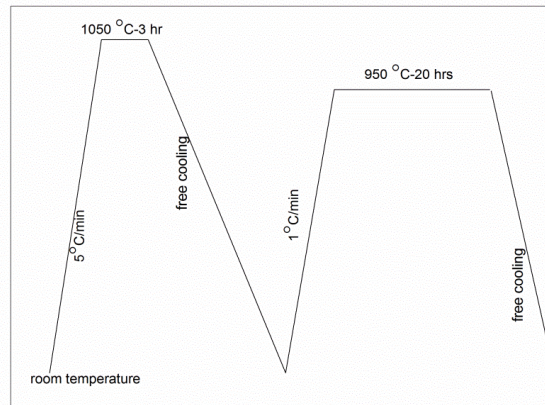


**Figure 6. 1: Optimized calcination profile employed to prepare the ceramic powder.**

Figure 6.2 shows the XRD patterns of KNN system prepared via different calcination schemes. All KNN powders showed the formation of a pure a Perovskite phase except the one calcined at 900 °C for 3 hrs. The powder calcined at 1000 and 1050 °C for 3 hrs was chosen for further milling and second calcination to improve the particle morphology and size distribution. The sharp crystalline peaks observed in the double calcined XRD pattern confirm the creation of a single well-developed crystalline phase.

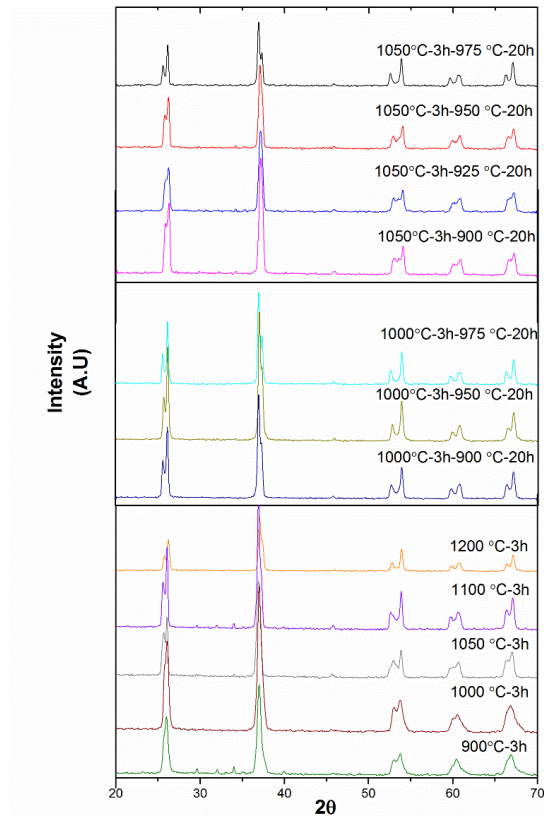


Figure 6. 2: XRD of KNN powder prepared through different calcination schemes.

SEM micrographs of the various powders produced are shown in Figure 6.3. The SEM micrographs reveal that the KNN particles processed by single step calcination have a bi-modal particle size distribution with particle size ranging from 0.5 - 3 $\mu$ m size. The powder processed at 1100 and 1200 °C for 3 hrs has big agglomerates which indicates that at 1100 °C and above [Figure 6.3(c)] the particles slowly start to sinter. Many studies reported that the sintering temperature of KNN ceramics is around 1100-1200 °C for 3 hrs either by hot pressing or normal sintering [10, 17, 18]. The

---

#### 6.4 Results and discussion

KNN powders processed through double calcination [Figure 6.3 (d) and (E)] procedure possess quite uniformly distributed grains whose average size is 1-2  $\mu\text{m}$  and 2-3  $\mu\text{m}$  for 900  $^{\circ}\text{C}$  and 950  $^{\circ}\text{C}$  for 20 hrs second calcination respectively. The one processed with the second calcination at 950  $^{\circ}\text{C}$  for 20 hrs shows well-faceted quite cubic particles. Table 6.1 summarises the effect of the different calcination temperatures on the particle size distribution. From this, it is clear that the second calcination step makes the submicron particles grow into 2-3  $\mu\text{m}$  cubic particles.

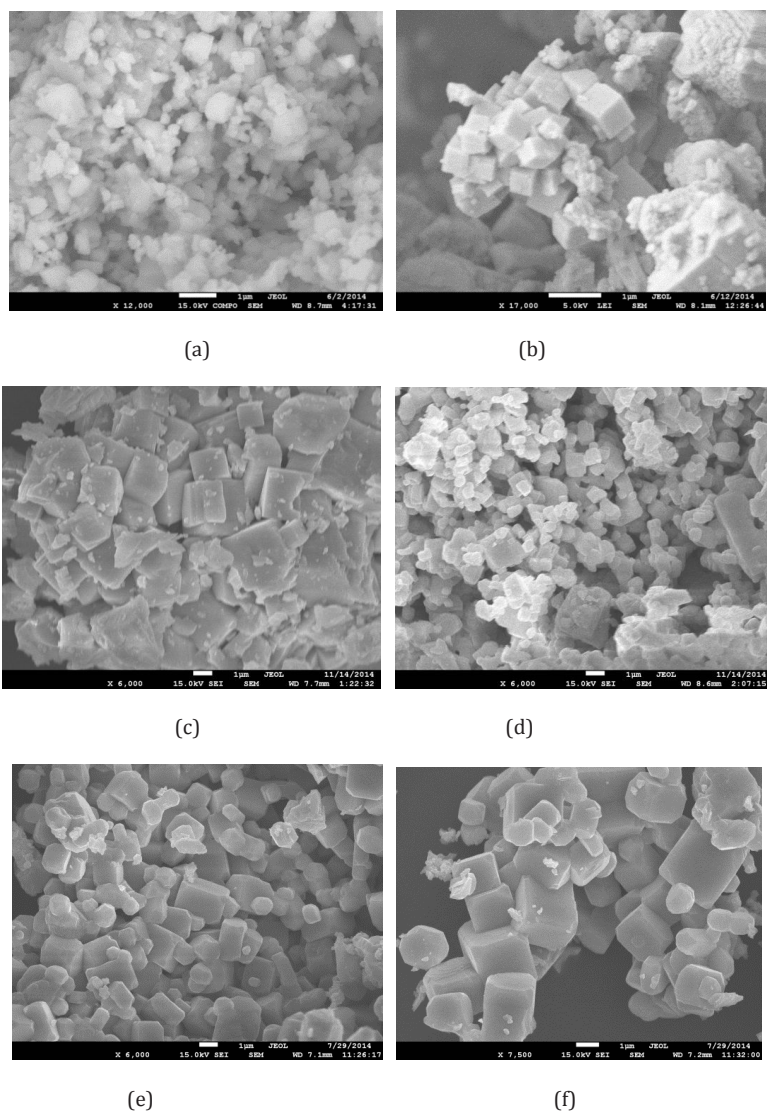


Figure 6. 3: Scanning Electron Micrograph of KNN particles processed at (a) 900-3h,(b) 1000-3h (c) 1100-3h (d) 1000 + 900 (20h) (e) 1050 + 950 (20h) (f) Higher magnified image of 1050 + 950 (20h).

**Table 6.1 Particle Size distribution of KNN ceramic particles calcined at different conditions.**

Processing condition	$d_{10}$ ( $\mu\text{m}$ )	$d_{50}$ ( $\mu\text{m}$ )	$d_{90}$ ( $\mu\text{m}$ )
900 °C -3h	0.6	1.3	4.6
1000 °C -3h	1.2	3.1	10.1
1100 °C -3h	4.9	51	120
1000 °C -3h + 950 °C -20h	1.3	2.2	4.3
1050 °C -3h + 950 °C -20h	1.8	3.7	9.6

#### 6.4.2 Microstructure

Figure 6.4(a) shows an X-ray tomographic image of dielectrophoretically structured KNN-epoxy composite having a KNN volume fraction of 10 %. Earlier work [13, 19] has shown that this volume fraction yields the optimal  $g_{33}$  value. At lower volume fractions the amount of active material is too low and at higher volume fractions the chain structure develops less well. The tomographic cross section shows the formation of well-developed chains in the DEP structured sample spanning the entire sample thickness of 1 mm. The typical effective width of a chain is about 1-2  $\mu\text{m}$  (i.e. one particle wide) and the average distance between the chains in lateral direction is of the order of 10  $\mu\text{m}$ . The extent and topological quality of the chains is much higher than that reported earlier for structured composites based on equiaxed PZT particles [13, 14]. The SEM images (Figure 6.4 (b) & (c)) of carefully polished cross sections confirm the presence of well-developed chains. In the 2D cross section the chains seem to be discontinuous along the length but this stereographic artefact is due to the chain not being exactly in the plane of the cross section. Figure. 6.4 (c) shows highly magnified image of a structured KNN chain which indicates a good arrangement of the particles. It should be mentioned that the particle arrangement is not perfect everywhere along the chain but many high perfection sections were

encountered. A mathematical model analysing the effect of topological packing defects on macroscopic piezo electric properties has been developed suggesting that the current imperfections lead to a reduction of about 20% in the macroscopic properties in comparison to a perfectly configured chain [20]. Finally, figure 6. 4 (d) shows a similar cross section but for a non-structured composite and shows that the epoxy wets the KNN particles well and as a result that there is no spontaneous agglomeration.

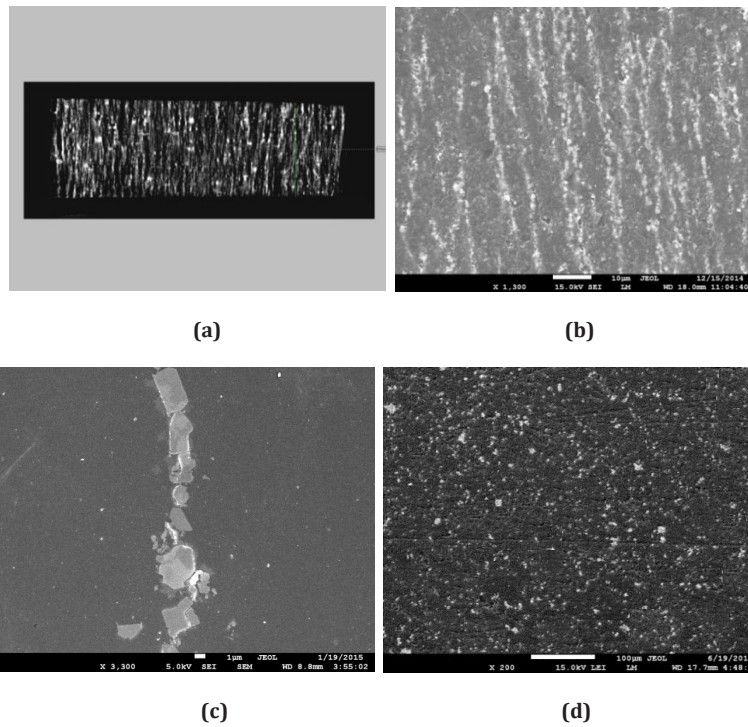


Figure 6. 4: (a) Tomography image of DEP aligned 5 vol. % KNN -epoxy composite (b) SEM image of aligned composite (c) Magnified image of KNN column (d) SEM image of random composite.

Figure 6.5 shows the variation of  $d_{33}$  of 10 vol. % structured composites prepared using KNN powder synthesized via different processing routes. Longer time second

calcination (<20 hrs) results in inferior piezoelectric properties which is due to the poor structuring of agglomerated KNN particles and the evaporation of alkaline metals which leads to inferior piezoelectric properties of KNN granules. The same facts prevents the further property improvement in the second calcination step. Table 6.2. present the piezoelectric charge and voltage coefficient for 10 vol. % structured composites for the same structuring conditions but with KNN ceramic powder processed through different processing route. It is clear that the piezoelectric charge and voltage constant for double calcined powder are almost double compared to those produced with a single step calcination.

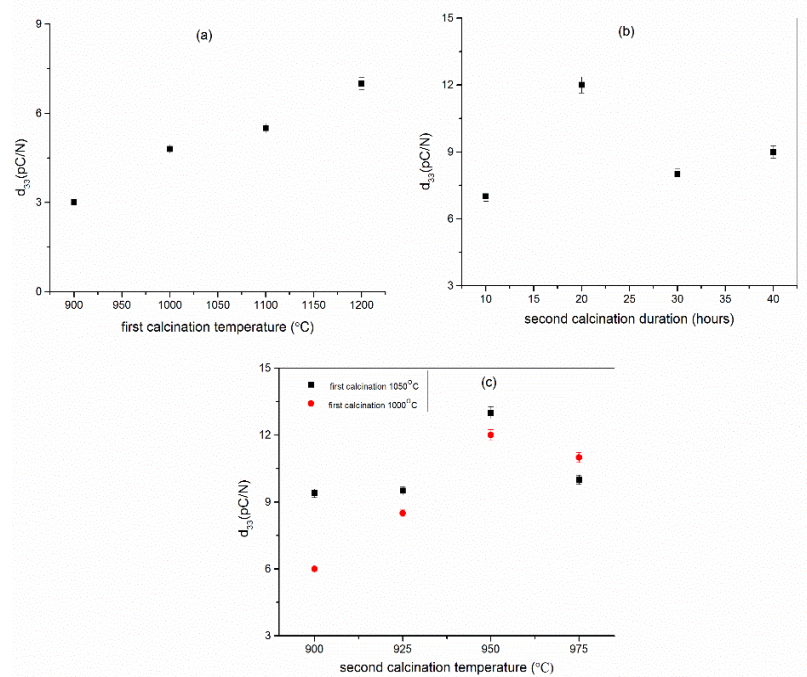


Figure 6.5:  $d_{33}$  values of 10 vol. % structured composites with KNN prepared via different routes

**Table 6.2: Variation of  $d_{33}$  of 10 vol. % structured composited with KNN prepared via different routes**

Processing condition	$d_{33}$ (pC/N)	$g_{33}$ (mV.m/N)
900 °C -3h	3	36
1000 °C -3h	4.8	42
1100 °C -3h	5.5	45
1200 °C -3h	7	65
1000 °C -3h + 900 °C -20h	6	58
1000 °C -3 + 925 °C -20h	8.5	85
1000 °C -3h + 950 °C -20h	12	98
1000 °C -3h + 975 °C -20h	11	83
1050 °C -3h + 900 °C -20h	9.4	89
1050 °C -3h + 925 °C -20h	9.5	100
1050 °C -3h + 950 °C -20h	13	118
1050 °C -3h + 975 °C -20h	10	106
1000 °C -3h + 950 °C -10h	7	74
1000 °C -3h + 950 °C -30h	8	82
1000 °C -3h + 950 °C -40h	9	105

#### 6.4.3 Dielectric and piezoelectric properties

Figure 6.6. shows the variation of dielectric constant of 0-3 and structured composites as function of KNN content along with the theoretical dependences. The dielectric constant of the neat epoxy and KNN ceramic phases were taken as 4.3 and 500 respectively. The experimental dielectric constants of the 0-3 composites fit to the Yamada model when assuming a depolarization factor  $n=5$  (i.e. slightly elongated particles) while a value of  $n=3$  would correspond to equiaxed (spherical) particles. At higher KNN ceramic loading fractions, the individual ceramic particulates are not always fully shielded by the polymer matrix. Therefore, at higher volume fractions the

composite develop a weak 1-3 composite character, leading to a higher dielectric constant as is indeed observed. The dielectrophoretically structured composites exhibit higher dielectric constant than the corresponding randomly dispersed (0-3) composites. The experimental values for the structured composites are compared to the Bowen model assuming inter-particle distances (ip) values along the chain ranging from 0.10 to 0.20  $\mu\text{m}$ . The experimental dielectric constant of the structured composite more or less matches for dielectric constant predicted by Bowen's model for an inter-particle distance,  $ip = 0.15\mu\text{m}$ . Such a small inter-particle distance is an attractive feature indicating the potential to get close to ideal piezoelectric properties. The inter-particle distance found here is clearly smaller than the value reported for structured PZT-epoxy composites. [13, 14, 21].

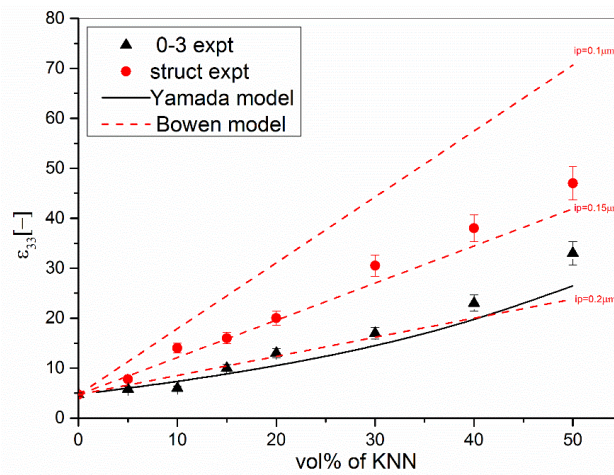


**Figure 6.6:** Variations of dielectric constant of the composite compared with theoretical models as a function of KNN volume fraction in epoxy matrix.

The piezoelectric charge constant ( $d_{33}$ ) of both structured and 0-3 KNN-epoxy composites fraction of KNN is shown in Figure 6.6. The  $d_{33}$  values for the unstructured 0-3 composites correlate well with values predicted by Yamada's model when using the same depolarization factor,  $n=5$ , as in the fitting of the dielectric data (Figure 6.6). The experimental values of  $d_{33}$  for the structured composites are compared with the model proposed by Van den Ende et al., [13] for different inter-particle distances

ranging from 0.20 to 0.10  $\mu\text{m}$ . As observed in the dielectric constant data for structured composite, the piezoelectric charge coefficient  $d_{33}$  also correlate well to the predicted values using the inter-particle distance,  $i_p = 0.15 \mu\text{m}$ . There seems to be a very good internal consistency in the data and the models.

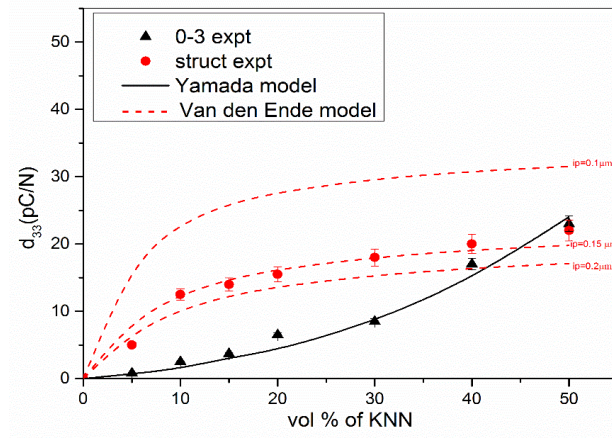


Figure 6.7: Variations of piezoelectric charge coefficient of the composite compared with theoretical models as a function of KNN volume fraction in epoxy matrix.

Finally the change in piezoelectric voltage coefficient ( $g_{33}$ ) as a function of KNN volume fraction for structured and unstructured composites is presented in Figure 6.8. The effective piezoelectric voltage coefficient of the composite results from a competition between the increase in  $d_{33}$  and the lowering of the dielectric constant of the composite. To obtain a high  $g_{33}$  value the dielectric constant should be as low as possible and at the same time the piezoelectric charge coefficient should be as high as possible. The bulk sintered KNN ceramics have a low dielectric constant approximately 500 contributing to a high  $g_{33}$  value around 50  $\text{mV}\cdot\text{m}/\text{N}$ . Figure 6.8 indicates that the  $g_{33}$  values for the (structured and unstructured) composites with a higher volume fraction nicely converge to the value of the bulk KNN material, From Figure 6.8 it is clear that the optimum KNN filler fraction for the highest  $g_{33}$  is 10 vol. %. At 10 vol. % KNN, the structured composite exhibits a  $g_{33}$  of around 118  $\text{mV}\cdot\text{m}/\text{N}$ .

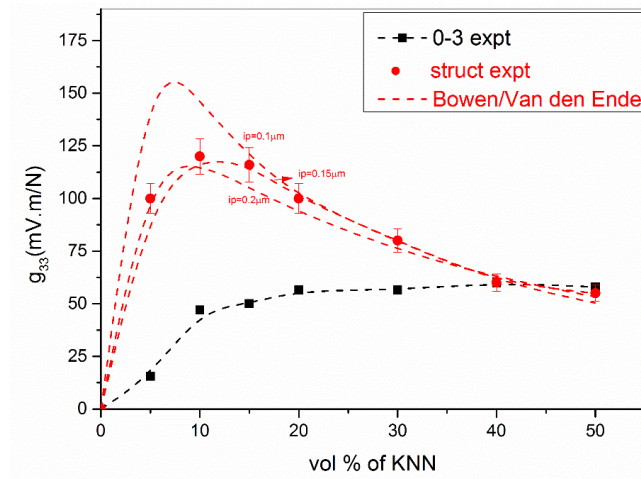


Figure 6.8: Variations of piezoelectric voltage coefficient of the composite as a function of KNN volume fraction in epoxy matrix.

Table 6.3 presents piezoelectric and dielectric properties for particulate piezoceramic composites reported recently in the literature. It is clear that the piezoelectric voltage coefficient of 10 vol % structured KNN-epoxy composites exceed those of all similar other systems. The high  $g_{33}$  value of the structured composite is due to the combination of the perfect cubic morphology of the particles, the well-developed chain formation for the dielectrophoretic conditions applied and the low dielectric constant of the KNN ceramic itself and the smaller inter-particle distance between the particles within the chain. Higher values of  $g_{33}$  are possible in case the formation of topological defects along the chains is reduced by a further improvement of particle morphology and size uniformity.

**Table 6. 3. Comparison of piezoelectric and dielectric properties of composites**

Composite	$d_{33}$ (pC/ N)	$\epsilon_{33}$ (-)	$g_{33}$ (mV.m/ N)	Ref.
Structured epoxy/0.2PT	8.5	11.2	85	[21]
Structured epoxy/0.1PZT507	6	8	65	[15]
Structured epoxy/0.1PZT5A4	7.5	10	77	[13]
<b>Structured epoxy/0.1KNN</b>	<b>13</b>	<b>13</b>	<b>118</b>	[Present Work]
LCT/PA/0.5PZT	73	42	65	[22]
PA/0.5PZT	28	68	48	[22]
LCT/0.4PZT	13	30	48	[23]
Epoxy/0.685 PZT	50	$\frac{12}{0}$	47	[24]
PVDF/0.7PZT	26	$\frac{10}{0}$	30	[25]
PVDF/0.67PZT	48	$\frac{15}{2}$	36	[15]
PVDF/0.5PZT (Hot press)	14	95	16	[26]
PVDF/0.5 PZT (solution cast)	9	30	36	[26]
Ionomer-0.3PZT	5.2	9	52	[19]

## 6.5 Conclusions

A novel double step calcination process route does lead to the formation of pure, 2  $\mu\text{m}$  large cubic Li-doped KNN particles. This allows the formation of long chain like structures with small topological defects during the dielectrophoretic structuring of KNN-epoxy composites while in their uncured state. The inter-particle distance between the particles within the chain is around 0.15  $\mu\text{m}$  which is very much lower than the similar systems. The value of the piezoelectric voltage coefficient of the structured 10 vol. % structured KNN- epoxy composites also exceeds that of all values for such functional composites reported in the literature. The double calcination strategy for KNN ceramic powder in combination with a dielectrophoretic structuring process opens a new route towards lead-free piezoelectric composites with enhanced properties for sensor and energy harvesting applications.

## References

- [1] B. Jaffe, W. R. Cook Jr and H. Jaffe, "*Piezoelectric ceramics*" vol. 3: Elsevier, 2012.
- [2] A. J. Moulson and J. M. Herbert, *Electroceramics: materials, properties, applications*: John Wiley & Sons, 2003.
- [3] J. Rödel, W. Jo, K. T. Seifert, E. M. Anton, T. Granzow and D. Damjanovic, "Perspective on the Development of Lead-free Piezoceramics," *Journal of the American Ceramic Society*, vol. 92, pp. 1153-1177, 2009.
- [4] P. Panda, "Review: environmental friendly lead-free piezoelectric materials," *Journal of Materials Science*, vol. 44, pp. 5049-5062, 2009.
- [5] T. R. Shrout and S. J. Zhang, "Lead-free piezoelectric ceramics: Alternatives for PZT?," *Journal of Electroceramics*, vol. 19, pp. 113-126, 2007.
- [6] T. Takenaka, H. Nagata and Y. Hiruma, "Current developments and prospective of lead-free piezoelectric ceramics," *Japanese Journal of Applied Physics*, vol. 47, pp. 3787-3801, 2008.

- [7] E. Ringgaard and T. Wurlitzer, "Lead-free piezoceramics based on alkali niobates," *Journal of the European Ceramic Society*, vol. 25, pp. 2701-2706, 2005.
- [8] L. Zhengfa, L. Yongxiang and Z. Jiwei, "Grain growth and piezoelectric property of KNN-based lead-free ceramics," *Current Applied Physics*, vol. 11, pp. S2-S13, 2011.
- [9] R. Gao, X. Chu, Y. Huan, X. Wang and L. Li, "(K, Na) NbO<sub>3</sub> based piezoceramics prepared by a two-step calcining and ball milling route," *Materials Letters*, vol. 123, pp. 242-245, 2014.
- [10] J. F. Li, K. Wang, F. Y. Zhu, L. Q. Cheng and F. Z. Yao, "(K, Na) NbO<sub>3</sub>-Based Lead-Free Piezoceramics: Fundamental Aspects, Processing Technologies and Remaining Challenges," *Journal of the American Ceramic Society*, vol. 96, pp. 3677-3696, 2013.
- [11] Y. Guo, K. I. Kakimoto and H. Ohsato, "Phase transitional behavior and piezoelectric properties of (Na<sub>0.5</sub> K<sub>0.5</sub>)NbO<sub>3</sub>-LiNbO<sub>3</sub> ceramics," *Applied Physics Letters*, vol. 85, pp. 4121-4123, 2004.
- [12] V. F. Janas and A. Safari, "Overview of Fine-Scale Piezoelectric Ceramic/Polymer Composite Processing," *Journal of the American Ceramic Society*, vol. 78, pp. 2945-2955, 1995.
- [13] D. A. van den Ende, B. Bory, W. A. Groen and S. Van der Zwaag, "Improving the d<sub>33</sub> and g<sub>33</sub> properties of 0-3 piezoelectric composites by dielectrophoresis," *Journal of Applied Physics*, vol. 107, pp. 024107, 1-8, 2010.
- [14] N. K. James, D. A. van den Ende, U. Lafont, S. van der Zwaag and W. A. Groen, "Piezoelectric and mechanical properties of structured PZT-epoxy composites," *Journal of Materials Research*, vol. 28, pp. 635-641, 2013.
- [15] T. Yamada, T. Ueda and T. Kitayama, "Piezoelectricity of a high-content lead zirconate titanate polymer composite," *Journal of Applied Physics*, vol. 53, pp. 4328-4332, 1982.
- [16] C. Bowen, R. E. Newnham and C. Randall, "Dielectric properties of dielectrophoretically assembled particulate-polymer composites," *Journal of Materials Research*, vol. 13, pp. 205-210, 1998.

- [17] H. Birol, D. Damjanovic and N. Setter, "Preparation and characterization of  $(K_{0.5}Na_{0.5})NbO_3$  ceramics," *Journal of the European Ceramic Society*, vol. 26, pp. 861-866, 2006.
- [18] F. Rubio-Marcos, P. Ochoa and J. Fernandez, "Sintering and properties of lead-free  $(K, Na, Li)(Nb, Ta, Sb)O_3$  ceramics," *Journal of the European Ceramic Society*, vol. 27, pp. 4125-4129, 2007.
- [19] N. K. James, U. Lafont, S. van der Zwaag and W. A. Groen, "Piezoelectric and mechanical properties of fatigue resistant, self-healing PZT-ionomer composites," *Smart Materials and Structures*, vol. 23, p. 055001, 2014.
- [20] S. E. van Kempen, "Optimisation of Piezoelectric Composite Materials Design through Improved Materials Selection and Property Prediction Methods," *M.Sc. Thesis, TU Delft*, 2012.
- [21] H. Khanbareh, S. van der Zwaag and W. A. Groen, "Effect of dielectrophoretic structuring on piezoelectric and pyroelectric properties of lead titanate-epoxy composites," *Smart Materials and Structures*, vol. 23, p. 105030, 2014.
- [22] I. Babu, D. A. van den Ende and G. de With, "Processing and characterization of piezoelectric 0-3 PZT/LCT/PA composites," *Journal of Physics D-Applied Physics*, vol. 43, pp. 425402,1-10, 2010.
- [23] D. A. van den Ende, P. de Almeida and S. van der Zwaag, "Piezoelectric and mechanical properties of novel composites of PZT and a liquid crystalline thermosetting resin," *Journal of Materials Science*, vol. 42, pp. 6417-6425, 2007.
- [24] G. Sa Gong, A. Safari, S. J. Jang and R. E. Newnham, "Poling flexible piezoelectric composites," *Ferroelectrics Letters Section*, vol. 5, pp. 131-142, 1986 1986.
- [25] B. Satish, K. Sridevi and M. S. Vijaya, "Study of piezoelectric and dielectric properties of ferroelectric PZT-polymer composites prepared by hot-press technique," *Journal of Physics D-Applied Physics*, vol. 35, pp. 2048-2050, 2002.
- [26] E. Venkatragavaraj, B. Satish, P. R. Vinod and M. S. Vijaya, "Piezoelectric properties of ferroelectric PZT-polymer composites," *Journal of Physics D-Applied Physics*, vol. 34, pp. 487-492, 2001.



## **Summary**

---



The main objective of this PhD thesis is to develop new routes and concepts for manufacturing piezoelectric ceramic-polymer composites with adequate piezoelectric properties while retaining ease of manufacturing and mechanical flexibility and explore new possibilities to maximize especially the voltage sensitivity while taking into account environmentally relevant issues such as avoiding the use of the chemical element Lead in the piezoelectric ceramics. The starting status of the field and the targets are described in Chapter 1.

The production of structured Lead Zirconium Titanate (PZT)-epoxy composites, fabricated using dielectrophoresis, is described in Chapter 2. The resulting thread-like arrangement of the PZT particles in the composites was found to enhance the piezoelectric and dielectric constants of the structured composites. The piezoelectric and dielectric properties of the composites as a function of PZT volume fraction were investigated and compared with the corresponding properties of unstructured composites. The experimentally observed piezoelectric and dielectric constants of the structured and unstructured composites could be described by existing theoretical models. It was found that an attractive combination of decent flexibility and good piezoelectric voltage sensitivity could be obtained for structured composites at around 10 vol.% PZT particles loading.

In Chapter 3, a Zn based ionomer was used as the new polymer matrix because of its high flexibility, decent electrical conductivity, excellent adhesion to the ceramic phase and most importantly its self-healing potential. The effective poling conditions for PZT-Zn ionomer composites were investigated and the results were compared with those for the reference PZT-EMAA (ethylene methacrylic acid copolymer) composites and monolithic PZT ceramic. The experimentally observed dielectric and piezoelectric coefficient were compared with Yamada's model. The tensile properties and high cycle fatigue of the composites for large strain levels were also studied. It was demonstrated that the partial loss of sensorial functionality of the composites after high cyclic tensile fatigue could be recovered by thermal healing, due to the self-healing character of the polymer matrix.

The goal of Chapter 4 was to develop an approach to quantify the state of poling of the PZT granules inside the Zn-ionomer matrix by using high energy synchrotron X-ray diffraction. For this study, we used a 30 vol.% Zn-ionomer PZT composite which was optimally poled as described in Chapter 3. The poling efficiency, crystallographic texture and lattice strain of the PZT particles inside the polymer matrix were determined and compared with the values for corresponding bulk ceramics reported in literature. It was shown that for an applied macroscopic field of  $15 \text{ kVmm}^{-1}$  the PZT particles are effectively poled, leading to a maximum  $v(002)$  domain reorientation volume fraction, of around 0.70. It is also found that a significant tensile lattice strain,  $\epsilon_{\{111\}}$ , of 0.6% occurs in the direction of the applied electric field, indicating the occurrence of residual stresses within the 2-4  $\mu\text{m}$  size diameter particles. The PZT particles within the polymeric matrix were found to experience significant elastic constraints.

In Chapter 5 the processing window of PZT based piezoelectric composites was unveiled over the entire phase diagram composition range and a material selection criterion for high  $g_{33}$  composites was formulated. The piezoelectric and dielectric properties for the complete set of PZT ceramics were reported and correlated to their microstructure, polarisation and strain hysteresis loops. The effect of the dielectric and piezoelectric properties of the filler particles on the effective properties of their composites was studied using theoretical models. It was demonstrated that the combination of low dielectric constant and moderately high  $d_{33}$  of the ceramic filler can lead to lead-free piezoelectric composites having sensorial properties not having been reported ever before for composite materials.

Finally, in Chapter 6 we describe the preparation of regular single phase cubic Lead-free  $(\text{K, Na})_x\text{Li}_{1-x}\text{NbO}_3$  (KNN) piezoceramic particles using a new solid state double calcination processing route. These particles were subsequently used to create random and structured KNN-epoxy composites. Using dielectrophoresis, these cubical KNN particles were structured into one dimensional chains in an epoxy matrix. Composites produced with these powders showed piezoelectric properties about a factor of 2 higher than those of composites processed with conventionally calcined

powder. The dielectrophoretically structured KNN-epoxy composites with optimized particle size and morphology showed excellent piezoelectric properties which can replace lead -containing piezoelectric composite for sensor applications in future.

In Figure S.1, we present an overview of the properties of the new composites created in the course of this graduation project and note with pleasure that in many cases the properties fall outside the domains of systems known at the start of the thesis project to yield attractive properties.

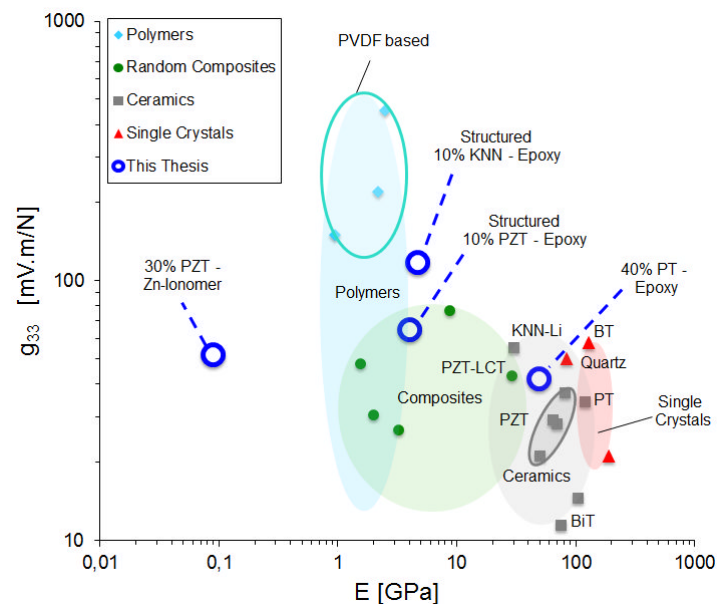


Figure S.1: Piezoelectric voltage coefficient of various types of piezoelectric materials as a function of their Young's modulus.



## **Samenvatting**

---



De belangrijkste doelstelling van dit proefschrift is om nieuwe routes en concepten te ontwikkelen voor de vervaardiging van piëzo-elektrische keramiek-polymeer composieten met voldoende piëzo-elektrische eigenschappen en behoud van productiegemak en mechanische flexibiliteit. Ook worden in dit proefschrift nieuwe mogelijkheden onderzocht om de veldgevoeligheid van de die composieten te maximaliseren veldgevoeligheid rekening houdend met ecologisch relevante vraagstukken zoals het vermijden van het gebruik van het chemische element lood in het keramiek. De aanvangstoestand van het onderzoeksveld en de doelstellingen van het uitgevoerde werk worden beschreven in Hoofdstuk 1.

De vervaardiging van met behulp van diëlektroforese gestructureerde lood zirkonium titanaat (PZT)-epoxy composieten wordt beschreven in Hoofdstuk 2. De resulterende draadvormige ordening van de PZT deeltjes in de composieten blijkt de piëzo-elektrische en diëlektrische constanten van de gestructureerde composieten te verbeteren. De piëzo-elektrische en diëlektrische eigenschappen van de composieten zijn onderzocht als functie van de PZT fractie en vergeleken met de overeenkomstige eigenschappen van ongestructureerde composieten. De bestaande theoretische modellen kunnen de experimenteel waargenomen piëzo- en diëlektrische constanten van de gestructureerde en ongestructureerde composieten voldoende beschrijven. Het blijkt dat een aantrekkelijke combinatie van redelijke mechanische flexibiliteit en goede piëzo-elektrische veldgevoeligheid in gestructureerde composieten verkregen kan worden bij een vulgraad van 10 vol.% PZT deeltjes.

In Hoofdstuk 3 is een Zink-bevattend ionomeer gekozen als nieuwe matrix vanwege de hoge flexibiliteit, redelijke goede elektrische geleiding, uitstekende hechting aan de keramische fase en vooral vanwege zijn zelfhelend vermogen. De effectieve polarisatievoorwaarden van PZT-Zn ionomeer composieten zijn onderzocht en de resultaten zijn vergeleken met die van de referentie PZT-EMAA (ethyleen methacrylzuur copolymeer) composieten almede die van puur PZT keramiek. De experimenteel waargenomen diëlektrische en piëzo-elektrische constanten worden vergeleken met het Yamada model. De mechanische eigenschappen, in het bijzonder de treksterkte en de vermoeiingssterktes bijna een groot aantal cycli met hoge

vervormingsniveaus, zijn onderzocht. Het is aangetoond dat, vanwege het zelfhelende vermogen van de polymeermatrix, een milde thermische behandeling kan leiden tot geheel of gedeeltelijk herstel van een door vermoeiing verloren gegane piezo-elektrische veldgevoeligheid.

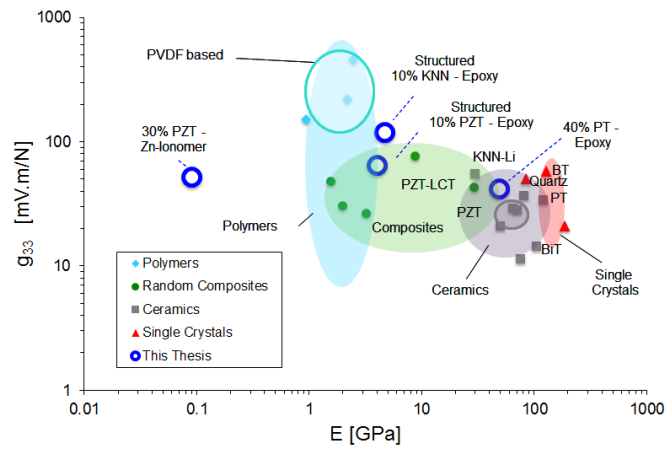
Het doel van Hoofdstuk 4 is het ontwikkelen van een methode om door middel van synchrotron röntgen diffractie de polarisatiestand van PZT deeltjes in de Zn-ionomeermatrix te kwantificeren. Voor dit onderzoek hebben we een optimaal gepolariseerd 30 vol.% PZT Zn-ionomeercomposiet gebruikt. De polarisatie-efficiëntie, kristallografische textuur en kristalroostervervorming van de PZT deeltjes in de polymeermatrix zijn gemeten en vergeleken met de waarden voor overeenkomstige piezo-keramieken uit de literatuur. Bij een toegepast macroscopisch elektrisch veld van  $15 \text{ kVmm}^{-1}$  blijkt dat de polarisatie van de PZT deeltjes effectief is, resulterend in een maximum van de  $v(002)$ -domein heroriëntatie volumefractie van ongeveer 0.70. Een aanzienlijke -kristalroostervervorming,  $\epsilon\{111\}$  in de richting van het toegepast elektrisch veld van + 0,6% is aangetoond, hetgeen wijst op het bestaan van restspanningen binnen de 2-4  $\mu\text{m}$  diameter deeltjes. Ook in een polymeermatrix blijken de deeltjes significante elastische restricties te ondervinden.

Hoofdstuk 5 legt de resultaten van een onderzoek naar het effect van chemische samenstelling van PZT vast en laat zien hoe samenstellingen leidend tot een hoge  $g_{33}$  waarde voor composieten gevonden kunnen worden. In Hoofdstuk 5 is het verwerkingsvenster van op PZT-gebaseerde piezo-elektrische composieten ontplooid over de gehele samenstellingsreeks van het fasesdiagram en wordt een materiaal selectie criterium voor hoge  $g_{33}$  composieten geformuleerd. De piezo-elektrische en diëlektrische eigenschappen zijn gemeten over het hele samenstellingsdomein en gecorreleerd aan hun microstructuur, polarisatie en vervormingshysterese-lussen. Het effect van de diëlektrische en piezo-elektrische eigenschappen van de granulaire vulstoffen op de effectieve eigenschappen van de composieten is theoretisch onderzocht. Aangetoond is dat de combinatie van een lage diëlektrische constante en redelijk hoge  $d_{33}$  van het loodvrije keramische vulmateriaal

kan leiden tot composieten met gevoeligheden die nog niet eerder met de op zich betere loodhoudende vulstoffen bereikt zijn. .

Tenslotte wordt in Hoofdstuk 6 de bereiding van één-fase kubische loodvrije  $(\text{K,Na})_x\text{Li}_{1-x}\text{NbO}_3$  (KNN) piëzo-keramiek deeltjes beschreven op basis van een nieuwe twee traps calcineerbehandeling. Deze deeltjes zijn vervolgens gebruikt om zowel ongeordende als gestructureerde KNN-epoxy composieten te maken. De kubische KNN deeltjes zijn wederom gestructureerd in ééndimensionale ketens in een epoxy matrix middels diëlektroforese. Dergelijke composieten hebben 2 keer zo hoge piëzo-elektrische eigenschappen als die gemaakt met conventioneel gecalcineerd poeder. De diëlektroforetisch gestructureerde KNN-epoxy composieten met geoptimaliseerde deeltjesgrootte en -morfologie laten uitstekende piëzo-elektrische eigenschappen zien, die suggereren dat voor sensortoepassingen in de toekomst loodhoudende composieten vervangen kunnen worden door loodvrije varianten zonder verlies van gevoeligheid.

In Figuur S.1, presenteren we een overzicht van twee belangrijke eigenschappen van de door ons ontwikkelde composieten, en stellen met genoeg vast dat in veel gevallen de nieuw gerealiseerde combinaties van eigenschappen buiten de domeinen van de bij het begin van het project bestaande materiaalgroepen vallen.



Figuur S.1: Piëzo-elektrische veldgevoeligheid van verschillende soorten piëzo-elektrische materialen als functie van hun Young's modulus.

## **Acknowledgements**

---



---

## Acknowledgements

While start writing acknowledgment, one might start feeling happy, relieved and bit proud. At the same time, I realize that the work in hand would never have been completed without the help from colleagues and friends. This thesis will not be completed without mentioning their names and expressing my sincere gratitude. I want to thank my promotor Prof. dr. ir. Sybrand van der Zwaag. It has been an honor to be his Ph.D. student. Without his help this thesis would not have completed in time. He is an inspiration as a powerful teacher. I have learned the basics to be good researcher and writing a good manuscript in his guidance. I am thankful for all his contributions of time, ideas, and funding to make my Ph.D. experience productive and stimulating. I also would like to thank him for high efficiency and time management in correcting this thesis. The joy and enthusiasm he has for his research is also contagious and motivational for me. I am also thankful for the excellent example he has provided as a successful material scientist and professor.

My special thanks and gratitude to Prof. dr. W.A. Groen. I feel fortunate to be his student. He have been more than a promotor to me. His encouragement and help made me feel confident to fulfill my desire and to overcome every difficulty I encountered from the day one of my PhD and still it continues. I am also very grateful for his scientific advice and knowledge and many insightful discussions and suggestions. He has given me immense support in the lab. His encouragement and support from the initial to the final day of my work has enabled me for the better understanding of the subject. He is my main resource for getting my science questions answered and was instrumental in helping me crank out this thesis, all in four years. He has been a figure of love, care and support in the career of 4 years. It is not sufficient to express my gratitude with only a few words.

I would like to thank Applied Piezo foundation and SMARTPIE programme members for initiating the project. The members of the NovAM group have contributed immensely to my personal and professional life at Delft. The group has been a source of friendships as well as good advice and collaboration. I am especially thankful to Dr. Ugo lafont and D. A. van den Ende for his initial help and support. I also thank Daniela and Jalmer who helped me with getting used to the dutch culture and food. I would

---

## Acknowledgements

really appreciate for being there on the best occasion of my life. You have been a very good friend and colleague. I especially would like to acknowledge Hamideh Khanbareh for providing me with all kinds of possible help, advice and feedback during the course of this work. I also would like to thank other members of the NovAM Group for making my tenure with the group an unforgettable experience, in random order, I would like mention Maruti (you are there from my interview itself till the end of the PhD, special thanks to your care and support), Santigo, Theo, Wei Xu, Qi Lu, Kevin, Marianella, Mladen, Hongli, Stanley van Kampen, Fedrick van Lock, Arianna, Srikanth, Jimmy, Jianwei, Wouter V, Wouter post, Ranjitha, Mina, Zelika, Martino, Antonio, Nan, Neola, Hussein and Johan. I warmly appreciate the help from Shanta Visser in taking care of administrative work and you have been a good friend. I specially remember all ISC Delft friends for their support and care.

I would like to thank Amal, my graduate student who helped me a lot in finishing the Non MPB composite work. I had a great time working with you. I am quite sure that you have a bright future ahead and wish you all success.

I am deeply indebted to my Mom and Dad for their persistent care and support. I love you both and I wish you all the happiness. My brother Jernet and my loving sister Nisha also deserve a special thanks. I also would like to make a special mention to Mr. Saji, Jeen who gave me a lot of strength to pursue my interest. My in laws Mr. Joseph Anto, Mrs. Saliamma Joseph and Ms. Elizabeth Joseph also deserve a special thanks for your support and encouragement. I also would like to thank all my family members. You have all contributed irreversibly to the person I have become. I cannot thank you enough.

Finally, I thank with love to Neena and Jovan. Understanding me best as a Ph.D. student, you have been my best friend and great companion, loved, supported, encouraged and helped me throughout this period in the most positive way. Big thanks to Jovan, you didn't cry that much during my writing time, I had enough sleep.

---

### Acknowledgements

Thank you very much to the doctoral committee members, who spared their time to review this thesis and the rich and fruitful discussions.



## Curriculum Vitae

---

Nijesh K James was born on 28 June 1984 in Kozhikode, Kerala, India. In 2007, he received his Master of Science degree in Physics from St. Berchman's college, M. G. University, Kerala. After that he moved to the Centre for Materials for Electronics Technology (C-MET), Trichur, Kerala as a Junior Research fellow in the microwave materials division where he engaged in developing composite substrates for high power solid state amplifiers. By the beginning of 2011 he moved to Delft University of Technology, within the group Novel Aerospace Materials group (NovAM) under the supervision of Prof. dr. ir. S. van der Zwaag and Prof. dr. W. A. Groen.



The main objective of his PhD thesis was to find new routes and concepts for manufacturing piezoelectric ceramic-polymer composites with adequate piezoelectric properties while retaining ease of manufacturing and explore new possibilities to maximize, especially, the voltage sensitivity. The breakthrough outcome of the project is the development of lead-free piezoelectric composites with enhanced properties for high precision sensor or energy harvesting applications.

Since March 2015, Nijesh is employed as a Post-doc in the group of Prof. Andrew Bell at the University of Leeds, in UK.



---

## List of publications

---

### 2014:

**N.K. James**, J. Kaliq, S van der Zwaag, WA Groen, Structure and unstructure KNN-epoxy composites, Patent submitted

**N.K. James**, U Lafont, S van der Zwaag, WA Groen, Piezoelectric and mechanical properties of fatigue resistant, self-healing PZT-ionomer composites, Journal of Smart Materials and structures 23(5), 055001, 2014.

**N. K. James**, T. Comyn, D. A. Hall, L. Daniel, A. K. Kleppe, S. van der Zwaag and W.A. Groen, Analysis of the state of poling of lead zirconate titanate (PZT) particles in an Zn-ionomer composite using high energy synchrotron X-ray diffraction, Journal of the American Ceramic Society, [under Review]

A. Shaji, **N. K. James**, H. Khanberek, S van der Zwaag, WA Groen

A. Shaji, **N. K. James**, S van der Zwaag, WA Groen

### 2013:

**N.K. James**, D.A. van den Ende, U Lafont, S van der Zwaag, WA Groen, Piezoelectric and mechanical properties of structured PZT-epoxy composites, Journal of Materials Research 28 (04), 635-64, 2013.

**N.K. James**, PS Simna, R. Ratheesh, Ba(Zn<sub>1/3</sub>Ta<sub>2/3</sub>)O<sub>3</sub> filled PTFE composites for microwave substrate applications, International Journal of Materials and structural Integrity 7 (1), 22-30, 2013.

**N.K. James**, U Lafont, S van der Zwaag, WA Groen Euromat 2013, Sevilla, Spain: Development of flexible ionomer – PZT composites and their piezoelectric and mechanical properties [ oral presentation].

**N.K. James**, U Lafont, S van der Zwaag, WA Groen, Piezoelectric and mechanical properties of fatigue resistant PZT-ionomer composites for sensors, ISPA 2013-

International Symposium on Piezocomposite applications September 19-20,  
2013 Fraunhofer Institute Center Dresden, Germany [poster presentation]

**2012:**

U. Lafont, **N.K. James**, W.A. Groen, H. Van Zeijl, S van der Zwaag, Self-healing composites with oriented fillers, Proceedings of the conference DYFP 2012.

**N.K. James**, D.A. van den Ende, U Lafont, S van der Zwaag, WA Groen, International Symposium on applications of Ferroelectrics 2012, Portugal, Piezoelectric and mechanical properties of structured PZT-epoxy composites [Oral presentation]

**N.K. James**, D.A. van den Ende, U Lafont, S van der Zwaag, WA Groen Electroceramics XIII 2012, Netherlands, Piezoelectric and mechanical properties of structured PZT-epoxy composites [Poster presentation]